COMPARISON AND EVALUATION OF
THREE DIMENSIONAL PASSIVE SOURCE LOCALIZATION TECHNIQUES

A THESIS SUBMITTED TO
THE GRADUATE SCHOOL OF NATURAL AND APPLIED SCIENCES
OF
MIDDLE EAST TECHNICAL UNIVERSITY

BY

EMRAH BATUMAN

IN PARTIAL FULLFILLMENT OF THE REQUIREMENTS
FOR
THE DEGREE OF MASTER OF SCIENCE
IN
ELECTRICAL AND ELECTRONICS ENGINEERING

JUNE 2010

Approval of the thesis:

COMPARISON AND EVALUATION OF THREE DIMENSIONAL PASSIVE SOURCE LOCALIZATION TECHNIQUES

submitted by **EMRAH BATUMAN** in partial fulfillment of the requirements for the degree of **Master of Science in Electrical and Electronics Engineering Department, Middle East Technical University** by,

Prof. Dr. Canan Özgen
Dean, Graduate School of **Natural and Applied Sciences**

Prof. Dr. İsmet Erkmen
Head of Department, **Electrical and Electronics Engineering**

Prof. Dr. Temel Engin Tuncer
Supervisor, **Electrical and Electronics Engineering Dept., METU**

Examining Committee Members:

Assoc. Prof. Dr. Özgür Barış Akan
Electrical and Electronics Engineering Dept., METU

Prof. Dr. Temel Engin Tuncer
Electrical and Electronics Engineering Dept., METU

Asst. Prof. Dr. Çağatay Candan
Electrical and Electronics Engineering Dept., METU

Dr. Arzu Tuncay Koç
Electrical and Electronics Engineering Dept., METU

Ç. Enis Doyuran (MSc.)
ASELSAN Inc.

Date: 07 June 2010

I hereby declare that all information in this document has been obtained and presented in accordance with academic rules and ethical conduct. I also declare that, as required by these rules and conduct, I have fully cited and referenced all material and results that are not original to this work.

Name, Last name   : Emrah Batuman

Signature   :

ABSTRACT

COMPARISON AND EVALUATION OF THREE DIMENSIONAL PASSIVE SOURCE LOCALIZATION TECHNIQUES

Batuman, Emrah

M. S., Department of Electrical and Electronics Engineering
Supervisor: Prof. Dr. Temel Engin Tuncer

June 2010, 158 pages

Passive source localization is the estimation of the positions of the sources or emitters given the sensor data. In this thesis, some of the well known methods for passive source localization are investigated and compared in a stationary emitter-sensor framework. These algorithms are discussed in detail in two and three dimensions for both single and multiple target cases.

Passive source localization methods can be divided into two groups as two-step algorithms and single-step algorithms. Angle-of-Arrival (AOA) based Maximum Likelihood (ML) and Least Squares (LS) source localization algorithms, Time-Difference-of-Arrival (TDOA) based ML and LS methods, AOA-TDOA based hybrid ML methods are presented as conventional two step techniques. Direct Position Determination (DPD) method is a well known technique within the single-

step approaches. In thesis, a number of variants of DPD technique with better computational complexity (the proposed methods do not need eigen-decomposition in the grid search) are presented. These are the Direct Localization (DL) with Multiple Signal Classification (MUSIC), DL with Deterministic ML (DML) and DL with Stochastic ML (SML) methods. The evaluation of these algorithms is done by considering the Cramer Rao Lower Bound (CRLB). Some of the CRLB expressions given in two dimensions in the literature are presented for three-dimensions.

Extensive simulations are done and the effects of different parameters on the performances of the methods are investigated. It is shown that the performance of the single step algorithms is good even at low SNR. DL with MUSIC algorithm performs as good as the DPD while it has significant savings in computational complexity. AOA, TDOA and hybrid algorithms are compared in different scenarios. It is shown that the improvement achieved by single-step techniques may be acceptable when the system cost and complexity are ignored. The localization algorithms are compared for the multiple target case as well. The effect of sensor deployments on the location performance is investigated.

Keywords: 3D Source Localization, AOA, TDOA, DPD, Single Step Location Estimation, Multiple Emitters

ÖZ

ÜÇ BOYUTLU PASİF KONUM BELİRLEME TEKNİKLERİNİN KARŞILAŞTIRILMASI VE DEĞERLENDİRİLMESİ

Batuman, Emrah

Yüksek Lisans, Elektrik Elektronik Mühendisliği Bölümü
Tez Yöneticisi: Prof. Dr. Temel Engin Tuncer

Haziran 2010, 158 sayfa

Konum belirleme, algılayıcı verileri kullanılarak yayıcıların veya vericilerinin konumlarının kestirilmesidir. Bu tez çalışmasında pasif konum kestirim teknikleri araştırılmış ve durağan algılayıcı-yayıcı geometrisi dâhilinde bu teknikler karşılaştırılmıştır. Söz konusu teknikler tek ve çoklu hedef durumları için iki ve üç boyutlu geometrilerde değerlendirilmiştir.

Pasif konum belirleme teknikleri, iki-adımlı ve tek-adımlı teknikler olarak iki gruba ayrılabilir. İki adımlı konum belirleme teknikleri olarak Varış Açısı (VA) tabanlı En Büyük Olabilirlik (EBO) ve En Küçük Kareler (EKK) teknikleri, Geliş Zaman Farkı (GZF) tabanlı EBO ve EKK teknikleri, VA-GZF tabanlı melez EBO tekniği sunulmuştur.

Doğrudan Konum Belirleme (DKB) metodu tek-adımlı iyi bilinen bir konum kestirim tekniğidir. Bu tez çalışmasında, DKB türevi olup DKB'den daha iyi hesaplama karmaşıklığına sahip (önerilen tekniklerde ızgara aramasında öz-ayrışıma gerek duyulmamaktadır) bazı tek-adımlı teknikler sunulmuştur. Bu teknikler, Çoklu Sinyal Sınıflandırma (ÇSS) ile Doğrudan Konum Kestirimi (DKK), Rastgele Olmayan EBO (ROEBO) ile DKK ve Rastgele EBO (REBO) ile DKK teknikleridir. Teknikler Cramer Rao Alt Sınırı (CRAS) ile karşılaştırılarak değerlendirilmiştir. Literatürde iki boyutlu verilen bazı CRAS ifadeleri üç boyutlu senaryolar için türetilerek sunulmuştur.

Kapsamlı benzetimler gerçekleştirilmiş, farklı değişkenlerin yöntemlerin başarımı üzerindeki etkileri araştırılmıştır. Yapılan benzetimlerde tek-adımlı tekniklerin başarımının düşük SNR seviyesinde dahi iyi olduğu gösterilmiştir. Hesaplama karmaşıklığını önemli derecede düşüren ÇSS-DKK tekniğinin başarımının DKB kadar iyi olduğu gözlemlenmiştir. VA, GZF ve melez teknikler değişik durumlarda karşılaştırılmıştır. Tek-adımlı teknikler ile elde edilen başarım artışı, sistem maliyeti ve karmaşıklığı göz ardı edildiğinde kabul edilebilir seviyededir. Ayrıca, konum belirleme teknikleri çoklu kaynak durumları için de karşılaştırılmıştır. Algılayıcı konuşlanmasının, konum kestirim başarımı üzerindeki etkileri araştırılmıştır.

Anahtar Kelimeler: 3B Konum Kestirimi, GA, GZF, DKB, Tek Adımlı Konum Kestirimi, Çoklu Kaynak

to My Family

and to Billur

ACKNOWLEDGEMENTS

I would like to express my sincere gratitude to my supervisor Prof. Dr. Temel Engin Tuncer for his guidance, advice, criticism, encouragement, endless patience and insight throughout the completion of the thesis.

I am indebted to all of my friends and colleagues for their support and encouragements.

I would like to express my special thanks to my fiancé Billur for her great support, encouragement, patience and understanding during the completion of this work.

My family, no words can help me to express my feelings, but at least I can say that I am grateful to you for the life you provide to me.

TABLE OF CONTENTS

LIST OF FIGURES

xiv

CHAPTER 1

INTRODUCTION

In this work, conventional two step and single step source localization approaches are investigated for unknown emitters with stationary emitter(s)-sensors (and sensor arrays) geometry.

Source localization is the estimation of the positions of the emitters given the sensor data. For defense, security and emergency purposes, estimating the location of the RF emitter with unknown waveform in a passive way incorporated the significance of this problem. The source localization problem may be classified for the geometrical scenarios of the targets and the sensors. When at least one of the targets and sensors are moving during the observation period, the Doppler shift is observed. This is called as a non-stationary geometrical scenario. In stationary geometry, it can be assumed that neither sources nor the sensors move in the data collection period.

Conventionally, the source localization problem is solved with two steps. The first step may be called as *Measurement Step* in which various parameters can be estimated such as Angle-of-Arrival (AOA) and Time-Difference-of-Arrival (TDOA) with respect to the sensor array structure. In other words, if separated sensors are deployed, TDOA between the sensor pairs can be estimated, whereas if the sensor arrays are used, AOA of the observed signal can be measured in each array. In some algorithms, TDOA information between the sensor array pairs is measured in addition to the AOA measurements to enhance the performance of the localization. The second step can be called as *Localization Step*. In the second step, by using the pre-measured parameters such as AOA, TDOA or both of AOA-TDOA sets, the location of the emitter(s) can be estimated.

However, in [1] it is shown that the source localization problem with stationary deployment geometry can be solved directly. In other words, the measurement and localization steps are merged to enhance the performance. The source location(s) of the target(s) can be estimated directly by processing all the observations taken by all of the sensors.

Certainly, the first emitter localization algorithm in the literature, which uses pre-measured AOA values, was presented by Stansfield [2]. Stansfield's pioneering approach has been adapted in different purposes [3, 4]. At least two sensor arrays are required for AOA based localization. In each sensor array, at least three sensors are required to estimate the AOA by measuring synchronous data. Well known AOA based localization algorithms are the Maximum Likelihood Estimation (MLE) approaches [5, 6]. Moreover Taylor Series approximations and Newton-Gauss iterations are used for non-linear minimization purposes in [5-7]. Another conventional localization algorithms using pre-measured AOA information are based on Least Squares (LS) approaches. One of the first LS localization solutions was proposed by Poirot in the sense of hemispheric LS error estimation in [4, 8]. Afterwards a new LS algorithm, which is based on minimizing the square of the miss distance of the position estimate from the measured AOAs, was presented by Brown in [9]. Another well known LS solution was proposed by Pages-Zamora in [10]. Moreover a Total Least Squares (TLS) solution to the localization problem was presented by Rao in [11]. Finally, a closed form approximate ML (AML) solution based on divide and conquers approach was presented by Pages-Zamora in [12]. The sources of error in the AOA based source localization problem are the effect of geometrical deployment of the sensor arrays and the target which can be called as Geometric Dilution of Precision (GDOP), Line-of-Bearing (LOB) errors, the effects of bias on AOA based localization, the effects of combining noisy AOA measurements and the effect of navigation errors. The effect of all of these error sources are investigated in the literature [5, 13-17].

TDOA based localization is used in Radar and Sonar applications and in emergency GSM localization purposes. At least four sensors (three TDOA measurements) are required for 3D TDOA based localization. Synchronized clock structure between

the sensors is required for accurate TDOA estimation. The TDOA estimation accuracy depends on the signal bandwidth [18-23]. The TDOA estimation accuracy degrades with decreasing signal bandwidth, in other words TDOA based localization methods are not suitable for narrowband communication waveforms. TDOA based localization methods give good performance for unknown signals with large bandwidths such as pulses, Code Division Multiple Access (CDMA) waveforms; known signals such as GSM waveforms with pilot, synchronization bursts etc. In this thesis, passive localization of the emitters with completely unknown waveforms is investigated. A well known ML solution and Gauss Newton iterations were presented in [5]. Fang proposed an exact solution to TDOA based localization problem when the number of TDOA measurements is equal to the number of unknown transmitter coordinates [24]. However Fang's algorithm cannot use the advantage of extra measurements. Closed form techniques dealing with extra measurements can be summarized as Spherical Interpolation Method, Divide and Conquer Method, Chan's Method, and Tyler Series Method which are presented respectively in [5, 25-27]. Divide and Conquer Method can achieve the optimum performance if the excessive number of sensors are used [28]. Chan's Method is better than the Spherical Interpolation and Divide and Conquer methods. Chan's Method gives approximately the same performance with the MLE when the TDOA measurement errors are small [28]. Finally, Doğançay presented new methods based on approximating the non linear hyperbolic equation sets to linear asymptotes [29-30]. The performance of the Doğançay's method degrades with respect to the ML solution in low SNR values due to the asymptotical linearization [28]. The comparison of the various TDOA based localization methods such as Analytical Method, LS Method, Taylor Series Method, Approximate ML (AML) Method, Two-Stage ML Method and Genetic Algorithm is presented in [31]. The sources of error in the TDOA based source localization problem are the effect of Geometric Dilution of Precision (GDOP), TDOA estimation errors, the effect of bias on TDOA based localization and navigation errors [13, 32-33].

Many localization algorithms based on the fusion of hybrid measurements have been developed. Almost all of these hybrid techniques address the localization of

the mobile users in the emergency situations. Basically, by using hybrid measurements, performance improvement over the single measurement type can be achieved, since the measurement noise for various types of measurements comes from different sources [28]. Consequently, location estimation errors of the different measurement types are assumed to be partially independent. This independence between the various measurement types provides designing estimators with better accuracies (by using data fusion techniques) than the estimators based on single measurement type [34]. Both ML and LS AOA-TDOA based hybrid localization algorithms depend on merging the AOA and TDOA based equation sets. MLE for 3D AOA-TDOA hybrid localization is derived in this work. In the literature, various methods have been presented such as LS Method, Two-Step LS Method, Divide and Conquer Method, methods specific to UWB and WCDMA systems, hybrid estimation with artificial neural networks [12, 35-40].

Weiss et al have proposed single step localization methods for various situations such as multiple number of emitters, known/unknown waveforms, stationary/non stationary geometries, for OFDM systems etc in [1, 41-45]. This method is called as Direct Position Determination (DPD), and the performance bounds of the DPD method under various cases are investigated in [46-48]. In this thesis, new single step localization techniques, which are applicable to multiple number of emitters, are introduced.

Various Cramer Rao Lower Bound (CRLB) expressions are presented for each different approach such as AOA, TDOA, AOA-TDOA Hybrid and Single Step based source localization algorithms to compare the performance of different techniques with the achievable ultimate performance. The reason of using CRLB expression is that CRLB gives the ultimate limit for an unbiased estimator. The CRLB for single step approaches was derived by Weiss for flexible geometric dimensions in [41]. For conventional two step localization methods, CRLB expressions are generally derived for 2D geometry for simplicity in the literature [7, 13]. In the literature, 3D CRLB expressions have been presented for TDOA based localization, however for AOA based methods due to the angular diversity (azimuth and elevation measurements) 2D expressions are preferred to be derived for

superficiality [7, 13, 49]. Moreover, due to the same reason CRLB expression for AOA-TDOA based hybrid methods, 2D representations are derived. However in this work, CRLB statements are derived for 3D for all methods.

The contributions in this thesis can be summarized as follows:

- 2D derivations in the literature are extended to 3D for AOA based and AOA-TDOA hybrid based Maximum Likelihood (ML) and Least Squares (LS) source localization methods.

- A two step LS technique for 3D source localization using only the AOA information is presented.

- 2D derivations in the literature are extended to 3D for CRLB expression for AOA based and AOA-TDOA hybrid based localization. Moreover, supplementary derivations for single step CRLB expression, namely, derivative of the combined manifold expression with respect to the source position vectors, are introduced.

- The approach in Direct Position Determination (DPD) technique is adapted for Multiple Signal Classification (MUSIC), Deterministic Maximum Likelihood (DML) and Stochastic Maximum Likelihood (SML) algorithms, and new single step localization algorithms with better computational complexities are proposed.

- The robustness of the localization algorithms to target-sensor deployments is investigated.

- Comparison of several different localization algorithms is done in a variety of scenarios for both single and multiple target cases.

The thesis is organized in six chapters. In Chapter 2 source localization techniques are classified with respect to various cases such as number of emitters, localization processors and target-sensor geometry. Moreover, basic mathematical expressions and illustrations are presented to emphasize the basic philosophy of the source localization approaches. In Chapter 3, conventional two step localization algorithms are presented. Namely, AOA based, TDOA based and AOA-TDOA based Hybrid

localization techniques are exhibited. Individual CRLB expressions are derived for each localization methods such as AOA, TDOA and AOA-TDOA Hybrid. Moreover some adaptive solutions are presented for the ML estimators. The work goes on with presenting the single step source localization methods such as Direct Position Determination (DPD), MUSIC, DML and SML localization algorithms for multiple emitters in Chapter 4. In addition, CRLB expression is presented for single step source localization problem. In Chapter 5, the comparison and the evaluation of the various localization methods are presented and explained for different cases. Finally, Chapter 6 summarizes the thesis and presents the conclusions.

CHAPTER 2

SOURCE LOCALIZATION PROBLEM

In this chapter, the source localization algorithms are classified with respect to the various factors which are referred in detail. The chapter goes on with the representation of the mathematical model for the observations taken by the sensors (or sensor arrays) from the target(s) for a stationary geometry.

2.1 CLASSIFICATION OF THE SOURCE LOCALIZATION TECHNIQUES

Paradowski [50] has classified the localization algorithms with respect to different concepts such as input data structure and the type of used geometrical quantities, object observation uncertainty model, input data collection and processing strategy. When the localization algorithms are classified with respect to the input data structure and the type of used geometrical quantities, the sub-classes are the homogenous and non-homogenous algorithms which are using the same type (i.e. AOA) and various types (i.e. AOA/TDOA Hybrid) of geometrical quantities, respectively. Secondly, Paradowski classified the algorithms with respect to the observation object uncertainty model, in which the sub-classes are Fisherian, Bayesian and Pseudo-Bayesian localization algorithms. In Fisherian algorithms, a priori knowledge concerning the emitter is not taken into the account. In Bayesian algorithms, a priori information about the emitter is used for location estimation, whereas in Pseudo-Bayesian algorithms are using joint particular features of the Fisherian and Bayesian algorithms. Pseudo-Bayesian algorithms can be classified as Fisherian-Bayesian and Bayesian-Fisherian algorithms. Finally Paradowski

classified the algorithms with respect to the input data collection and processing strategy in which the sub classes are simultaneous and asynchronous observations.

In this work, it is mainly interested in localization of the emitters without any prior information. In other words, it can be said that in this work the comparison and evaluation of the Fisherian localization algorithms are investigated. Some adaptive Bayesian solutions are presented for the Fisherian ML solutions.

Weiss [51] has classified algorithms as single step and two step algorithms which is tried to be illustrated in Figure 2.1. In single step algorithms, the source localization is directly estimated from the observed data. However in two step algorithms the source location is estimated via the premeasured parameters such as AOA, Time-of-Arrival (TOA), TDOA, Received-Signal-Strength (RSS), Frequency-of-Arrival (FOA), Frequency-Difference-of-Arrival (FDOA) (or any hybrid combination of these) which are measured with the observed data at separated sensors (or sensor arrays).
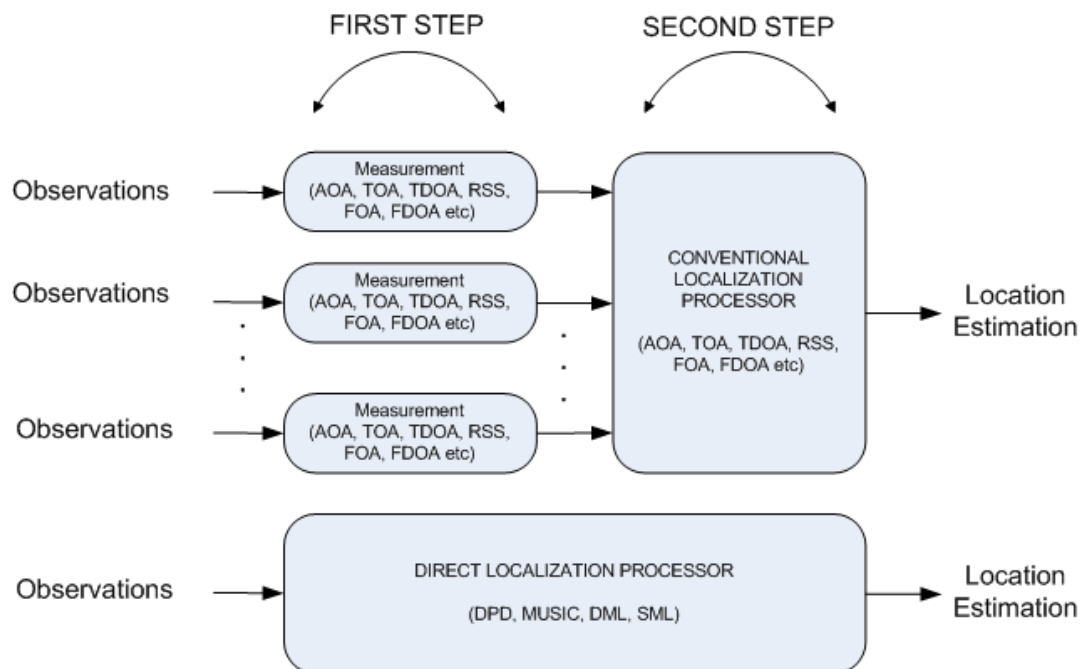
Figure 2.1: Conventional Two Step and Single Step Source Localization

By considering the geometrical deployment of the emitters and the sensors, source localization algorithms covered in this work is presented in Figure 2.2.
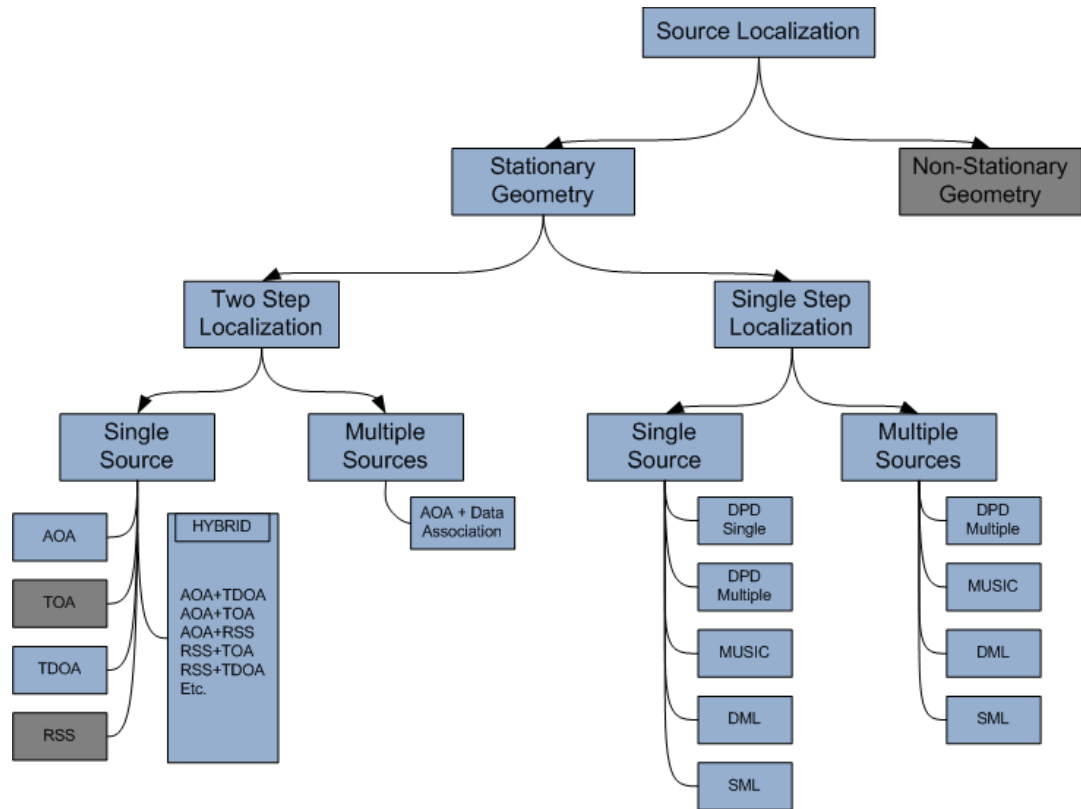
Figure 2.2: Source Localization Techniques Covered in This Thesis

The localization problem is classified with respect to the emitters-sensors geometry. If one of the emitters or the sensors (or sensor arrays) is moving, the geometry can be named as non-stationary. In this work, targets and the sensors are assumed to be stationary in the observation period, so it can be called as there is a stationary geometry of targets-sensors. In multiple emitter scenarios, there are at least two sources emitting at the same frequency. As a second classification step, it is preferred to classify the algorithms for the number of sources since many algorithms such as TOA, TDOA (except CDMA networks), and RSS cannot resolve the emitters for continuously emitting targets. High resolution AOA algorithms can

handle this problem by using an association algorithm [52]. The necessity of the data association is expressed exhaustively in the next chapter.

TOA and RSS based localization methods for stationary geometries and the localization algorithms for non-stationary geometries are not referred in this work, since this work focuses on the localization of continually emitting unknown source(s). Brief conceptual information about these algorithms is presented in the following paragraphs.

When the transmitting power of the emitter is known, by measuring received signal strength (RSS) at all sensors, the target localization can be estimated. Different propagation loss models are used to estimate the range of arrival (ROA), in other words the distance between the target and the sensor due to the terrain variations such as urban rural etc and the frequency of the transmission. Various RSS based localization algorithms are presented in the literature for different aspects such as GSM localization [53-57]. The geometrical interpretation of the RSS based localization is identical to the TOA based localization since both of them use ROA information.

Moreover, some fingerprint techniques are used for mobile positioning in GSM networks, which are based on searching the likelihood coordinate in the terrain. In such systems, a mobile emitter is located each point in the city and the RSS is measured from all sensors. By using the pre-measured RSS tables (comparing the RSSs measured during the localization operation), the localization of the GSM users can be done.

When the transmission frequency of the moving and emitting source is known, the Frequency-of Arrival (FOA) of the received signal can be estimated. However, if the transmission frequency is not known, the Frequency-Difference-of-Arrival (FDOA) between the separated sensors can be measured. There are various methods based on geometric and statistical approaches in the literature [13-14, 58]. By using the frequency differences between sources, Iso-Doppler curves are obtained on which the emitter position lies. Conversely these techniques (FOA and FDOA) are used with scenarios at least one of the sensors or target is non stationary. The

mathematical equation sets of the FDOA based localization correspond to the derivative of the TDOA equations with respect to the time.

Moreover, Weiss et al. have studied the single step localization techniques for non-stationary scenarios presented in [42]. In single step methods, all FOA and TOA information are embedded into the manifold model. By using all of the information, moreover the entire sensor pairs jointly, the performance of the single step localization algorithms outperforms the traditional FDOA measurement plus FDOA based localization techniques. However, the computational complexity of the single step method is much higher than that of the traditional FDOA based method.

2.2 BASIC OBSERVATION MODEL FOR STATIONARY GEOMETRY

In this section, the snapshot model for the stationary geometry is presented. The model is based on amplitude, phase and time differences of the received waveforms. Since, there is no relative movement between the targets and the sensors; frequency difference between the sensors is not used.

Under the assumption that the source is far away from the sensor array (a plane wave), a phase difference occurs between the antennas. In other words, the wave travels $d\ sin(\theta)$ path between the two sensors due to the illustration given in Figure 2.3, where d is the distance between the two antenna in y-axis.
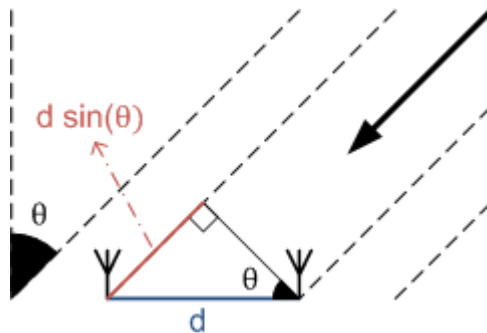
Figure 2.3: Basic Concept of AOA Estimation

The narrowband snapshot model received by the DF system can be written as

$$y_l(t) = b_l \ a_l(p) \ s(t) \ + \ n_l(t)$$

$$0 \le t \le T$$

<div align="right">(2.1)</div>

under some assumptions such as, the receiver channels, antennas and all cabling are phase identical. L is the total number of sensor arrays, M is the number of sensors used in each array for AOA estimation. In the snapshot representation, b_l is the complex attenuation coefficient between the emitter and the lth sensor array, $s(t)$ is the signal waveform of the emitter, $\boldsymbol{a_l(p)}$ is the steering vector with respect to the emitter and $n_l(t)$ is the zero mean Gaussian noise at the lth sensor.

However, in real (3D) world, the manifold representation is a bit different from the illustration given in Figure 2.3. Each entry of the $Mx1$ manifold vector $\boldsymbol{a_l(p)}$ can be represented as

$$a_{lm} = e^{j\frac{2\Pi}{\lambda}\left(P_{lm_x}sin(\theta_l)cos(\phi_l)+P_{lm_y}cos(\theta_l)cos(\phi_l)+P_{lm_z}sin(\phi_l)\right)}$$

<div align="right">(2.2)</div>

where P_{lm_x}, P_{lm_y} and P_{lm_z} are the x, y and z coordinates of the mth sensor of the lth array, respectively. θ_l is the azimuth angle of the source signal to the lth array, whereas ϕ_l is the elevation angle.

If there is more than one emitter in the environment, namely, Q number of emitters, at the observation period, then the MxQ array manifold matrix which consists of manifold column vectors for each target should be constructed.

For TDOA localization, in each sensor the snapshot model can be written as

$$y_l(t) = b_l \ s(t-\tau_l(p) - t^0) + \ n_l(t)$$

<div align="right">(2.3)</div>

where b_l is the complex attenation coefficient between the emitter and the lth sensor, $s(t)$ is the signal waveform of the emitter, $\tau_l(p)$ is the flight time of the signal between the target and the lth sensor, t^0 is the transmission time of the signal at the emitter and $n_l(t)$ is the zero mean Gaussian noise at the lth sensor.
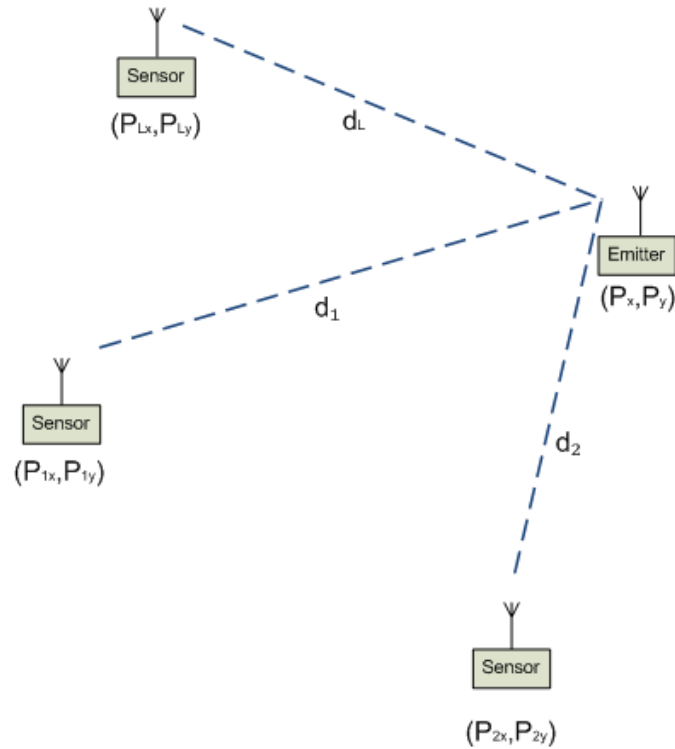
Figure 2.4: Basic Concept of TDOA estimation

The signal transmitted at time t^0 arrives at the sensors with delays, which may be called as flight times of the signal or TOAs. By cross-correlating the received waveforms, the TDOA between the sensor pairs can be estimated. By using the TDOA pairs and the coordinate of the sensors, the source localization can be estimated, which is presented in detail in the next chapter.

In AOA estimation of the received signal, the phase difference between the sensors with respect to the carrier (of the received signal) is measured, whereas in TDOA estimation, time delays between the sensors with respect to the message signal is calculated. Measuring the phase difference with respect to the carrier frequency requires calibration between the channels of the Direction Finder (DF) receivers. All the components (antennas, RF front ends, down-converters, ADCs) should give the same response, or should be calibrated. Consequently, there is no need for calibration data or phase identical requirements between the sensors for proper TDOA estimation. However, good time synchronization between the sensors is needed.

CHAPTER 3

CONVENTIONAL TWO STEP SOURCE

LOCALIZATION ALGORITHMS

In this chapter, conventional two step source localization algorithms which are applicable to unknown emitters are presented. The chapter consists of three main parts. In each part, different localization methods which are based on different pre-measured parameters are investigated. Pre-measured parameters are Angle-of-Arrival (AOA) and Time-Difference-of-Arrival (TDOA) values. Moreover, hybrid based methods which use both AOA and TDOA measurements are presented.

The chapter starts with AOA Based Source Localization. First, AOA based localization problem is formulated. AOA based localization algorithms are derived for 2D and 3D localization scenarios such as Maximum Likelihood (ML) and Least Squares (LS) based methods. Adaptive techniques are presented for ML solutions. AOA based localization accuracy is investigated in two different ways such as giving the Cramer Rao Lower Bound (CRLB) expression and defining the error ellipse. Ghost node concept is presented for multiple source localization with AOA measurements and relevant data association algorithms are presented.

In the second part, TDOA Based Source Localization is investigated. TDOA based source localization problem is formulated for 3D localization. TDOA based localization algorithms are derived for 3D localization scenarios such as Maximum Likelihood (ML) and Least Squares (LS) based methods. Adaptive techniques are presented for ML solutions. This part ends with deriving the CRLB expression for 3D TDOA based localization problem.

Finally, AOA plus TDOA Based Hybrid Source Localization is investigated. Hybrid based source localization problem is formulated. Maximum Likelihood (ML) expression is derived for 3D localization and literature survey about LS based hybrid methods is briefly presented. This part ends with deriving the CRLB expression for 3D AOA-TDOA based localization problem.

3.1 AOA BASED SOURCE LOCALIZATION

Position estimation concept starts with using AOA measurements taken from different sensor arrays. As mentioned in the previous chapter, by using amplitude or phase differences or observation correlation between the sensors, AOA measurement is performed. Different techniques have been developed for AOA estimation. Most of these techniques depend on amplitude or phase differences between the sensors such as Watson-Watt Method, Interferometer Algorithm and Single Rotating Directional Antenna Method whereas some techniques such as Pseudo-Doppler Technique depends on the frequency difference [13, 14, 51, 59]. Moreover High Resolution (HR) techniques have been developed to estimate AOAs for multiple sources by using the observation covariance of the sensors such as MUSIC, ESPRIT, and Min-Norm [60-63]. Some fast HR algorithms (search free) which depend on polynomial root finding have been developed to reduce the algorithmic complexity such as Root MUSIC, Root Min-Norm methods [64]. However uniform linear arrays are required for these fast algorithms. For this reason, array interpolation techniques, which are used to transform real arbitrary array data to virtual ULA data, have been developed. Various fast AOA estimation algorithms and array interpolation techniques have been presented in [51, 59].

AOA estimation accuracy depends on many factors such as observation covariance, array geometry, SNR, number of snapshots, covariance of the signal waveforms etc. [65].

3.1.1 Problem Formulation

After performing AOA measurement in all sensor arrays, the position of the source can be estimated, by using the location of the sensor arrays. Noise-free 2D illustration is given in Figure 3.1.
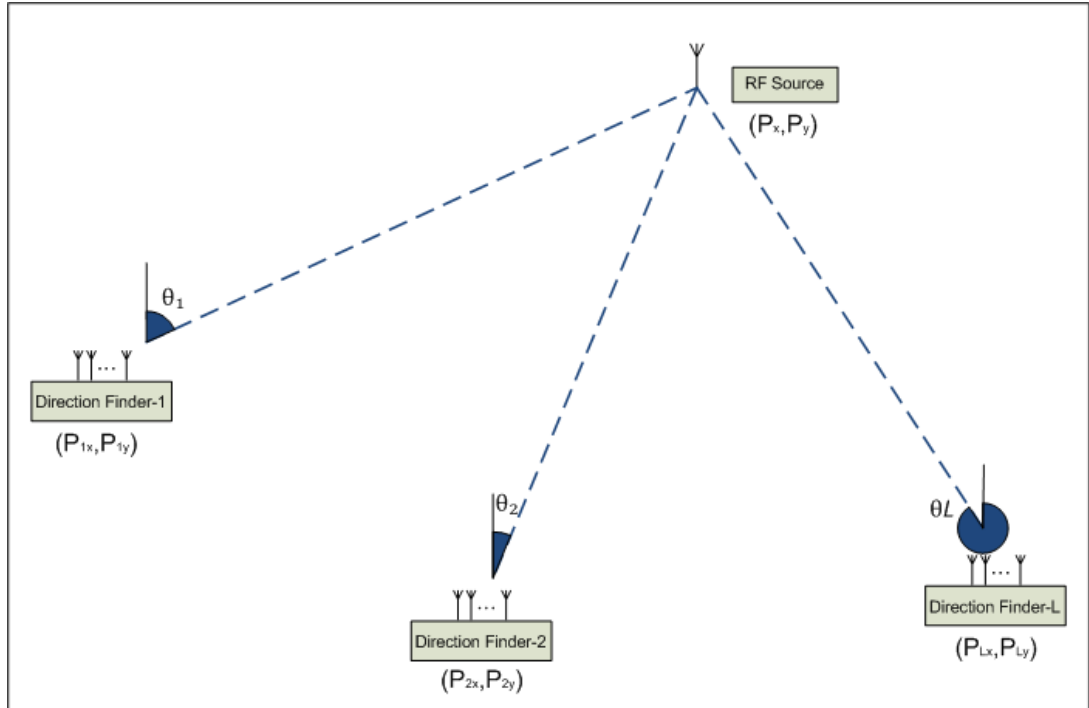
Figure 3.1: Noise Free Scenario for 2D AOA Based Source Localization

By the effect of observation noise, Line-of-Bearings (LOBs) are distorted. Noisy observation scenario is illustrated in Figure 3.2. Some non-statistical triangulization techniques have been developed to estimate the position of the source that depends on intersection of medians, intersection of angle bisectors and Steiner point [66]. These classical techniques and the statistical analysis have been summarized by Poisel [13]. Some deployment techniques such as concave and convex deployments are suggested for tactical Electronic Warfare (EW) scenarios for the accurate localization [14].

The problem is estimating the position of the source by using noisy LOB measurements taken from different sensor arrays and array locations. Many

techniques depend on geometric solutions have been developed whereas, Maximum Likelihood (ML) based techniques depend on some statistical properties of the measured LOBs such as covariance of the LOB measurements for accurate positioning.
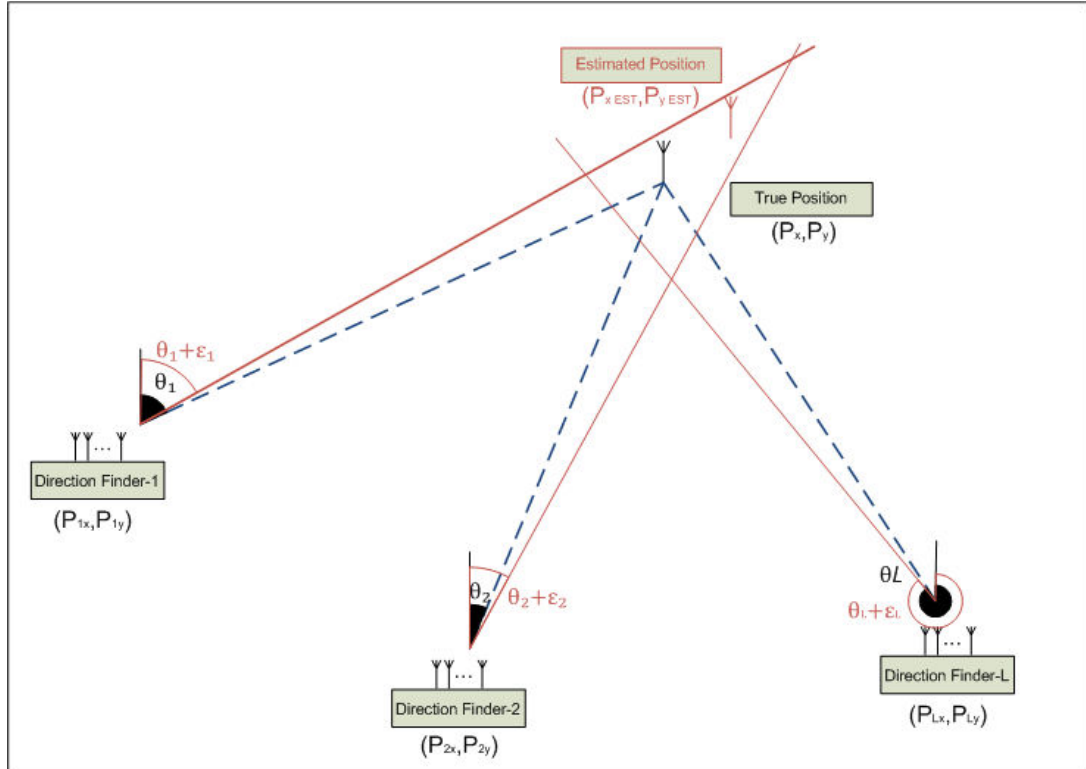
Figure 3.2: Noisy Scenario for 2D AOA Based Source Localization

However, in 3D geometry both azimuth and elevation deviations should be taken into account. The target lies inside the elliptic cones. The radiuses of the elliptic cone depend on the deviations of the azimuth and elevation measurements. An illustrative scenario is shown in Figure 3.3. When the observations are noiseless, target position is the intersection of the rays coming from the sensor arrays, which is tried to be visualized with the dashed lines.
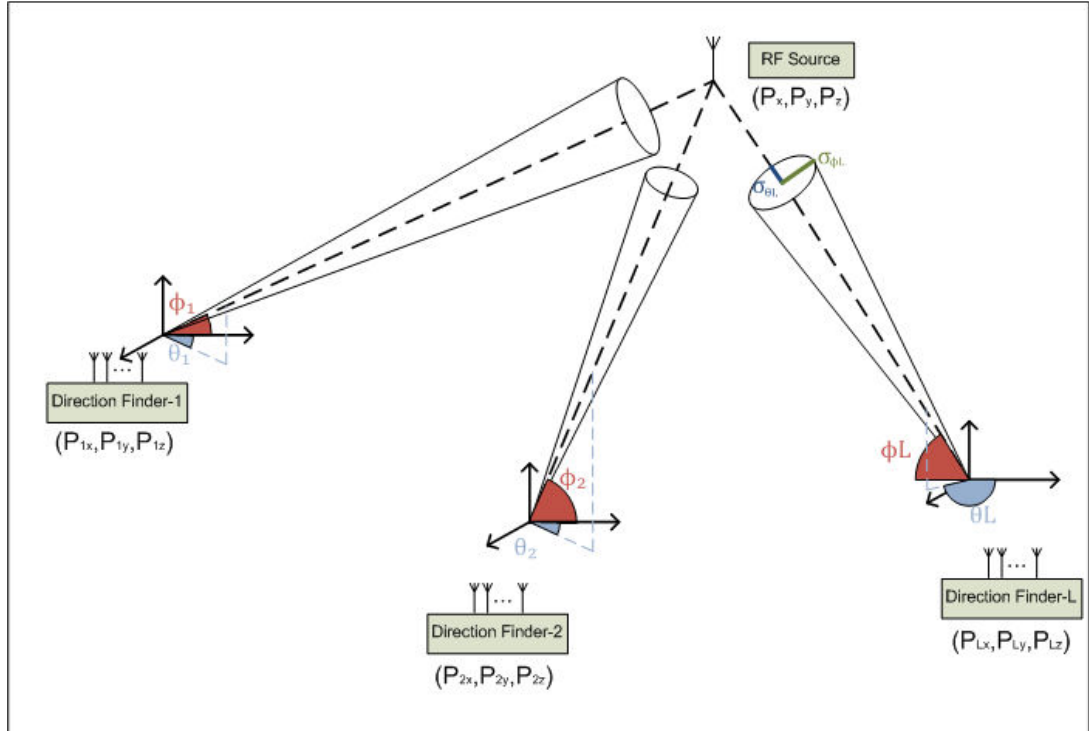
Figure 3.3: Noisy and Noise Free Scenario for 3D AOA Based Source Localization

3.1.2 AOA Based Source Localization Algorithms

In this section AOA based source localization algorithms have been presented. Section starts with deriving the Maximum Likelihood (ML) cost function of the localization problem. Iterative technique is presented for this ML cost function and the section ends with giving the Least Squares (LS) solution to the problem.

3.1.2.1 AOA Based Maximum Likelihood Source Localization Algorithms

In this section Maximum Likelihood (ML) algorithms and iterative solutions are presented. The definitions start with 2D localization problem, then goes with 3D expressions.

By assuming the noise is zero mean Gaussian, the Maximum Likelihood Estimation (MLE) of the 2D source position can be written as [7]

$$\hat{\boldsymbol{p}} = argmin_p \, F(p, \theta) \tag{3.1}$$

where the cost function $F(p, \theta)$ is

$$F(p, \theta) = \frac{1}{2}[\, \boldsymbol{g}(\boldsymbol{p}) - \boldsymbol{\theta}\,]^T \boldsymbol{S}^{-1} [\, \boldsymbol{g}(\boldsymbol{p}) - \boldsymbol{\theta}\,] \tag{3.2}$$

The cost function depends on the azimuth measurements, covariance of these AOA measurements and the angles with respect to the search point $\boldsymbol{g}(\boldsymbol{p})$. At each search point, the angle between the lth sensor array and the search point is calculated as

$$g_l(p) = tan^{-1}\left(\frac{P_x - P_{lx}}{P_y - P_{ly}}\right) \tag{3.3}$$

then, these angles are combined in $Lx1$ vector $\boldsymbol{g}(\boldsymbol{p})$ as

$$\boldsymbol{g}(\boldsymbol{p}) = [g_1(p), \, g_2(p), \dots, g_L(p)]^T \tag{3.4}$$

The azimuth measurements of each sensor array are merged into a $Lx1$ vector $\boldsymbol{\theta}$ as

$$\boldsymbol{\theta} = [\theta_1, \, \theta_2, \dots, \theta_L]^T \tag{3.5}$$

Finally LxL covariance matrix $\boldsymbol{S}$ contains the covariance of the AOA measurements on its diagonals as

$$\boldsymbol{S} = diag\{\sigma_{\theta_1}^2, \sigma_{\theta_2}^2, \dots, \sigma_{\theta_L}^2\} \tag{3.6}$$

The pre-mentioned ML cost function $F(p, \theta)$ can be rewritten as

$$F(p, \theta) = \frac{1}{2}\boldsymbol{f}^T \boldsymbol{S}^{-1} \boldsymbol{f} = \frac{1}{2}\sum_{l=1}^{L} \frac{f_l^2}{\sigma_{\theta_l}^2} \tag{3.7}$$

where f_l represents the error between the measured angle of the lth sensor array and the angle with respect to the search point.

$$\boldsymbol{f} = [f_1, \, f_2, \dots, f_L]^T = \boldsymbol{g}(\boldsymbol{p}) - \boldsymbol{\theta} \tag{3.8}$$

MLE Algorithm:

1. Estimate the Angle-of Arrival (AOA) of the received signal in each sensor array by using any DOA estimation algorithm.

2. As mentioned in equations (3.5) and (3.6), obtain the measurement vector $\boldsymbol{\theta}$ and the measurement covariance matrix $\boldsymbol{S}$.

3. Perform a grid search, in each search point

    i.   Calculate the angle between the search point and the sensor arrays, and obtain vector $\boldsymbol{g}(\boldsymbol{p})$

    ii.   Calculate the cost function $F(p, \theta)$

4. After performing the grid search, find the position estimate $\hat{\boldsymbol{p}}$, which gives the minimum cost.

The solution of the MLE of the source position can be found by using Newton-Gauss iterations as [13]

$$\hat{\boldsymbol{p}}_{i+1} = \hat{\boldsymbol{p}}_i + \left[g_p^T S^{-1} g_p \right]^T g_p^T S^{-1} \left[\boldsymbol{\theta} - \boldsymbol{g}(\hat{\boldsymbol{p}}_i) \right] \tag{3.9}$$

where $\hat{\boldsymbol{p}}_i$ and $\hat{\boldsymbol{p}}_{i+1}$ are the position estimates at the ith and $(i+1)^{st}$ iterations respectively. $\boldsymbol{g}_p$ represents the derivative of $\boldsymbol{g}(\boldsymbol{p})$ evaluated at the true target position, which yields to

$$\boldsymbol{g}_p = \frac{\partial \boldsymbol{g}}{\partial \boldsymbol{p}} = \begin{bmatrix} \dfrac{-(P_x - P_{1x})}{\|\boldsymbol{P} - \boldsymbol{P}_1\|} & \dfrac{-(P_x - P_{2x})}{\|\boldsymbol{P} - \boldsymbol{P}_2\|} & \cdots & \dfrac{-(P_x - P_{Lx})}{\|\boldsymbol{P} - \boldsymbol{P}_L\|} \\ \dfrac{(P_y - P_{1y})}{\|\boldsymbol{P} - \boldsymbol{P}_1\|} & \dfrac{(P_y - P_{2y})}{\|\boldsymbol{P} - \boldsymbol{P}_2\|} & \cdots & \dfrac{(P_y - P_{Ly})}{\|\boldsymbol{P} - \boldsymbol{P}_L\|} \end{bmatrix} \tag{3.10}$$

The adaptive implementation of the MLE algorithm can be described as follows:

Adaptive MLE Algorithm:

1. Estimate the Angle-of Arrival (AOA) of the received signal in each sensor array by using any DOA estimation algorithm.

2. As mentioned in equations (3.5) and (3.6), obtain the measurement vector $\boldsymbol{\theta}$ and the measurement covariance matrix $\boldsymbol{S}$.

3. Obtain an initial position estimate $\hat{\boldsymbol{p}}_0$ by using any source localization algorithm.

4. By using a stopping criterion (i.e. $(\hat{\boldsymbol{p}}_{i+1} - \hat{\boldsymbol{p}}_i) < \boldsymbol{\varepsilon}$), start the iterations with the initial position estimate until the stopping criterion is satisfied.

5. In each iteration step,

    i.   Calculate the matrix $\boldsymbol{g_p}$ with the previously estimated position.

    ii.   By using equation (3.9), estimate the new position.

Stansfield's Algorithm:

Stansfield's Algorithm is one of the first algorithms developed for estimating the location of the emitter source based on AOA measurements [2, 13]. AOA measurement errors are assumed to be Gaussian. The main idea is minimizing the joint probability density function of the miss distances. The geometry of the Stansfield's Algorithm is illustrated in Figure 3.4. The previously mentioned original ML cost function is given by

$$F(p, \theta) = \frac{1}{2} \boldsymbol{f}^T \boldsymbol{S}^{-1} \boldsymbol{f} = \frac{1}{2} \sum_{l=1}^{L} \frac{f_l^2}{\sigma_{\theta_l}^2} \qquad (3.11)$$

where f_l represents the difference between the measured AOA and the angle between the sensor array and the estimated target location $\hat{\boldsymbol{p}}$. As shown in Figure 3.4, these differences are represented by $\Delta\theta_l$ as

$$f_l = g_l(p) - \theta_l = \Delta\theta_l \qquad (3.12)$$

Stansfield's approach is based on assuming that the measurement errors are small. By assuming small errors, the *sine function approximation* can be performed on errors as

$$\sin(\Delta\theta) \approx \Delta\theta \qquad (3.13)$$
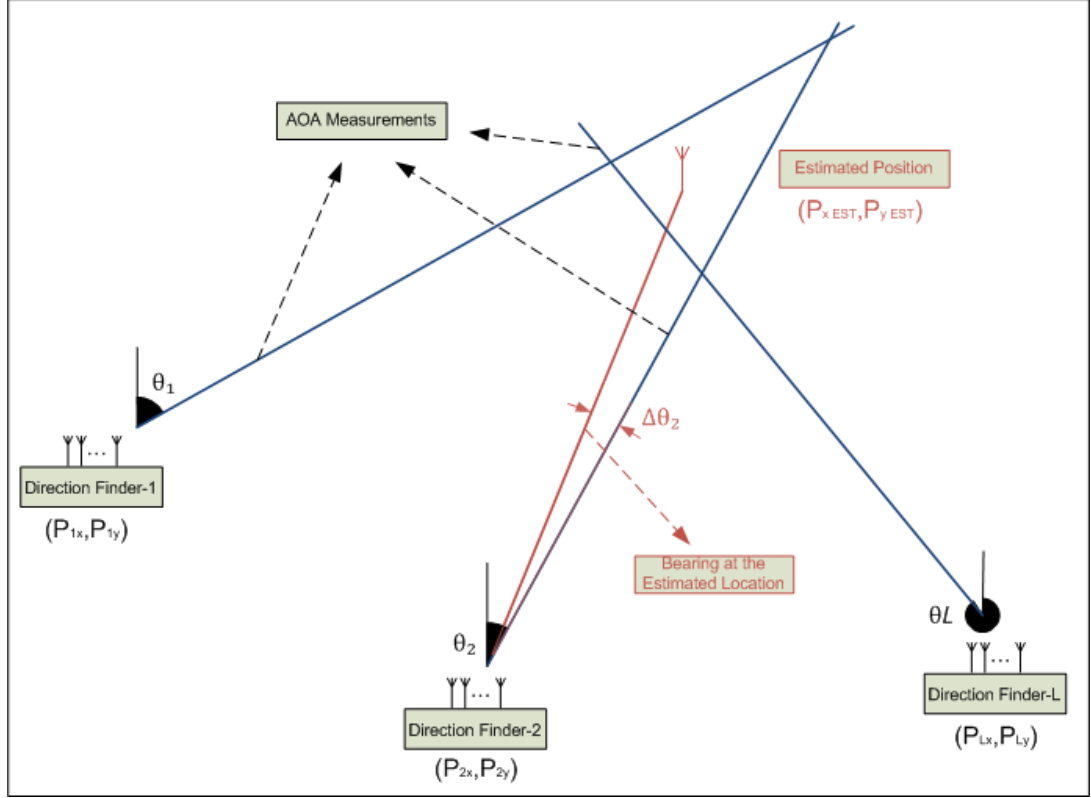
Figure 3.4: Stansfield's Geometry for 2D AOA Based Source Localization

Then, the Stansfield's ML cost function can be written as

$$F_{ST}(p, \theta) = \frac{1}{2} \sum_{l=1}^{L} \frac{sin^2(\Delta\theta_l)}{\sigma_{\theta_l}^2} \qquad (3.14)$$

By using trigonometric identities, the cost function can be rewritten a

$$F_{ST}(p, \theta) = \frac{1}{2}(Ap - b)^T D^{-1} S^{-1}(Ap - b) \qquad (3.15)$$

where the $Lx2$ matrix A and the $Lx1$ vector b are written as

$$A = \begin{bmatrix} cos(\theta_1) & -sin(\theta_1) \\ cos(\theta_2) & -sin(\theta_2) \\ \vdots & \vdots \\ cos(\theta_L) & -sin(\theta_L) \end{bmatrix} \qquad (3.16)$$

22

$$b = \begin{bmatrix} P_{1x}cos(\theta_1) - P_{1y}sin(\theta_1) \\ P_{2x}cos(\theta_2) - P_{2y}sin(\theta_2) \\ \vdots \\ P_{Lx}cos(\theta_L) - P_{Ly}sin(\theta_L) \end{bmatrix} \tag{3.17}$$

The *LxL* diagonal matrix $\boldsymbol{D}$ contains the distances between the estimated target position and the sensor arrays on its diagonals.

$$\boldsymbol{D} = diag\{\|\boldsymbol{P} - \boldsymbol{P_1}\|^2, \|\boldsymbol{P} - \boldsymbol{P_2}\|^2, \ldots, \|\boldsymbol{P} - \boldsymbol{P_L}\|^2\} \tag{3.18}$$

The solution which minimizes the Stansfield's cost function with the weighting matrix $\boldsymbol{W} = \boldsymbol{D^{-1}S^{-1}}$, can be given as

$$\widehat{\boldsymbol{p}}_{ST} = (\boldsymbol{A^T D^{-1} S^{-1} A})^{-1} \boldsymbol{A^T D^{-1} S^{-1} b} \tag{3.19}$$

Note that, the matrix $\boldsymbol{D}$ is assumed to be known or a rough estimate is used without affecting the solution significantly since the cost function is a weak function of $\boldsymbol{D}$.

This solution is non-iterative and has accuracy close to the original MLE. However, Gavish and Weiss showed that Stansfield's estimator is biased [7]. Moreover, the bias and the RMS error do not decrease with the number of observations.

Stansfield's Algorithm:

1. Estimate the Angle-of Arrival (AOA) of the received signal in each sensor array by using any DOA estimation algorithm.
2. As mentioned in equations (3.16) and (3.17), obtain the matrix $\boldsymbol{A}$, vector $\boldsymbol{b}$ and the measurement covariance matrix S by using the AOA measurements and the positions of the sensor arrays.
3. By using any source localization algorithm, obtain a rough position estimate $\widehat{\boldsymbol{p}}_0$. Obtain matrix $\boldsymbol{D}$, by using this estimate and the sensor array locations.
4. Estimate the source position $\widehat{\boldsymbol{p}}_{ST}$ by using closed form solution given in equation (3.19).

Extension to 3D Localization:

By assuming the noise is zero mean Gaussian, the Maximum Likelihood Estimation (MLE) of the 3D source position can be written as [49]

$$\hat{\boldsymbol{p}} = argmin_p \, F(p, \theta, \phi) \tag{3.20}$$

where the cost function $F(p, \theta, \phi)$ is

$$F(p, \theta, \phi) = \frac{1}{2} (\hat{\boldsymbol{g}} - \boldsymbol{g}(\boldsymbol{p}))^T \boldsymbol{R}^{-1} (\hat{\boldsymbol{g}} - \boldsymbol{g}(\boldsymbol{p})) \tag{3.21}$$

The derivation goes on with defining $\hat{\boldsymbol{g}}$ which represents the azimuth and elevation measurements as

$$\hat{\boldsymbol{g}} = \left[\hat{\boldsymbol{g}}_\theta^T, \, \hat{\boldsymbol{g}}_\phi^T \right]^T \tag{3.22}$$

$2Lx1$ vector $\hat{\boldsymbol{g}}$ consists of two $Lx1$ vectors; $\hat{\boldsymbol{g}}_\theta$ and $\hat{\boldsymbol{g}}_\phi$, which represent the azimuth and elevation values measured by the sensor arrays. These vectors are

$$\hat{\boldsymbol{g}}_\theta = \left[\hat{\theta}_1, \, \hat{\theta}_2, \dots, \hat{\theta}_L \right]^T \tag{3.23}$$

$$\hat{\boldsymbol{g}}_\phi = \left[\hat{\phi}_1, \, \hat{\phi}_2, \dots, \hat{\phi}_L \right]^T \tag{3.24}$$

The $2Lx2L$ matrix $\boldsymbol{R}$ represents the covariance of the AOA measurements. Assuming that the elevation and azimuth angles are independent and noise is independent between azimuth and elevation measurements, the measurement covariance matrix can be written as

$$\boldsymbol{R} = \begin{bmatrix} \boldsymbol{R}_\theta & \boldsymbol{0} \\ \boldsymbol{0} & \boldsymbol{R}_\phi \end{bmatrix} \tag{3.25}$$

where the LxL matrices $\boldsymbol{R_\theta}$ and $\boldsymbol{R_\phi}$ are the covariances of the azimuth and elevation measurements, respectively. The covariance matrices of the azimuth and elevation measurements can be written as

$$\boldsymbol{R_\theta} = diag\{\sigma_{\theta_1}^2, \sigma_{\theta_2}^2, \dots, \sigma_{\theta_L}^2\} \tag{3.26}$$

$$\boldsymbol{R_\phi} = diag\{\sigma_{\phi_1}^2, \sigma_{\phi_2}^2, \dots, \sigma_{\phi_L}^2\} \tag{3.27}$$

by assuming that the angle measurements are independent between the sensor arrays. The $2Lx1$ vector $\boldsymbol{g(p)}$ represents angles with respect to the search point $\boldsymbol{p}$, i.e.

$$\boldsymbol{g(p)} = \begin{bmatrix} \boldsymbol{g_1^T(p)} & \boldsymbol{g_2^T(p)} \end{bmatrix}^T \tag{3.28}$$

This vector consists of two $Lx1$ vectors; $\boldsymbol{g_1(p)}$ and $\boldsymbol{g_2(p)}$, which represents the azimuth and elevation angles with respect to the search point.

$$\boldsymbol{g_1(p)} = [\theta_1, \ \theta_2, \dots, \theta_L]^T \tag{3.29}$$

$$\boldsymbol{g_2(p)} = [\phi_1, \ \phi_2, \dots, \phi_L]^T \tag{3.30}$$

The lth element of the azimuth vector $\boldsymbol{g_1(p)}$ can be calculated with respect to the search point and the position of the lth sensor array as

$$\theta_l(p) = tan^{-1}\left(\frac{P_x - P_{l,x}}{P_y - P_{l,y}}\right) \tag{3.31}$$

Similarly, the lth element of the elevation vector $\boldsymbol{g_2(p)}$ can be calculated as

$$\phi_l(p) = tan^{-1}\left(\frac{P_z - P_{l,z}}{\sqrt{\left(\left(P_x - P_{l,x}\right)^2 + \left(P_y - P_{l,y}\right)^2\right)}}\right) \tag{3.32}$$

3D MLE Algorithm:

1. Estimate the Angle-of Arrival (AOA) of the received signal in each sensor array by using any DOA estimation algorithm.
2. As mentioned in equations (3.22) and (3.25), obtain the measurement vector $\hat{g}$ and the measurement covariance matrix R.
3. Perform a 3D grid search, in each search point
    i. Calculate the azimuth and elevation angles between the search point the sensor arrays, and obtain vector $g(p)$
    ii. Calculate the cost function $F(p, \theta, \phi)$
4. After performing the grid search, find the position estimate $\hat{p}$, which gives the minimum cost.

Newton-Gauss Iterations can be easily modified for 3D scenario by replacing the measurement vector, covariance of the measurements for 3D definitions given in this section.

3.1.2.2 AOA Based Least Squares Source Localization Algorithms

Least Squares based solution was proposed by Pages Zamora for single source localization problem [10].

First, the position vectors are defined as P_l and P for the lth sensor array and the source, respectively. The source position can be written in terms of the position of each sensor array by using the distance between the sensor array and the emitter d_l, and the unitary vector v_l. These mentioned parameters are seen in Figure 3.5 for 2D noiseless scenario.

26
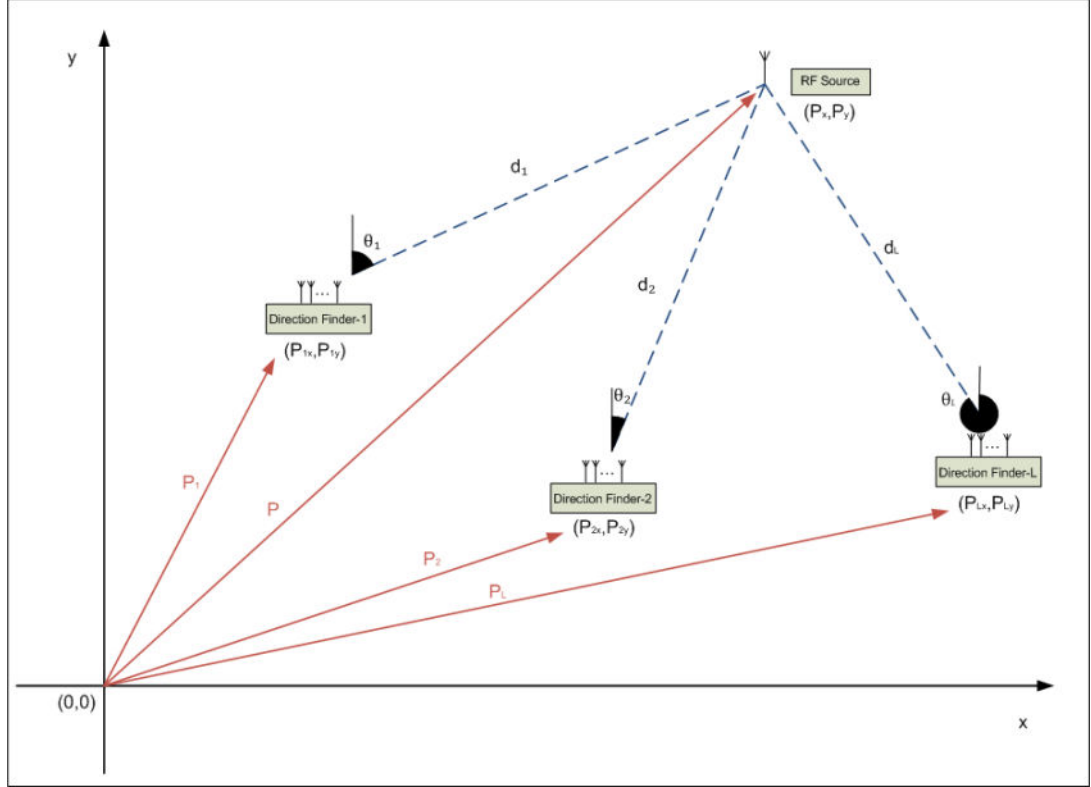
Figure 3.5: Pages-Zamora's Geometry for 2D AOA Based Source Localization

As mentioned before, the source position can be written in terms of the position of each sensor array as

$$P = P_l + d_l v_l$$

$$l = 1, 2, \ldots, L$$

(3.33)

where d_l is the distance between the sensor array and the source. Unitary vector v_l is defined in terms of the angle between the source and the array with respect to the north.

$$v_l = \begin{bmatrix} sin(\theta_l) \\ cos(\theta_l) \end{bmatrix}$$

(3.34)

Then equation (3.33) can be rewritten in vector equations as

$$P = \begin{bmatrix} P_x \\ P_y \end{bmatrix} = \begin{bmatrix} P_{lx} \\ P_{ly} \end{bmatrix} + d_l \begin{bmatrix} sin(\theta_l) \\ cos(\theta_l) \end{bmatrix} \tag{3.35}$$

When the first and second rows of the equation set are multiplied by $Cos(\theta_l)$ and $Sin(\theta_l)$, respectively, the equations can be rewritten as

$$P_x \, cos(\theta_l) = P_{lx} \, cos(\theta_l) + d_l \, sin(\theta_l) \, cos(\theta_l) \tag{3.36}$$

$$P_y \, sin(\theta_l) = P_{ly} \, sin(\theta_l) + d_l \, sin(\theta_l) \, cos(\theta_l) \tag{3.37}$$

When the first equation is subtracted from the second equation, the below equation can be written for each sensor array as

$$-P_x \, cos(\theta_l) + P_y \, sin(\theta_l) = -P_{lx} \, cos(\theta_l) + P_{ly} \, sin(\theta_l)$$

$$l = 1,2, \dots, L \tag{3.38}$$

The equations can be merged into a matrix equation representation as

$$\boldsymbol{b(\theta)} = \boldsymbol{H(\theta)} \, \boldsymbol{P} \tag{3.39}$$

where the $Lx1$ vector $\boldsymbol{b(\theta)}$ and the $Lx2$ matrix $\boldsymbol{H(\theta)}$ are defined as

$$\boldsymbol{b(\theta)} = \begin{bmatrix} -P_{1x} \, cos(\theta_1) + P_{1y} \, sin(\theta_1) \\ -P_{2x} \, cos(\theta_2) + P_{2y} \, sin(\theta_2) \\ \vdots \\ -P_{Lx} \, cos(\theta_L) + P_{Ly} \, sin(\theta_L) \end{bmatrix} \tag{3.40}$$

$$\boldsymbol{H(\theta)} = \begin{bmatrix} -cos(\theta_1) & sin(\theta_1) \\ -cos(\theta_2) & sin(\theta_2) \\ \vdots & \vdots \\ -cos(\theta_L) & sin(\theta_L) \end{bmatrix} \tag{3.41}$$

At least two sensor arrays are required to obtain an over-determined set of equations for 2-D localization. Then the least squares solution for the set of over-determined equations can be written as

$$\widehat{P} = H^{\#}(\theta)b(\theta) = \left(H^{H}(\theta)\,H(\theta)\right)^{-1}H^{H}(\theta)\,b(\theta) \qquad (3.42)$$

where the operator $(.)^{\#}$ represents the Moore-Penrose pseudo inverse and the resulting expression is shown above.

LS Pages-Zamora Algorithm:

1. Estimate the Angle-of Arrival (AOA) of the received signal in each sensor array by using any DOA estimation algorithm.
2. As mentioned in equations (3.40) and (3.41), obtain the $b(\theta)$ and $H(\theta)$ expressions by using the AOA estimates and the array positions.
3. Estimate the source position by using LS solution given in equation (3.42).

Extension to 3D Geometry:

Similarly, d_l is the distance between the lth sensor array and the source. In 3D unitary vector v_l is defined in terms of the azimuth and elevation angles between the source and the array with respect to the north (y-axis) and the ground (x-y plane), respectively.

$$v_l = \begin{bmatrix} sin(\theta_l)cos(\phi_l) \\ cos(\theta_l)cos(\phi_l) \\ sin(\phi_l) \end{bmatrix} \qquad (3.43)$$

These mentioned parameters are seen in Figure 3.6 for 3D noiseless scenario.
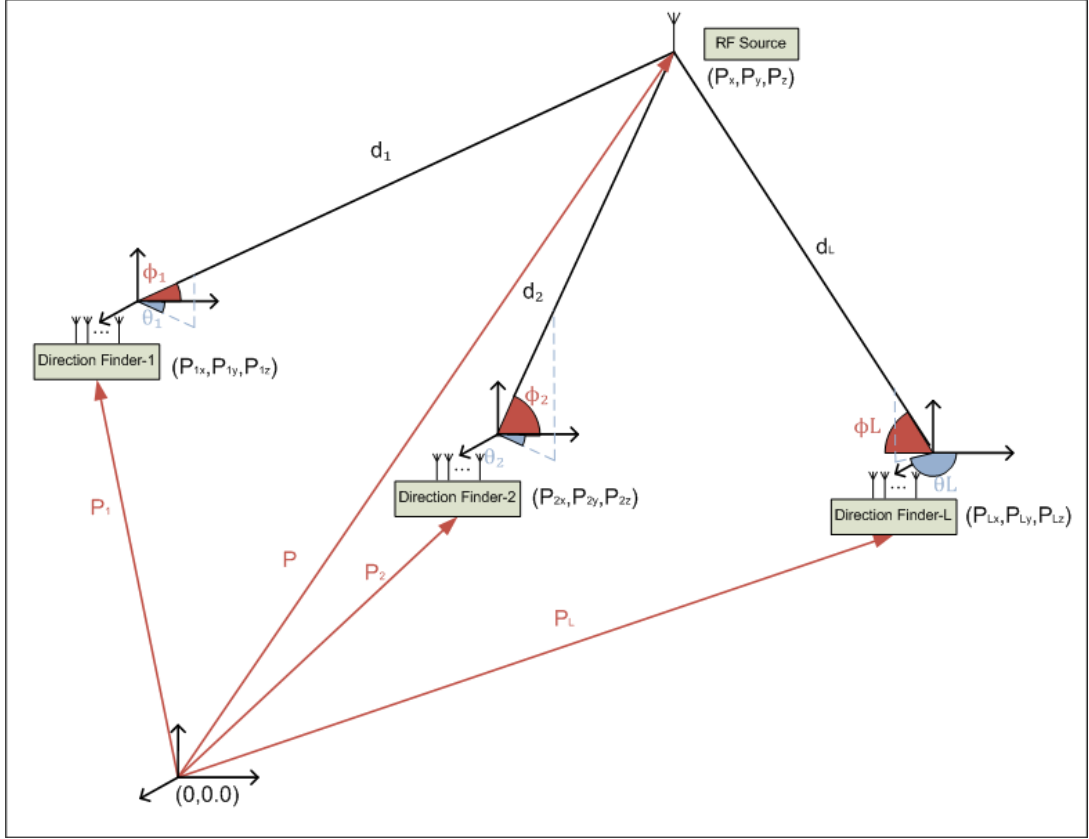
Figure 3.6: Pages-Zamora's Geometry for 3D AOA Based Source Localization

Then the source position can be rewritten in vector equations as

$$\boldsymbol{P} = \begin{bmatrix} P_x \\ P_y \\ P_z \end{bmatrix} = \begin{bmatrix} P_{lx} \\ P_{ly} \\ P_{lz} \end{bmatrix} + d_l \begin{bmatrix} sin(\theta_l)cos(\phi_l) \\ cos(\theta_l)cos(\phi_l) \\ sin(\phi_l) \end{bmatrix} \qquad (3.44)$$

When the rows of the equation set are multiplied by $Cos(\theta_l)\,Sin(\phi_l)$, $Sin(\theta_l)\,Sin(\phi_l)$ and $Sin(\theta_l)\,Cos(\theta_l)\,Cos(\phi_l)$ respectively, the equations can be rewritten as

$$\begin{aligned} P_x\,cos(\theta_l)sin(\phi_l) \\ = P_{lx}\,cos(\theta_l)sin(\phi_l) \\ + d_l\,sin(\theta_l)\,cos(\phi_l)cos(\theta_l)sin(\phi_l) \end{aligned} \qquad (3.45)$$

$$P_y \, sin(\theta_l) Sin(\phi_l)$$
$$= P_{ly} \, sin(\theta_l) sin(\phi_l)$$
$$+ d_l \, cos(\theta_l) cos(\phi_l) sin(\theta_l) sin(\phi_l)$$

$$P_z \, sin(\theta_l) \, cos(\theta_l) \, cos(\phi_l)$$
$$= P_{lz} \, sin(\theta_l) \, cos(\theta_l) \, cos(\phi_l)$$
$$+ d_l \, sin(\theta_l) \, sin(\theta_l) \, cos(\theta_l) \, cos(\phi_l)$$

When twice of the third equation is subtracted from the sum of first two equations, the below equation can be written for each sensor array as

$$P_x \, cos(\theta_l) sin(\phi_l) + P_y \, sin(\theta_l) sin(\phi_l) - 2 \, P_z \, sin(\theta_l) \, cos(\theta_l) \, cos(\phi_l)$$
$$= P_{lx} \, cos(\theta_l) sin(\phi_l) + P_{ly} \, sin(\theta_l) sin(\phi_l)$$
$$- 2 P_{lz} \, sin(\theta_l) \, cos(\theta_l) \, cos(\phi_l) \tag{3.46}$$

$$l = 1,2, \ldots, L$$

The equations can be merged into a matrix equation representation as

$$\boldsymbol{b}(\boldsymbol{\theta}, \boldsymbol{\phi}) = \boldsymbol{H}(\boldsymbol{\theta}, \boldsymbol{\phi}) \, \boldsymbol{P} \tag{3.47}$$

where the $Lx1$ vector $\boldsymbol{b}(\boldsymbol{\theta}, \boldsymbol{\phi})$ and the $Lx3$ matrix $\boldsymbol{H}(\boldsymbol{\theta}, \boldsymbol{\phi})$ are defined as

$$\boldsymbol{b}(\boldsymbol{\theta}, \boldsymbol{\phi})$$
$$= \begin{bmatrix} P_{1x} \, cos(\theta_1) sin(\phi_1) + P_{1y} \, sin(\theta_1) sin(\phi_1) - 2P_{1z} \, sin(\theta_1) \, cos(\theta_1) \, cos(\phi_1) \\ P_{2x} \, cos(\theta_2) sin(\phi_2) + P_{2y} \, sin(\theta_2) sin(\phi_2) - 2P_{2z} \, sin(\theta_2) \, cos(\theta_2) \, cos(\phi_2) \\ \vdots \\ P_{Lx} \, cos(\theta_L) sin(\phi_L) + P_{Ly} \, sin(\theta_L) sin(\phi_L) - 2P_{Lz} \, sin(\theta_L) \, cos(\theta_L) \, cos(\phi_L) \end{bmatrix} \tag{3.48}$$

$H(\theta, \phi)$

$$= \begin{bmatrix} \cos(\theta_1)\sin(\phi_1) & \sin(\theta_1)\sin(\phi_1) & -2\sin(\theta_1)\cos(\theta_1)\cos(\phi_1) \\ \cos(\theta_2)\sin(\phi_2) & \sin(\theta_2)\sin(\phi_2) & -2\sin(\theta_2)\cos(\theta_2)\cos(\phi_2) \\ \vdots & \vdots & \vdots \\ \cos(\theta_L)\sin(\phi_L) & \sin(\theta_L)\sin(\phi_L) & -2\sin(\theta_L)\cos(\theta_L)\cos(\phi_L) \end{bmatrix} \quad (3.49)$$

At least three sensor arrays are required to obtain an over-determined set of equations for 3D localization. Then the least squares solution for the set of over-determined equations can be written as

$$\widehat{P} = H^{\#}(\theta, \phi)b(\theta, \phi) = \left(H^H(\theta, \phi)\, H(\theta, \phi)\right)^{-1} H^H(\theta, \phi)\, b(\theta, \phi) \quad (3.50)$$

where the operator $(.)^{\#}$ represents the Moore-Penrose pseudo inverse and the resulting expression is shown above.

3D LS Pages-Zamora Algorithm:

1. Estimate the azimuth and elevation angles of the received signal in each sensor array by using any DOA estimation algorithm.
2. As mentioned in equations (3.48) and (3.49), obtain the $b(\theta, \phi)$ and $H(\theta, \phi)$ expressions by using the AOA estimates and the array positions.
3. Estimate the source position by using LS solution given in equation (3.50).

However this algorithm gives solution when the number of sensor arrays is larger than 2. Moreover, the trigonometric functions of the noisy angles are multiplied in the expressions $b(\theta, \phi)$ and $H(\theta, \phi)$, which degrades the performance of the algorithm. The reason of this situation can be explained with simple statistics. The multiplication of random variables with any variances gives larger variance. Consequently the performance of the algorithm degrades with increasing residuals of the least squares equation system.

To avoid this performance reduction and to find a solution with 2 Line-of-Bearings (LOBs), a straightforward 2 step LS approach can be written. The equation in (3.39) can be written as

$$b(\theta) = H(\theta)\,\xi \tag{3.51}$$

where

$$\hat{\xi} = \begin{bmatrix} \hat{P}_x \\ \hat{P}_y \end{bmatrix} = H^{\#}(\theta)b(\theta) = \left(H^H(\theta)\,H(\theta)\right)^{-1} H^H(\theta)\,b(\theta) \tag{3.52}$$

where the $Lx1$ vector $b(\theta)$ and the $Lx2$ matrix $H(\theta)$ are defined as

$$b(\theta) = \begin{bmatrix} -P_{1x}\cos(\theta_1) + P_{1y}\sin(\theta_1) \\ -P_{2x}\cos(\theta_2) + P_{2y}\sin(\theta_2) \\ \vdots \\ -P_{Lx}\cos(\theta_L) + P_{Ly}\sin(\theta_L) \end{bmatrix} \tag{3.53}$$

$$H(\theta) = \begin{bmatrix} -\cos(\theta_1) & \sin(\theta_1) \\ -\cos(\theta_2) & \sin(\theta_2) \\ \vdots & \vdots \\ -\cos(\theta_L) & \sin(\theta_L) \end{bmatrix} \tag{3.54}$$

Then the projection of the distances onto the x-y plane can be written as

$$d_l^{x\&y} = \left\| \begin{bmatrix} \hat{P}_x - P_{lx} \\ \hat{P}_y - P_{ly} \end{bmatrix} \right\| \tag{3.55}$$

where the operator $\|.\|$ represents the Euclidean norm of the inside vector. $d_l^{x\&y}$ becomes the distance between the lth sensor array and the estimated position in x-y plane. By using exactly the same geometrical relationship between the source and the sensor array positions, the expressions $b(\phi)$ and $H(\phi)$ can be written as

$$b(\boldsymbol{\phi}) = \begin{bmatrix} d_1^{x\&y} \sin(\phi_1) + P_{1z} \sin(\phi_1) \\ d_2^{x\&y} \sin(\phi_2) + P_{2z} \sin(\phi_2) \\ \vdots \\ d_L^{x\&y} \sin(\phi_L) + P_{Lz} \sin(\phi_L) \end{bmatrix} \tag{3.56}$$

$$H(\boldsymbol{\phi}) = \begin{bmatrix} \cos(\phi_1) \\ \cos(\phi_2) \\ \vdots \\ \cos(\phi_L) \end{bmatrix} \tag{3.57}$$

The z-coordinate of the source position can be estimated as

$$\widehat{P}_z = H^{\#}(\boldsymbol{\phi})b(\boldsymbol{\phi}) = \left(H^H(\boldsymbol{\phi}) \, H(\boldsymbol{\phi})\right)^{-1} H^H(\boldsymbol{\phi}) \, b(\boldsymbol{\phi}) \tag{3.58}$$

By combining the separate coordinate estimates, the source position estimate can be written as

$$\widehat{P} = \begin{bmatrix} \widehat{P}_x \\ \widehat{P}_y \\ \widehat{P}_z \end{bmatrix} \tag{3.59}$$

3D Two Step LS Algorithm:

1. Estimate the azimuth and elevation angles of the received signal in each sensor array by using any DOA estimation algorithm.
2. As mentioned in equations (3.53) and (3.54), obtain the $b(\boldsymbol{\theta})$ and $H(\boldsymbol{\theta})$ expressions by using the azimuth measurements and the array positions.
3. Estimate the x and y coordinates of the source position by using LS solution given in equation (3.52).

4. By using estimates found in Step (3), calculate the projection of the distances between the sensor arrays and source onto the x-y plane; obtain the expression $d_l^{x\&y}$ for each array.

5. As mentioned in equations (3.56) and (3.57), obtain the $\boldsymbol{b}(\boldsymbol{\phi})$ and $\boldsymbol{H}(\boldsymbol{\phi})$ expressions by using the elevation measurements and the array positions.

6. Estimate the z coordinate of the source position by using LS solution given in equation (3.58).

The performances of the *3D LS Pages-Zamora* and the *3D Two Step LS Algorithms* are compared. First, the sensor arrays are assumed to be located at the corners of $10x10\ km^2$ square region, whereas the target is located at the Cartesian coordinates (15, 15, 5) km. Both azimuth and elevation deviations are assumed to be 1° and 100 experiments are performed with each method.

i.   *3D LS Pages-Zamora*   ii.   *3D Two Step LS*
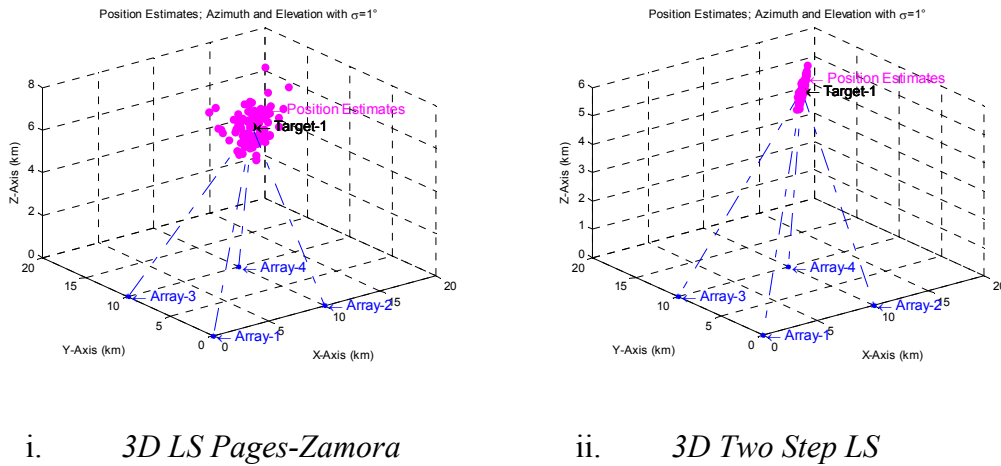
Figure 3.7: 3D Position Estimates Found with LS Pages-Zamora and 3D Two Step LS Methods

It is obviously seen from Figure 3.7 that *3D Two Step LS Algorithm* is better than *3D LS Pages-Zamora Method.* Moreover, the performances of these methods are compared with varying angle deviations. Also, the 3D MLE method and the 3D CRLB for AOA based source localization are evaluated and compared with the LS methods. The performance comparison and the lower bound are shown in Figure 3.8.
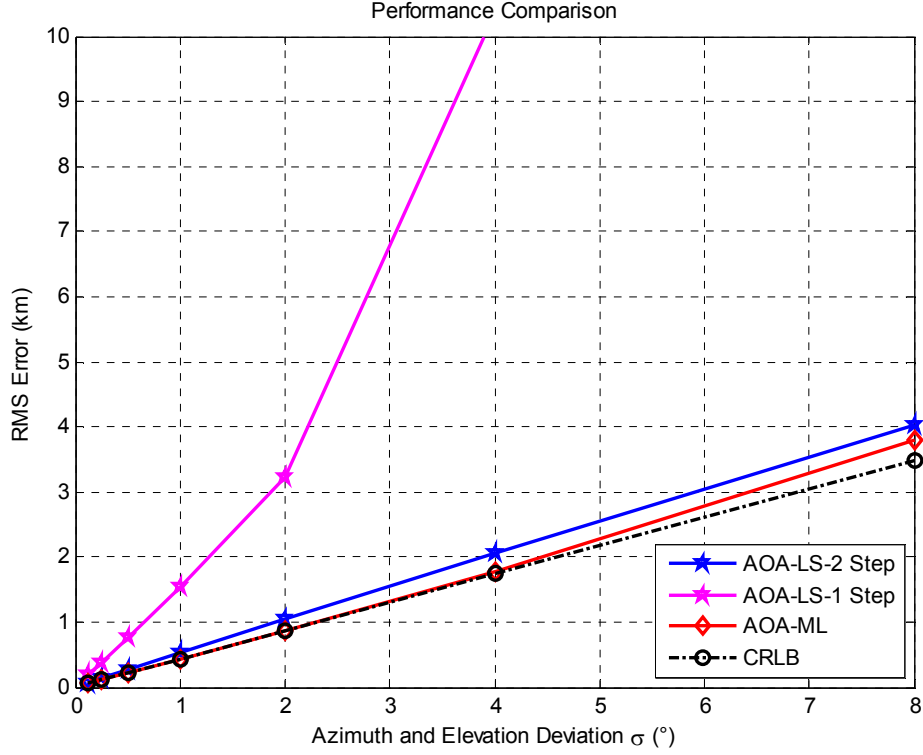
Figure 3.8: 3D Performance Comparison for AOA Based Methods and CRLB

It is shown in Figure 3.8 that, ML and Two Step LS methods give better results, than Pages-Zamora method. The reason of this situation is mentioned at the end of the algorithmic steps for 3D LS Pages-Zamora method.

3.1.3 Cramer Rao Lower Bound for AOA Based Source Localization

In this part the Cramer Rao Lower Bound (CRLB) is presented for 3D AOA based source localization problem. The CRLB is the minimum achievable error covariance matrix by an unbiased estimator [82]. The CRLB is found by inverting the Fisher Information Matrix (FIM). The lq^{th} block of the **FIM** is given by [49]

$$[\boldsymbol{FIM}(\boldsymbol{p})]_{lq} = E\left\{\frac{\partial}{\partial p_l}ln\big(f_{\hat{g}}(\hat{g}:p)\big)\frac{\partial}{\partial p_q}ln\big(f_{\hat{g}}(\hat{g}:p)\big)\right\} \qquad (3.60)$$

where p_l is the lth element of the true target location vector P; $f_{\hat{g}}(\hat{g}:p)$ is the likelihood function with respect to the true target position and R^{-1} is the inverse of the covariance of the angle measurements. The natural log-likelihood function can be written as

$$ln\big(f_{\hat{g}}(\hat{g}:p)\big) = \frac{1}{2}(\hat{g} - g(p))^T R^{-1}(\hat{g} - g(p)) + \gamma \tag{3.61}$$

where γ is constant term independent from the target position. The complete FIM can be written as

$$FIM(p) = \big(\nabla_p g(p)\big)^T R^{-1}\big(\nabla_p g(p)\big) \tag{3.62}$$

The 3D derivation of the CRLB expression goes on with defining the operator ∇_p which represents the gradient vector.

$$\nabla_p g(p) = \left[\frac{\partial g(p)}{\partial p_x} \quad \frac{\partial g(p)}{\partial p_y} \quad \frac{\partial g(p)}{\partial p_z}\right] \tag{3.63}$$

Under the assumption that azimuth and elevation measurements are independent from each other, the covariance of the angle measurements can be written as

$$R = \begin{bmatrix} R_\theta & 0 \\ 0 & R_\phi \end{bmatrix} \tag{3.64}$$

where the LxL matrices R_θ and R_ϕ are the covariances of the azimuth and elevation measurements respectively. The covariance matrices of the azimuth and elevation measurements can be written as

$$R_\theta = diag\{\sigma_{\theta_1}^2, \sigma_{\theta_2}^2, ..., \sigma_{\theta_L}^2\} \tag{3.65}$$

$$R_\phi = diag\{\sigma_{\phi_1}^2, \sigma_{\phi_2}^2, ..., \sigma_{\phi_L}^2\} \tag{3.66}$$

by assuming the angle measurements are independent between the sensor arrays. The $2Lx1$ vector $g(p)$ represents the true angles with respect to the true target

position. This vector consists of two $Lx1$ vectors; $\boldsymbol{g_1(p)}$ and $\boldsymbol{g_2(p)}$, which represent the true azimuth and elevation angles.

$$g(p) = \left[g_1^T(p) \ g_2^T(p)\right]^T \tag{3.67}$$

$$g_1(p) = [\theta_1, \ \theta_2, \dots, \theta_L]^T \tag{3.68}$$

$$g_2(p) = [\phi_1, \ \phi_2, \dots, \phi_L]^T \tag{3.69}$$

The lth element of the true azimuth vector $\boldsymbol{g_1(p)}$ can be calculated with respect to the true target position and the position of the lth sensor array as

$$\theta_l(p) = tan^{-1}\left(\frac{P_x - P_{l,x}}{P_y - P_{l,y}}\right) \tag{3.70}$$

Similarly, the lth element of the true elevation vector $\boldsymbol{g_2(p)}$ can be calculated as

$$\phi_l(p) = tan^{-1}\left(\frac{P_z - P_{l,z}}{\sqrt{\left((P_x - P_{l,x})^2 + (P_y - P_{l,y})^2\right)}}\right) \tag{3.71}$$

The expression $\boldsymbol{\nabla_p g(p)}$, can be separated as

$$\nabla_p g(p) = \begin{bmatrix} \nabla_p g_1(p) \\ \nabla_p g_2(p) \end{bmatrix} \tag{3.72}$$

The separated $Lx3$ matrix $\boldsymbol{\nabla_p g_1(p)}$ can be represented as

$$\nabla_p g_1(p) = \begin{bmatrix} \dfrac{\partial g_1(p)}{\partial p_x} & \dfrac{\partial g_1(p)}{\partial p_y} & \dfrac{\partial g_1(p)}{\partial p_z} \end{bmatrix} \tag{3.73}$$

where $\frac{\partial g_1(p)}{\partial p_x}$ is the partial derivate of the azimuth angles with respect to the x-coordinate of the true target position,

38

$$\frac{\partial \boldsymbol{g_1}(\boldsymbol{p})}{\partial p_x} = \begin{bmatrix} \left(\dfrac{-(P_y - P_{1,y})}{(P_x - P_{1,x})^2 + (P_y - P_{1,y})^2} \right) \\[3ex] \left(\dfrac{-(P_y - P_{2,y})}{(P_x - P_{2,x})^2 + (P_y - P_{2,y})^2} \right) \\[3ex] \vdots \\[3ex] \left(\dfrac{-(P_y - P_{L,y})}{(P_x - P_{L,x})^2 + (P_y - P_{L,y})^2} \right) \end{bmatrix} \tag{3.74}$$

Similarly expressions $\dfrac{\partial \boldsymbol{g_1}(\boldsymbol{p})}{\partial p_y}$ and $\dfrac{\partial \boldsymbol{g_1}(\boldsymbol{p})}{\partial p_z}$ are the partial derivates of the azimuth angles with respect to the y and z coordinates of the true target position respectively. These expressions can be written as

$$\frac{\partial \boldsymbol{g_1}(\boldsymbol{p})}{\partial p_y} = \begin{bmatrix} \left(\dfrac{(P_x - P_{1,x})}{(P_x - P_{1,x})^2 + (P_y - P_{1,y})^2} \right) \\[3ex] \left(\dfrac{(P_x - P_{2,x})}{(P_x - P_{2,x})^2 + (P_y - P_{2,y})^2} \right) \\[3ex] \vdots \\[3ex] \left(\dfrac{(P_x - P_{L,x})}{(P_x - P_{L,x})^2 + (P_y - P_{L,y})^2} \right) \end{bmatrix} \tag{3.75}$$

$$\frac{\partial \boldsymbol{g_1}(\boldsymbol{p})}{\partial p_z} = \boldsymbol{0}_{Lx1} \tag{3.76}$$

Moreover, the separated $Lx3$ matrix $\boldsymbol{\nabla_p g_2}(\boldsymbol{p})$ can be represented as

$$\nabla_p g_2(p) = \left[\frac{\partial g_2(p)}{\partial p_x} \quad \frac{\partial g_2(p)}{\partial p_y} \quad \frac{\partial g_2(p)}{\partial p_z} \right] \tag{3.77}$$

where $\frac{\partial g_2(p)}{\partial p_x}$ is the partial derivate of the elevation angles with respect to the x-coordinate of the true target position,

$$\frac{\partial g_2(p)}{\partial p_x} = \begin{bmatrix} \left(\dfrac{-\left(P_x - P_{1,x}\right)\left(P_z - P_{1,z}\right)}{\|P - P_1\|^2 \sqrt{\left(P_x - P_{1,x}\right)^2 + \left(P_y - P_{1,y}\right)^2}} \right) \\ \left(\dfrac{-\left(P_x - P_{2,x}\right)\left(P_z - P_{2,z}\right)}{\|P - P_2\|^2 \sqrt{\left(P_x - P_{2,x}\right)^2 + \left(P_y - P_{2,y}\right)^2}} \right) \\ \vdots \\ \left(\dfrac{-\left(P_x - P_{L,x}\right)\left(P_z - P_{L,z}\right)}{\|P - P_L\|^2 \sqrt{\left(P_x - P_{L,x}\right)^2 + \left(P_y - P_{L,y}\right)^2}} \right) \end{bmatrix} \tag{3.78}$$

Similarly expressions $\frac{\partial g_2(p)}{\partial p_y}$ and $\frac{\partial g_2(p)}{\partial p_z}$ are the partial derivates of the elevation angles with respect to the y and z coordinates of the true target position respectively. These expressions can be written as

$$\frac{\partial \boldsymbol{g_2}(\boldsymbol{p})}{\partial p_y} = \begin{bmatrix} \left(\dfrac{-\left(P_y - P_{1,y}\right)\left(P_z - P_{1,z}\right)}{\|\boldsymbol{P} - \boldsymbol{P_1}\|^2 \sqrt{\left(P_x - P_{1,x}\right)^2 + \left(P_y - P_{1,y}\right)^2}} \right) \\[2em] \left(\dfrac{-\left(P_y - P_{2,y}\right)\left(P_z - P_{2,z}\right)}{\|\boldsymbol{P} - \boldsymbol{P_2}\|^2 \sqrt{\left(P_x - P_{2,x}\right)^2 + \left(P_y - P_{2,y}\right)^2}} \right) \\[2em] \vdots \\[2em] \left(\dfrac{-\left(P_y - P_{L,y}\right)\left(P_z - P_{L,z}\right)}{\|\boldsymbol{P} - \boldsymbol{P_L}\|^2 \sqrt{\left(P_x - P_{L,x}\right)^2 + \left(P_y - P_{L,y}\right)^2}} \right) \end{bmatrix} \tag{3.79}$$

$$\frac{\partial \boldsymbol{g_2}(\boldsymbol{p})}{\partial p_z} = \begin{bmatrix} \dfrac{\sqrt{\left(P_x - P_{1,x}\right)^2 + \left(P_y - P_{1,y}\right)^2}}{\|\boldsymbol{P} - \boldsymbol{P_1}\|^2} \\[2em] \dfrac{\sqrt{\left(P_x - P_{2,x}\right)^2 + \left(P_y - P_{2,y}\right)^2}}{\|\boldsymbol{P} - \boldsymbol{P_2}\|^2} \\[2em] \vdots \\[2em] \dfrac{\sqrt{\left(P_x - P_{L,x}\right)^2 + \left(P_y - P_{L,y}\right)^2}}{\|\boldsymbol{P} - \boldsymbol{P_L}\|^2} \end{bmatrix} \tag{3.80}$$

After calculating the complete FIM, CRLB matrix is written as

$$\boldsymbol{CRLB} = (\boldsymbol{FIM})^{-1} \tag{3.81}$$

The $3x3$ **CRLB** matrix contains the axial minimum achievable variances on its diagonals, i.e.

41

$$diag(\boldsymbol{CRLB}) = \left\{\sigma_{P_x}^2, \sigma_{P_y}^2, \sigma_{P_z}^2\right\} \tag{3.82}$$

The trace of the CRLB matrix gives the minimum achievable localization variance,

$$\sigma_P^2 = tr(\boldsymbol{CRLB}) \tag{3.83}$$

3.1.4 Error Ellipse

The error ellipse defined by the Stansfield represents the accuracy of the source localization [2]. Moreover, the error ellipse may be used for the selection of the locations of the sensor arrays. By exploring the ellipse parameters, the best locations can be chosen for the sensor arrays for the target source region.

The error ellipse covers the region, in which the true target position lies with a probability of ₱. The center of the error ellipse is the estimated position of the source. An illustration of the mentioned scenario is given in Figure 3.9. There is no significance of the estimator model on the ellipse parameters.
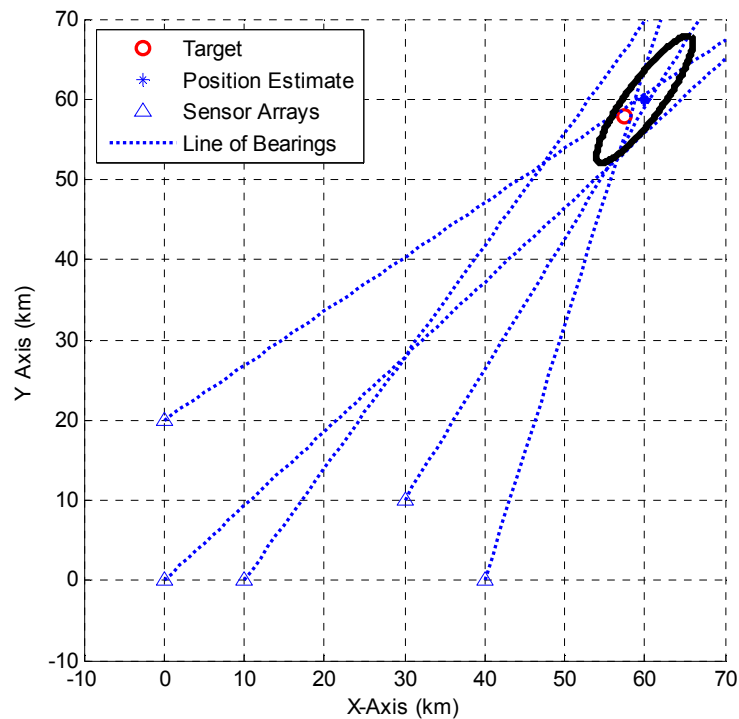
Figure 3.9: Error Ellipse with σ_θ=2° and ₱ =0.9

The ellipse parameters depend on the estimated source position, positions of the sensor arrays, AOAs and the standard deviation of the AOAs. The distance between the estimated source position and the lth sensor array can be written as

$$d_l = \|\boldsymbol{P}_{est} - \boldsymbol{P}_l\|$$ (3.84)

where the operator $\|.\|$ represents the Euclidean norm. The ellipse equation can be written as [2]

$$\frac{x^2}{b^2} + \frac{y^2}{a^2} = -2ln(1 - \mathbb{P})$$ (3.85)

The parameters b and a represent the major and minor radiuses of the ellipse. The radiuses are found in terms of the DOAs and the standard deviation of the AOAs as

$$\frac{2}{a^2} = \left[\lambda + \mu + \sqrt{((\lambda - \mu)^2 + 4v^2)}\right]$$ (3.86)

$$\frac{2}{b^2} = \left[\lambda + \mu - \sqrt{((\lambda - \mu)^2 + 4v^2)}\right]$$ (3.87)

The parameters λ, μ and v can be written as

$$\lambda = \sum_{l=1}^{L} \left(\frac{cos^2(\tilde{\theta}_l)}{\sigma_{\theta_l}^2 d_l^2}\right)$$ (3.88)

$$\mu = \sum_{l=1}^{L} \left(\frac{sin^2(\tilde{\theta}_l)}{\sigma_{\theta_l}^2 d_l^2}\right)$$ (3.89)

$$v = \sum_{l=1}^{L} \left(\frac{cos(\tilde{\theta}_l) sin(\tilde{\theta}_l)}{\sigma_{\theta_l}^2 d_l^2}\right)$$ (3.90)

where $\tilde{\theta}_l$ is the estimated azimuth angle of the lth sensor array and $\sigma_{\theta_l}^2$ represents the variance of this measurement.

The ellipse equation can be simplified as

$$\frac{x^2}{L_b^2} + \frac{y^2}{L_a^2} = 1 \tag{3.91}$$

where the radiuses can be presented as

$$L_a = \sqrt{\left(a^2\left(-2\ln(1-\mathbb{P})\right)\right)} \tag{3.92}$$

$$L_b = \sqrt{\left(b^2\left(-2\ln(1-\mathbb{P})\right)\right)} \tag{3.93}$$

Finally, the orientation of the ellipse with respect to the y-axis can be written as

$$\alpha = \tan^{-1}\left(\frac{\sum_{l=1}^{L}\left(\frac{P_x - P_{lx}}{\|\boldsymbol{P}_{est} - \boldsymbol{P}_l\|^2}\right)}{\sum_{l=1}^{L}\left(\frac{P_y - P_{ly}}{\|\boldsymbol{P}_{est} - \boldsymbol{P}_l\|^2}\right)}\right) \tag{3.94}$$

In practical EW systems, error ellipse is calculated with both fixed and varying angle variation $\sigma_{\theta_l}^2$. In earlier systems, this variation is fixed to the DF accuracy of the system (i.e. $\sigma_{\theta_l} = 2°\ RMS$). However, in some systems, the variation of the Direction Finding (DF) results for the same received signal is used to calculate $\sigma_{\theta_l}^2$. The error ellipse is drawn around the estimated source position, and it means that the true position of the emitter is inside this ellipse with a probability of $\mathbb{P}$.

An illustration is given in Figure 3.10 (The same scenario mentioned in Figure 3.9). The error ellipses are calculated for different probabilities. By using a little analogy, the center of the ellipse is chosen as the true source position. 20 experiments are performed to estimate the source location. Each source position estimate is plotted in the figure.
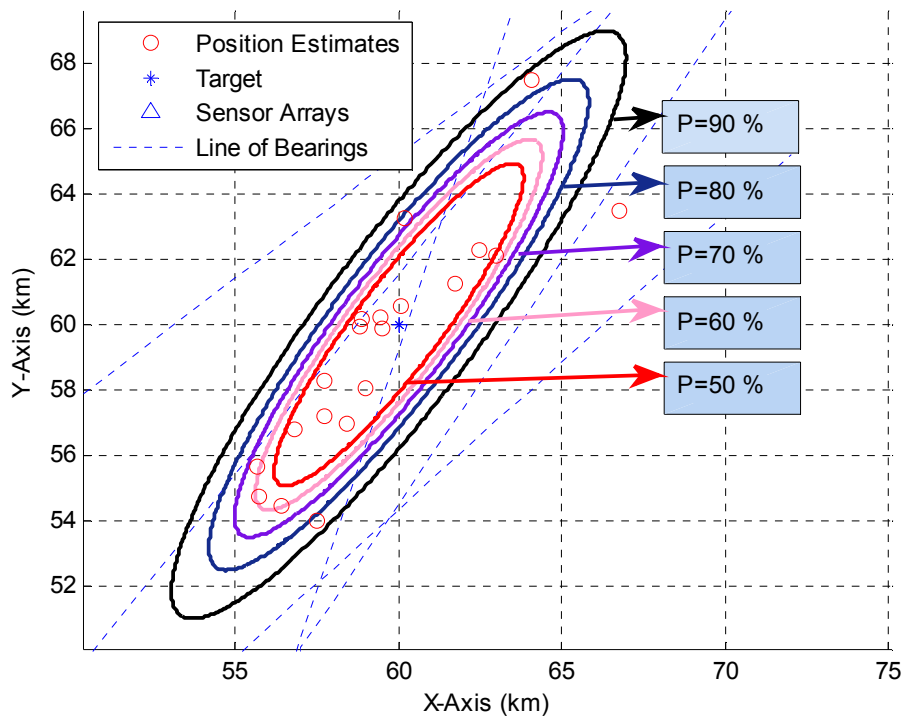
Figure 3.10: 20 Position Estimates and the Error Ellipse with $\sigma_\theta=2°$ and varying ℗

It is obviously seen from the illustration that the number of the position estimates covered by the error ellipses is consistent with the mentioned probabilities.

As mentioned in the first paragraph of this part, the positions of the sensor arrays and the source highly affect the minor and major radiuses of the ellipse. Consequently, the position of the sensor arrays and the source affect the localization accuracy. This fact is illustrated by two different scenarios seen in Figure 3.11 and Figure 3.12.
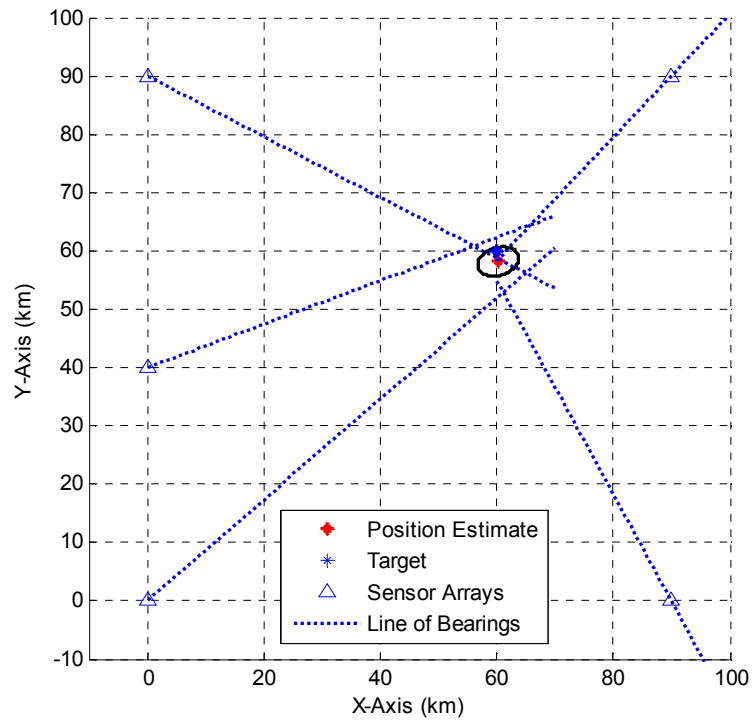
Figure 3.11: Error Ellipse with $\sigma_\theta=2°$ and $P=0.9$ for the "Array Deployment-1"

When the target is surrounded by the sensor arrays, the radiuses of the ellipse are small. However, when the target is separated from the arrays the radiuses become larger. This fact is directly in accordance with the localization accuracy. For accurate source localization, source should be surrounded by the sensor arrays.
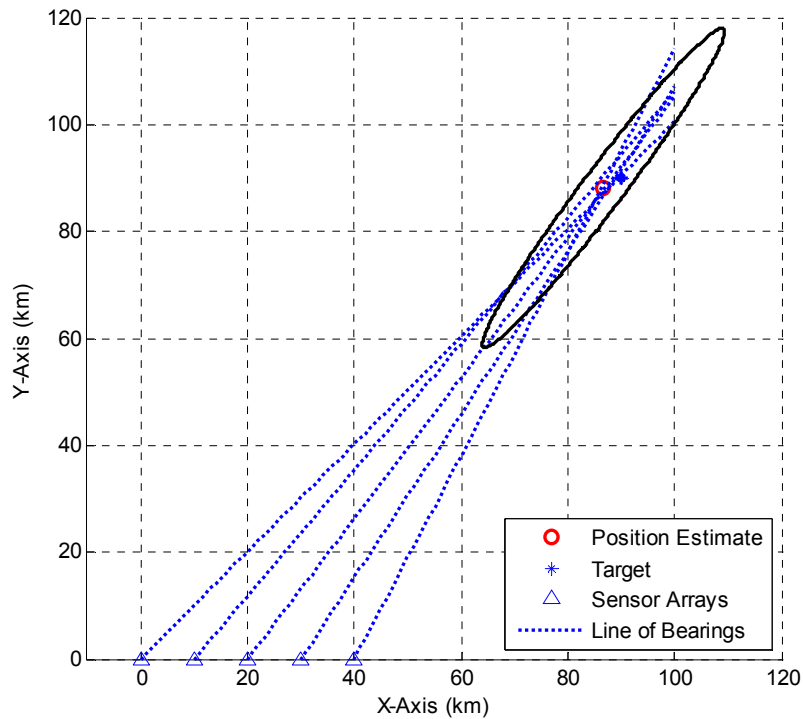
Figure 3.12: Error Ellipse with $\sigma_\theta = 2°$ and $P = 0.9$ for the "Array Deployment-2"

The same effect is tried to be simulated for 3D localization. 100 experiments are performed with two step Least Square Algorithm. Both azimuth and elevation angles have 1° standard deviation. Each position estimate, array and target coordinates are labeled in the figures. In Figure 3.13, the target is far away from the sensor arrays. When the position estimates are investigated, they compose a volume like rugby ball. This rugby ball figure may be called as error ellipsoid with probability of one.
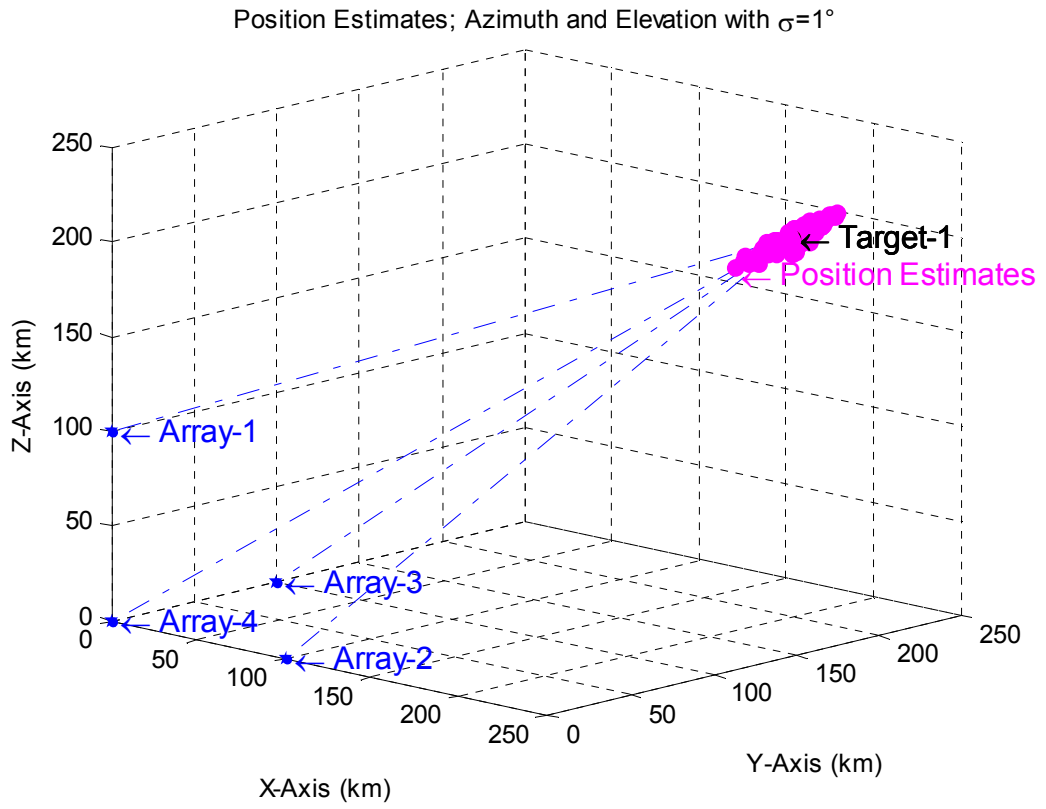
Figure 3.13: 100 Position Estimates with $\sigma_\theta = 1°$ and $\sigma_\phi = 1°$ for the "Target-1"
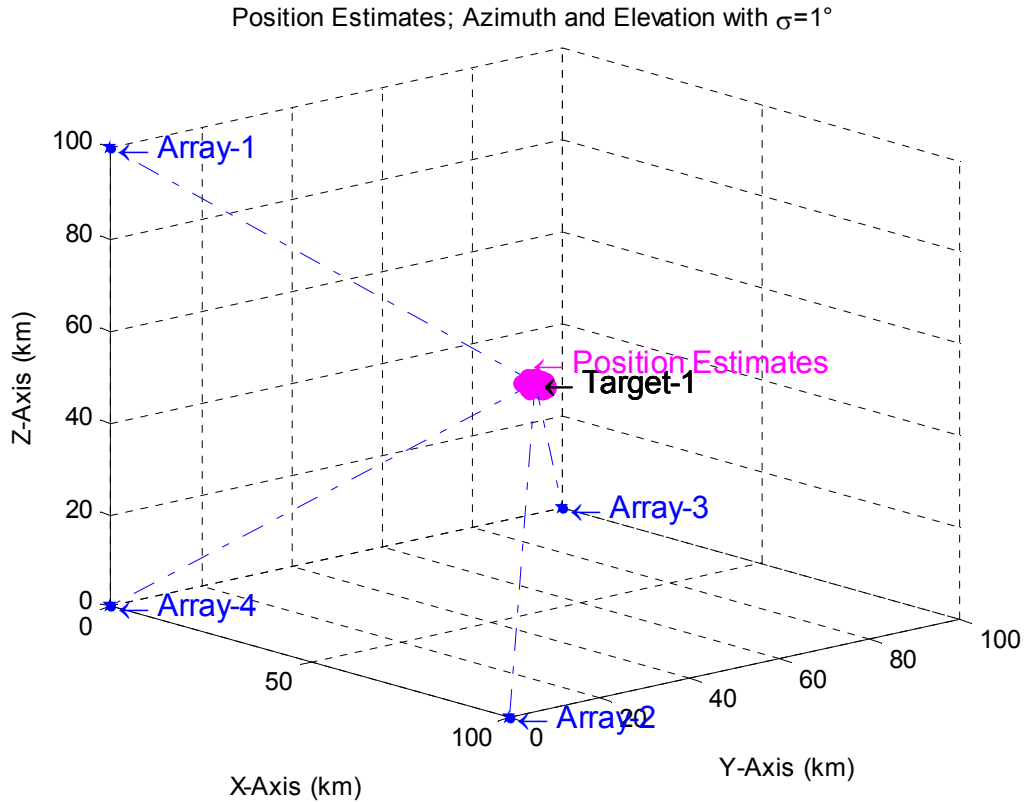
Figure 3.14: 100 Position Estimates with $\sigma_\theta=1°$ and $\sigma_\phi=1°$ for the "Target-2"

When the target is located closer to the sensor arrays, it is seen from Figure 3.14 that the deviation of position estimates becomes smaller. Consequently, it is seen that the localization accuracy is affected by the target and array locations.

3.1.5 Data Association Techniques for AOA Based Multiple Source Localization

When the number of RF sources is more than one, the DOAs of the sources can be found with High Resolution-Direction Finding (HR-DF) or Maximum Likelihood DF (ML-DF) algorithms. The AOA based localization algorithms work for single source. The AOA based source localization algorithms are insufficient for this problem. Individual AOA sets should be classified for each transmitter. The problem is illustrated in Figure 3.15. When three LOBs from each sensor array become closer, it seems like a position estimate. This situation is defined as *Ghost Node Concept* [52]. True source positions and the ghost nodes are seen in the figure.
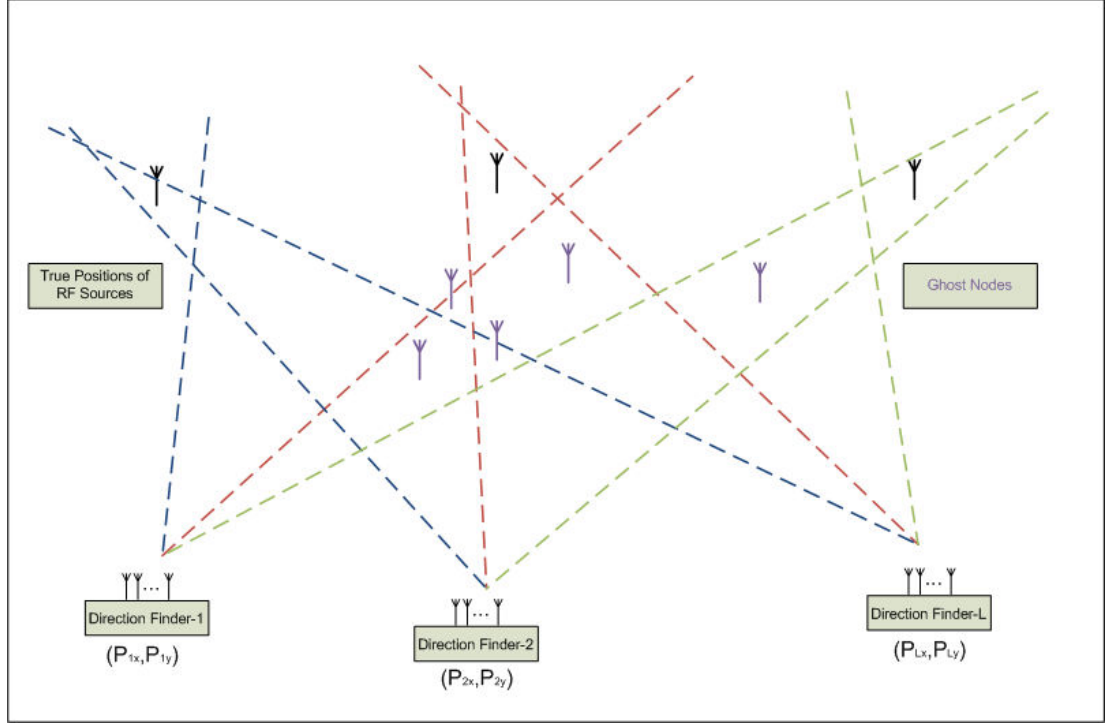
Figure 3.15: AOA Association Problem, Ghost Node Concept and Localization via Multiple LOBs

When the associated results are collected in the localization processor, the DOA estimates should be shown as,

$$
\boldsymbol{\Psi} = \begin{bmatrix} \Psi_{1,1} & \Psi_{1,2} & ... & \Psi_{1,Q} \\ \Psi_{2,1} & \Psi_{2,2} & ... & \Psi_{2,Q} \\ \vdots & \vdots & ... & \vdots \\ \Psi_{L,1} & \Psi_{L,2} & ... & \Psi_{L,Q} \end{bmatrix} \tag{3.95}
$$

where $\boldsymbol{\Psi_{l,q}}$ represents the DOA estimates (associated azimuth and elevation pairs) of the lth sensor array with respect to the qth source, i.e., $\boldsymbol{\Psi_{l,q}} = \{\theta_{l,q}, \phi_{l,q}\}$. Then the source localization is performed for each column of $\boldsymbol{\Psi}$.

However, the rows of the matrix $\boldsymbol{\Psi}$ are taken arbitrarily from the sensor arrays, since there is no priori information about the source locations.

Different techniques have been developed to solve AOA association problem [52]. Some of these techniques are based on clustering the AOA measurements. Moreover, Cyclic MUSIC spectrum can be used for an AOA association. However, the cycle rate (typically, twice the carrier rate and multiples of the baud rate) cannot be used for completely unknown signals [67]. In this section, the *Brute Force Method,* which gives more accurate association results, is presented. The AOA association algorithms (*Clustering Method, Signal Selectivity with Cyclic MUSIC*) are developed to reduce the algorithmic complexity of Brute Force Method which is given in the end of the next part.

Brute Force AOA Association Method:

In Brute Force Method (BFM), an exhaustive search is performed over the set of all possible sets of AOA combinations to find the most likely one.

For each set of the AOA combinations, each source position is estimated by using the relevant column of the AOA set.

Then the angles between the estimated target position and the sensor array is calculated for each source and each sensor array as

$$\hat{\theta}_{l,q} = tan^{-1}\left(\frac{\hat{p}_{q,x} - P_{l,x}}{\hat{p}_{q,y} - P_{l,y}}\right) \tag{3.96}$$

where $\hat{p}_{q,x}$, $\hat{p}_{q,y}$ and $\hat{p}_{q,z}$ represent the x, y and z Cartesian coordinates of the qth emitter respectively. Similarly $P_{l,x}$, $P_{l,y}$, and $P_{l,z}$ represent the Cartesian coordinates of the lth sensor array.

$$\hat{\phi}_{l,q} = tan^{-1}\left(\frac{\hat{p}_{q,z} - P_{l,z}}{\sqrt{\left((\hat{p}_{q,x} - P_{l,x})^2 + (\hat{p}_{q,y} - P_{l,y})^2\right)}}\right) \tag{3.97}$$

where $\hat{\theta}_{l,q}$ and $\hat{\phi}_{l,q}$ are the azimuth and elevation angles between the lth sensor array and the qth transmitter. The azimuth residual of the combination set is defined as

$$\Delta\theta = \sum_{l=1}^{L}\sum_{q=1}^{Q}\left|\theta_{l,q} - \hat{\theta}_{l,q}\right| \tag{3.98}$$

Similarly, the elevation residual of the combination set is defined as

$$\Delta\phi = \sum_{l=1}^{L}\sum_{q=1}^{Q}\left|\phi_{l,q} - \hat{\phi}_{l,q}\right| \tag{3.99}$$

Finally the total angle residual can be calculated as

$$\Delta\Psi = \Delta\theta + \Delta\phi \tag{3.100}$$

At the end of the residual calculation for all unique combination sets, the combination which gives the minimum residual is selected as the associated set of AOA measurements.

Brute Force AOA Association Algorithm:

1. Obtain a unique combination set of AOA measurements (combination in row-wise in measurement matrix $\boldsymbol{\Psi}$), and define this combination set as $\boldsymbol{\Psi}$.
2. By using any AOA based localization algorithm, compute the location of each source by using the relevant column of the combination set found in Step 1.
3. Calculate the angles between each sensor array and each source estimated in Step 2 by using the equations (3.96) and (3.97).
4. Calculate the residual of the combination set by using equation (3.100).
5. Repeat steps 1-4 until all the combinations are finished. Choose the combination set which gives the minimum residual as the *Associated AOA Set*.

As seen from the algorithmic steps, the complexity of the BFM is very high. Total number of computations used in BFM is calculated by Buehrer et al. as [52]

$$(41 \, L \, Q - 1) \, (Q!)^{L-1} \qquad\qquad (3.101)$$

For easier view of the concept, Data Association Technique for 2D localization problem is given in [52].

3.2 TDOA BASED SOURCE LOCALIZATION

Time Difference of Arrival (TDOA) based localization is usually used for Radar applications and GSM based localization services [19-23].

By using cross correlation processors and parabolic interpolators, TDOA values between the separated sensors are measured [68]. Moreover super resolution techniques have been developed for Code Division Multiple Access (CDMA) systems which use Pseudo Noise (PN) sequences. One of the best of these methods is called as Super Resolution PN Correlation Method (SPM Algorithm) which is presented in [69-70]. Moreover the performance of the SPM algorithm is given in [71]. The noise and the measurement errors are the main sources of TDOA estimation error. Measurement errors are systematic and unique to each implementation [13]. Stein derived Cramer Rao Lower Bound (CRLB) for TDOA estimation in his study [18]. TDOA estimation accuracy depends on various parameters such as noise bandwidth of the receiver, signal bandwidth, observation time and effective input SNR which is calculated by using the SNR values at the separated sensors used for TDOA estimation. CRLB expression for the TDOA estimation highly depends on the bandwidth of the signal. Good time synchronization (i.e. several nanoseconds) between the sensors is a must to estimate the accurate TDOA values between the sensors. Moreover, in digital TDOA estimation applications, oversampling factor affects the TDOA estimation accuracy [72]. TDOA based location estimation is directly proportional with the TDOA measurement accuracy. Finally the geometry formed by the sensors and the target location is one of the most important characteristic that determines the localization accuracy [13]. Optimum sensor geometries for 2D and 3D localization problems are presented by Yang and Scheuing [73]. Sensor array configurations with geometry of

a platonic solid are defined as optimum sensor geometry for 3D localization problem for single emitter case. Sample platonic solids are seen in Figure 3.16.
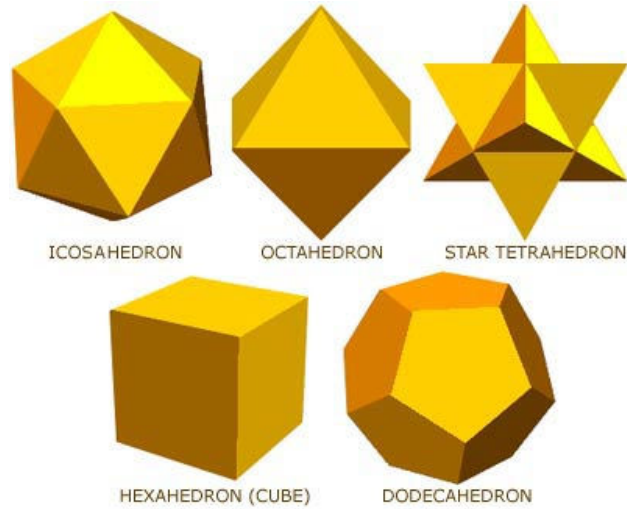
Figure 3.16: Sample Platonic Solid Geometries

The parameters that affect the TDOA based localization estimation accuracy and the mathematical relations between these parameters and localization accuracy can be summarized as,

- By increasing the integration time, location estimation accuracy increases
- By increasing the oversampling factor, location estimation accuracy increases
- By increasing the synchronization error, location estimation accuracy decreases
- By increasing the signal bandwidth, location estimation accuracy increases
- By increasing the noise bandwidth of the receiver, location estimation accuracy increases
- Platonic solid array configurations (or Uniform Angular Array (UAA) for 2D) should be used for accurate 3D positioning

3.2.1 Problem Formulation

Each TDOA value represents a unique hyperbola which lies on the target positions. However, in 3D geometry each TDOA value represents a branch of hyperboloid and the target position lies on the surface of it.

By using these unique hyperbolas (hyperboloids in 3D), the location of the emitter can be estimated. An illustrative noise free scenario is seen in Figure 3.17 which illustrates the 2D geometric interpretation.
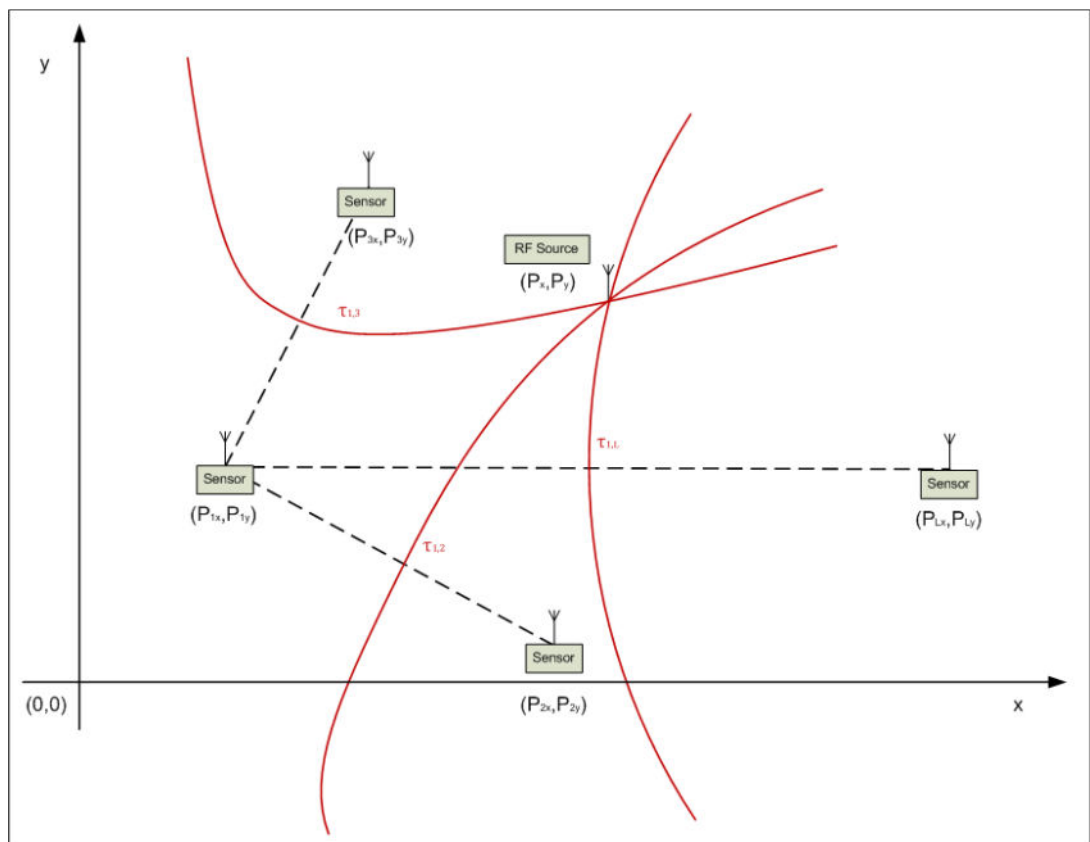
Figure 3.17: Noise Free Scenario for 2D TDOA Based Source Localization

For easier illustration, the 2D problem is considered in geometric sense in the previous figure. This part starts with defining the mathematical expressions of the problem.

In a constant velocity medium, let's define the distance between the target and the lth sensor as

$$r_l = c\, t_l$$
$$l = 1,2,\dots,L$$

(3.102)

where c is the propagation speed of the signal (for an electromagnetic wave, speed of light); L is the total number of sensors and t_l is the propagation time between the target and the relevant sensor. Then τ_{lk} is defined as the time difference of arrival between the lth and k^{th} sensors,

$$\tau_{lk} = t_l - t_k = \left(\frac{r_l - r_k}{c}\right)$$
$$l, k = 1,2,\dots,L$$

(3.103)

$$r_l = \sqrt{(P_x - P_{l,x})^2 + (P_y - P_{l,y})^2 + (P_z - P_{l,z})^2}$$

(3.104)

where (P_x, P_y, P_z) and $(P_{l,x}, P_{l,y}, P_{l,z})$ are the Cartesian coordinates of the target and l^{th} sensor, respectively.

A non-linear relationship between the "TDOA values between the sensor pairs" and the "target location" is obviously seen in the above equations. The problem is estimating the target location with using sensor position and noisy TDOA measurements.

3.2.2 TDOA Based Source Localization Algorithms

In this part, some TDOA based localization algorithms are given such as Maximum Likelihood (ML) and Least Squares (LS) localization algorithms. Moreover, iterative techniques are presented for ML solution.

3.2.2.1 TDOA Based Maximum Likelihood Source Localization Algorithms

By assuming the noise is zero mean Gaussian, the Maximum Likelihood Estimation (MLE) of the source position can be written as [49]

$$\hat{p} = argmin_P \{F_\tau(p)\} \tag{3.105}$$

where the cost function $F_\tau(p)$ is

$$F_\tau(p) = \frac{1}{2}(\hat{h} - h(p))^T R_\tau^{-1}(\hat{h} - h(p)) \tag{3.106}$$

The cost function depends on the range difference measurements, covariance of these range difference measurements and the range differences with respect to the search point $h(p)$.

The $(L - 1)x1$ vector $h(p)$ represents the range differences between the first sensor and the others with respect to the search point.

$$h(p) = [h_2(p) \, h_3(p) \, ... \, h_L(p) \,]^T \tag{3.107}$$

At each search point, the range difference between the lth sensor and the first one with respect to the search point is calculated as

$$h_l(p) = \|P_l - P\| - \|P_1 - P\| \tag{3.108}$$

The $(L - 1)x1$ vector $\hat{h}$ represents the range difference measurements between the first sensor and the others.

$$\hat{h} = c \left[\tau_{2,1}, \tau_{3,1}, ..., \tau_{L,1}\right]^T \tag{3.109}$$

Assuming that the range (Time of Arrival (TOA) values multiplied by propagation speed c) measurements are independent from each other, the covariance of the range difference measurements can be written as [27]

$$R_\tau = c^2\sigma_{TOA}^2 \begin{bmatrix} 1 & \frac{1}{2} & \cdots & \frac{1}{2} \\ \frac{1}{2} & 1 & \ddots & \vdots \\ \vdots & \ddots & \ddots & \frac{1}{2} \\ \frac{1}{2} & \cdots & \frac{1}{2} & 1 \end{bmatrix} \qquad (3.110)$$

MLE Algorithm:

1. Estimate the Time Difference of Arrival (TDOA) of the received signal between the sensor pairs by using any TDOA estimation algorithm.

2. As mentioned in equations (3.109) and (3.110), obtain the measurement vector $\hat{h}$ and the measurement covariance matrix R_τ.

3. Perform a grid search; in each search point
   i. Calculate the range difference between the first sensor and the others with respect to the search point; obtain vector $h(p)$
   ii. Calculate the cost function $F_\tau(p)$

4. After performing the grid search, find the position estimate $\hat{p}$, which gives the minimum cost.

Localization with Stochastic Gradient:

Gustafsson and Gunnarsson presented a Normalized Least Mean Squares (NLMS) type iterative algorithm to the TDOA Based ML localization problem [74].

Let P denote the target position and $\hat{p}_i$ be the estimate of the target location P in the ith iteration. In this algorithm, iterations are performed due to least mean squares as

$$\hat{p}_{i+1} = \hat{p}_i - \mu^i h_p'(\hat{p}_i)\left[\hat{h} - h(\hat{p}_i)\right] \qquad (3.111)$$

The definitions for h and $\hat{h}$ are given in equations (3.107-3.109). The step size is found by

$$\mu^i = \frac{\mu}{\left[h_p'(\hat{p}_i)\right]^T h_p'(\hat{p}_i)} \tag{3.112}$$

where μ is the LMS step size which is selected due to stability conditions for convergence. h_p' is the gradient of h_p with respect to the global coordinate axis.

$$h_p' = \nabla_p h(p) = \left[\frac{\partial h(p)}{\partial p_x} \quad \frac{\partial h(p)}{\partial p_y} \quad \frac{\partial h(p)}{\partial p_z}\right] \tag{3.113}$$

The partial derivatives are given in CRLB derivation for TDOA Based Localization (equations 3.131-3.133). The LMS step size should satisfy the below condition for convergence.

$$0 < \mu < \frac{1}{\lambda_{max}} \tag{3.114}$$

where λ_{max} is the maximum eigenvalue of matrix R_τ. Typically faster convergence is obtained with larger step sizes.

The weights $h_p'(\hat{p}_i)$ are adjusted adaptively in the algorithm. For an initial guess LS target location estimate may be used for this algorithm.

Adaptive MLE Algorithm:

1. Estimate the Time Difference of Arrival (TDOA) of the received signal between the sensor pairs by using any TDOA estimation algorithm.
2. As mentioned in equations (3.109) and (3.110), obtain the measurement vector $\hat{h}$ and the measurement covariance matrix R_τ.
3. Obtain an initial position estimate $\hat{p}_0$ by using any source localization algorithm.
4. By using a stopping criterion (i.e. $(\hat{p}_{i+1} - \hat{p}_i) < \varepsilon$), start the iterations with the initial position estimate until the stopping criterion is satisfied.
5. In each iteration step,
    i. Calculate the matrix $h_p'(\hat{p}_i)$ with the previously estimated position.
    ii. Calculate the step size μ^i with equation (3.112).

iii.　　By using equation (3.111), estimate the new position.

3.2.2.2 TDOA Based Least Squares Source Localization Algorithms

Similar derivations were performed by Bard and Mellen to obtain closed form LS solutions for target location [75-76]. The idea is linearizing the non-linear relationships by adding a new unknown into the equations. The distance between the target and the 1st sensor is introduced as a new unknown in this algorithm. Let's assume that this distance is r , then

$$r^2 = (P_x - P_{1,x})^2 \; + \; (P_y - P_{1,y})^2 + (P_z - P_{1,z})^2 \qquad (3.115)$$

Let τ_i be the TDOA between the lth and the 1st sensor,

$$\tau_l = t_l - t_1$$
$$l = 2, ..., L \qquad\qquad (3.116)$$
$$r = c\, t_1$$

Then, for each sensor, the non linear equations can be re-written as

$$(c\, t_l)^2 = (r + c\, \tau_l)^2 = (P_x - P_{l,x})^2 + (P_y - P_{l,y})^2 + (P_z - P_{1,z})^2 \qquad (3.117)$$

The equations are written for all sensors except the reference one,

$$(r + c\, \tau_2)^2 = (P_x - P_{2,x})^2 + (P_y - P_{2,y})^2 + (P_z - P_{2,z})^2$$
$$(r + c\, \tau_3)^2 = (P_x - P_{3,x})^2 + (P_y - P_{3,y})^2 + (P_z - P_{3,z})^2$$
$$\vdots \qquad\qquad (3.118)$$
$$(r + c\, \tau_L)^2 = (P_x - P_{L,x})^2 + (P_y - P_{L,y})^2 + (P_z - P_{L,z})^2$$

When the differences are taken between the above equations and the r^2 expression, the resulting equations are

$$-2\,r\,c\,\tau_2 + (c\,\tau_2)^2$$
$$= P_{1,x}^2 + P_{1,y}^2 + P_{1,z}^2 - P_{2,x}^2 - P_{2,y}^2 - P_{2,z}^2$$
$$+ 2(P_{2,x} - P_{1,x})P_x + 2(P_{2,y} - P_{1,y})P_y + 2(P_{2,z} - P_{1,z})P_z$$

$$-2\,r\,c\,\tau_3 + (c\,\tau_3)^2$$
$$= P_{1,x}^2 + P_{1,y}^2 + P_{1,z}^2 - P_{3,x}^2 - P_{3,y}^2 - P_{3,z}^2$$
$$+ 2(P_{3,x} - P_{1,x})P_x + 2(P_{3,y} - P_{1,y})P_y + 2(P_{3,z} - P_{1,z})P_z \qquad (3.119)$$

$$\vdots$$

$$-2\,r\,c\,\tau_L + (c\,\tau_L)^2$$
$$= P_{1,x}^2 + P_{1,y}^2 + P_{1,z}^2 - P_{L,x}^2 - P_{L,y}^2 - P_{L,z}^2$$
$$+ 2(P_{L,x} - P_{1,x})P_x + 2(P_{L,y} - P_{1,y})P_y + 2(P_{L,z} - P_{1,z})P_z$$

These equations can be written in the matrix form as

$$\mathbf{y} = 2\,\mathbf{A}\,\mathbf{x} \qquad (3.120)$$

where vectors $\mathbf{x}$, $\mathbf{y}$ and matrix $\mathbf{A}$ are defined as

$$\mathbf{x} = \begin{bmatrix} P_x \\ P_y \\ P_z \\ r \end{bmatrix} \qquad (3.121)$$

$$\mathbf{y} = \begin{bmatrix} P_{1,x}^2 + P_{1,y}^2 + P_{1,z}^2 - P_{2,x}^2 - P_{2,y}^2 - P_{2,z}^2 + (c\,\tau_2)^2 \\ P_{1,x}^2 + P_{1,y}^2 + P_{1,z}^2 - P_{3,x}^2 - P_{3,y}^2 - P_{3,z}^2 + (c\,\tau_3)^2 \\ \vdots \\ P_{1,x}^2 + P_{1,y}^2 + P_{1,z}^2 - P_{L,x}^2 - P_{L,y}^2 - P_{L,z}^2 + (c\,\tau_L)^2 \end{bmatrix} \qquad (3.122)$$

$$A = \begin{bmatrix} \left(P_{1,x} - P_{2,x}\right) & \left(P_{1,y} - P_{2,y}\right) & \left(P_{1,z} - P_{2,z}\right) & \left(-c\,\tau_2\right) \\ \left(P_{1,x} - P_{3,x}\right) & \left(P_{1,y} - P_{3,y}\right) & \left(P_{1,z} - P_{3,z}\right) & \left(-c\,\tau_3\right) \\ \vdots & \vdots & \vdots & \vdots \\ \left(P_{1,x} - P_{L,x}\right) & \left(P_{1,y} - P_{L,y}\right) & \left(P_{1,z} - P_{L,z}\right) & \left(-c\,\tau_L\right) \end{bmatrix} \qquad (3.123)$$

Then the LS solution can be written as;

$$\hat{x}_{LS} = \frac{1}{2} A^{\#} y = \frac{1}{2} (A^{H}A)^{-1} A^{H} y \qquad (3.124)$$

As seen from the matrix structures, for an over-determined equation system $(L - 1) \geq 4$. For 3D localization at least 5 sensors should be used in Least Squares Localization Algorithm.

Algorithm:

1. Estimate the Time-Difference-of Arrival (TDOA) between the 1st sensor and the rest of the sensors for the received signals by using any TDOA estimation algorithm.
2. As mentioned in equations (3.122) and (3.123), obtain the y and A expressions by using the TDOA estimates and the sensor positions.
3. Estimate the source position by using LS solution given in equation (3.124).

As obviously seen from the LS solution expression, this solution highly depends on the location of the sensors and the target. When TDOAs are close to each other or sensor positions badly chosen, the expression $(A^{H}A)$ becomes close to singular. To prevent ill-conditioned inverse situations the locations of the sensors should be chosen well. The pseudo inverse operations are performed via SVD in the simulations. The effect of this case is investigated in Chapter 5.

3.2.3 Cramer Rao Lower Bound for TDOA Based Source Localization

Many different Cramer-Rao Lower Bound expressions for TDOA based source localization have been derived in the literature [77]. However, some of these are the approximate solutions to the lower bound.

The lq^{th} block of the **FIM** is given by [49]

$$[\boldsymbol{FIM(p)}]_{lq} = E\left\{\frac{\partial}{\partial p_l}ln\big(f_{\hat{h}}(\hat{h}\!:\!p)\big)\frac{\partial}{\partial p_q}ln\big(f_{\hat{h}}(\hat{h}\!:\!p)\big)\right\} \qquad (3.125)$$

where $\boldsymbol{p_l}$ is the lth element of the true target location vector $\boldsymbol{P}$; $f_{\hat{g}}(\hat{h}\!:\!p)$ is the likelihood function with respect to the true target position and $\boldsymbol{R_\tau^{-1}}$ is the inverse of the covariance of the range difference measurements. The natural log-likelihood function can be written as

$$ln\big(f_{\hat{h}}(\hat{h}\!:\!p)\big) = \frac{1}{2}\big(\hat{\boldsymbol{h}}-\boldsymbol{h(p)}\big)^T\boldsymbol{R_\tau^{-1}}\big(\hat{\boldsymbol{h}}-\boldsymbol{h(p)}\big)+\gamma \qquad (3.126)$$

where γ is constant term independent from the target position. The complete FIM can be written as

$$\boldsymbol{FIM(p)} = \big(\boldsymbol{\nabla_p h(p)}\big)^T\boldsymbol{R_\tau^{-1}}\big(\boldsymbol{\nabla_p h(p)}\big) \qquad (3.127)$$

The derivation starts with defining the operator $\boldsymbol{\nabla_p}$ which represents the gradient vector,

$$\boldsymbol{\nabla_p h(p)} = \left[\frac{\partial \boldsymbol{h(p)}}{\partial p_x} \quad \frac{\partial \boldsymbol{h(p)}}{\partial p_y} \quad \frac{\partial \boldsymbol{h(p)}}{\partial p_z}\right] \qquad (3.128)$$

The $(L-1)x1$ vector $\boldsymbol{h(p)}$ represents the true range differences between the first sensor and the others with respect to the true target position.

$$\boldsymbol{h(p)} = c\left[\tau_{2,1},\tau_{3,1},\dots,\tau_{L,1}\right]^T \qquad (3.129)$$

Assuming that the range (Time of Arrival (TOA) values multiplied by propagation speed c) measurements are independent from each other, the covariance of the range difference measurements can be written as

$$R_\tau = c^2 \sigma_{TOA}^2 \begin{bmatrix} 1 & \frac{1}{2} & \cdots & \frac{1}{2} \\ \frac{1}{2} & 1 & \ddots & \vdots \\ \vdots & \ddots & \ddots & \frac{1}{2} \\ \frac{1}{2} & \cdots & \frac{1}{2} & 1 \end{bmatrix} \tag{3.130}$$

where the $(L-1)x(L-1)$ matrix R_τ is the covariance of the range difference measurements.

The expression $\frac{\partial h(p)}{\partial p_x}$ is the partial derivate of the range difference values with respect to the x-coordinate of the true target position,

$$\frac{\partial h(p)}{\partial p_x} = \begin{bmatrix} \dfrac{(P_x - P_{2,x})}{\|P - P_2\|} - \dfrac{(P_x - P_{1,x})}{\|P - P_1\|} \\ \dfrac{(P_x - P_{3,x})}{\|P - P_3\|} - \dfrac{(P_x - P_{1,x})}{\|P - P_1\|} \\ \vdots \\ \dfrac{(P_x - P_{L,x})}{\|P - P_L\|} - \dfrac{(P_x - P_{1,x})}{\|P - P_1\|} \end{bmatrix} \tag{3.131}$$

Similarly expressions $\frac{\partial h(p)}{\partial p_y}$ and $\frac{\partial h(p)}{\partial p_z}$ are the partial derivates of the range differences with respect to the y and z coordinates of the true target position respectively. These expressions can be written as

$$\frac{\partial \boldsymbol{h}(\boldsymbol{p})}{\partial p_y} = \begin{bmatrix} \dfrac{(P_y - P_{2,y})}{\|\boldsymbol{P} - \boldsymbol{P_2}\|} - \dfrac{(P_y - P_{1,y})}{\|\boldsymbol{P} - \boldsymbol{P_1}\|} \\[2ex] \dfrac{(P_y - P_{3,y})}{\|\boldsymbol{P} - \boldsymbol{P_3}\|} - \dfrac{(P_y - P_{1,y})}{\|\boldsymbol{P} - \boldsymbol{P_1}\|} \\[2ex] \vdots \\[2ex] \dfrac{(P_y - P_{L,y})}{\|\boldsymbol{P} - \boldsymbol{P_L}\|} - \dfrac{(P_y - P_{1,y})}{\|\boldsymbol{P} - \boldsymbol{P_1}\|} \end{bmatrix} \tag{3.132}$$

$$\frac{\partial \boldsymbol{h}(\boldsymbol{p})}{\partial p_z} = \begin{bmatrix} \dfrac{(P_z - P_{2,z})}{\|\boldsymbol{P} - \boldsymbol{P_2}\|} - \dfrac{(P_z - P_{1,z})}{\|\boldsymbol{P} - \boldsymbol{P_1}\|} \\[2ex] \dfrac{(P_z - P_{3,z})}{\|\boldsymbol{P} - \boldsymbol{P_3}\|} - \dfrac{(P_z - P_{1,z})}{\|\boldsymbol{P} - \boldsymbol{P_1}\|} \\[2ex] \vdots \\[2ex] \dfrac{(P_z - P_{L,z})}{\|\boldsymbol{P} - \boldsymbol{P_L}\|} - \dfrac{(P_z - P_{1,z})}{\|\boldsymbol{P} - \boldsymbol{P_1}\|} \end{bmatrix} \tag{3.133}$$

After calculating the complete FIM, CRLB matrix is written as

$$\boldsymbol{CRLB} = (\boldsymbol{FIM})^{-1} \tag{3.134}$$

The $3x3$ **CRLB** matrix contains the axial minimum achievable variances on its diagonals.

$$diag(\boldsymbol{CRLB}) = \left\{ \sigma_{P_x}^2, \sigma_{P_y}^2, \sigma_{P_z}^2 \right\} \tag{3.135}$$

The trace of the **CRLB** matrix gives the minimum achievable localization variance.

$$\sigma_P^2 = tr(\boldsymbol{CRLB}) \tag{3.136}$$

3.3 AOA-TDOA BASED HYBRID SOURCE LOCALIZATION

In this part, AOA-TDOA based hybrid source localization is investigated. After formulating the hybrid localization problem, Maximum Likelihood (ML) based hybrid localization algorithm is presented for 3D localization. Literature survey on Least Squares (LS) based hybrid localization algorithms is briefly presented. This part ends with derivation of the Cramer Rao Lower Bound (CRLB) expression for 3D AOA-TDOA based hybrid source localization problem.

3.3.1 Problem Formulation

To estimate the position of the target with AOA-TDOA based hybrid localization algorithms, the pre-measured AOA and TDOA values are needed. The TDOA values are measured between the different sensor arrays and AOA values are measured at each sensor array. As mentioned before, each TDOA value represents a branch of hyperboloid and the target position lies on the surface of it. Moreover the target lies on rays (azimuth and elevation), each starts from the sensor arrays. By using these unique hyperboloids and the rays the location of the emitter can be estimated. An illustrative noise free scenario is seen in Figure 3.18 which illustrates the 2D geometric interpretation.
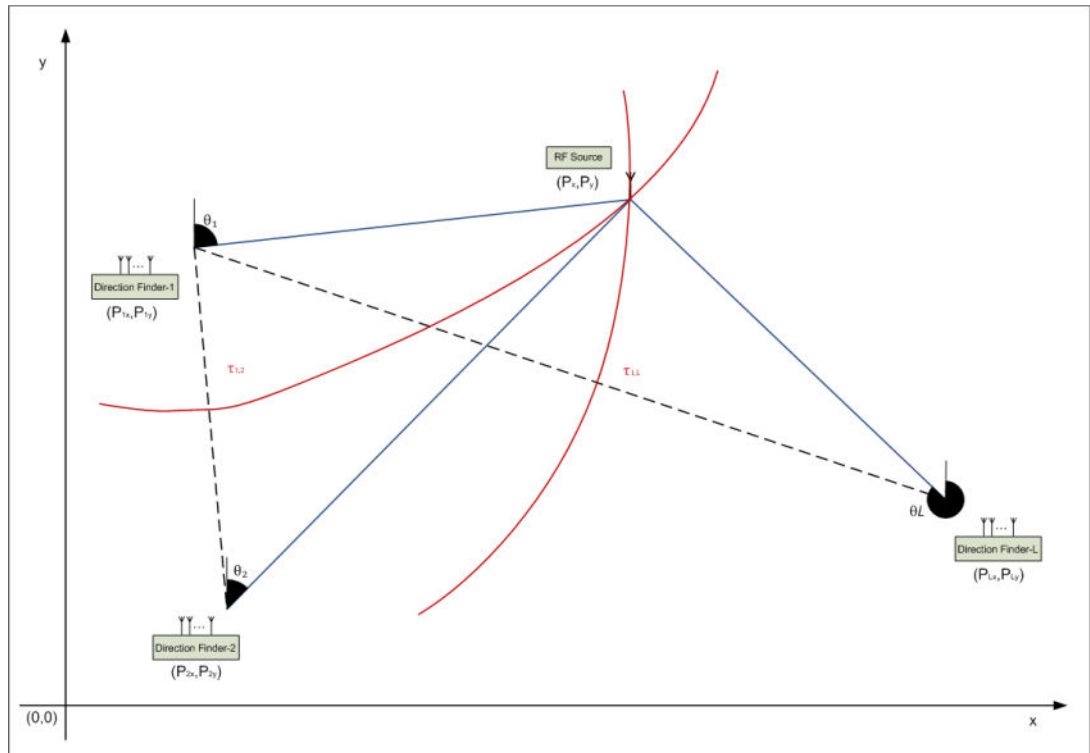
Figure 3.18: Noise Free Scenario for 2D Hybrid Based Source Localization

The problem is estimating the position of the target with using noisy LOB measurements taken from different sensor arrays, noisy TDOA measurements calculated between the sensor arrays and array locations. Many techniques depend on geometric solutions have been developed whereas, Maximum Likelihood (ML) based techniques depend on some statistical properties of the pre-measured parameters such as covariance of the LOB measurements and covariance of the TDOA measurements for accurate positioning.

3.3.2 Hybrid Based Source Localization Algorithms

In this part, AOA-TDOA based hybrid source localization algorithms are given such as Maximum Likelihood (ML) and Least Squares (LS) based hybrid localization algorithms. Maximum Likelihood (ML) based hybrid localization algorithm is presented for 3D localization. Literature survey on Least Squares (LS) based hybrid localization algorithms is briefly presented.

3.3.2.1 Hybrid Based Maximum Likelihood Source Localization Algorithms

By assuming the noise is zero mean Gaussian, the Maximum Likelihood Estimation (MLE) of the source position can be written as [49]

$$\widehat{p} = argmin_P\{F(\theta, \phi, \tau, p)\} \tag{3.137}$$

where the cost function $F(\theta, \phi, \tau, p)$ is

$$F(\theta, \phi, \tau, p) = \frac{1}{2}\left(\widehat{\psi} - \psi(p)\right)^T R_\psi^{-1}\left(\widehat{\psi} - \psi(p)\right) \tag{3.138}$$

The cost function depends on the angle and range difference measurements, covariance of these measurements and the angles and range differences with respect to the search point. $(3L - 1)x1$ vector $\widehat{\psi}$ represents the angle and range difference measurements.

$$\widehat{\psi} = \begin{bmatrix} \widehat{g}_\theta^T & \widehat{g}_\phi^T & \widehat{h}^T \end{bmatrix}^T \tag{3.139}$$

The measurement vector components are defined in equations (x-y-z).

The $(3L - 1)x1$ vector $\psi(p)$ represents the azimuth and elevation angles; the range differences between the first sensor and the others; with respect to the search point.

$$\psi(p) = \begin{bmatrix} g_\theta^T(p) & g_\phi^T(p) & h^T(p) \end{bmatrix}^T \tag{3.140}$$

where the $Lx1$ vectors $g_\theta(p)$ and $g_\phi(p)$ represent the azimuth and elevation angles with respect to the search point respectively. Moreover $(L - 1)x1$ vector $h(p)$ represents the range differences between the first sensor and the others with respect to the search point. The expressions for these vectors are given in sections 3.1 and 3.2.

Assuming that the range measurements and angle measurements are independent from each other, the covariance of AOA and TDOA measurements can be written as

$$R_\psi = \begin{bmatrix} R_\theta & 0 & 0 \\ 0 & R_\phi & 0 \\ 0 & 0 & R_\tau \end{bmatrix} \qquad (3.141)$$

MLE Algorithm:

1. Estimate the Angle of Arrival values of the sensors arrays and Time Difference of Arrival (TDOA) of the received signal between the sensor array pairs by using any AOA and TDOA estimation algorithms.

2. As mentioned in equations (3.139) and (3.141), obtain the measurement vector $\widehat{\psi}$ and the measurement covariance matrix R_ψ.

3. Perform a grid search; in each search point

   i. Calculate the range difference between the first sensor and the others with respect to the search point; obtain vector $h(p)$

   ii. Calculate the relative azimuth and elevation angles for each sensor array with respect to the search point; obtain vectors $g_\theta(p)$ and $g_\phi(p)$

   iii. By using vectors found in (i) and (ii) obtain $(3L-1)x1$ vector $\psi(p)$

   iv. Calculate the cost function $F(\theta, \phi, \tau, p)$

4. After performing the grid search, find the position estimate $\widehat{p}$, which gives the minimum cost.

3.3.2.2 Hybrid Based Least Squares Source Localization Algorithms

Many closed form localization algorithms based on fusion of hybrid measurements have been developed. LS AOA-TDOA based hybrid localization algorithms depend on merging the AOA and TDOA based equation sets. In the literature, various methods have been presented such as LS Method, Two-Step LS Method, Divide and Conquer Method, methods specific to UWB and WCDMA systems, hybrid estimation with artificial neural networks [12, 35-40]. Both of these methods depend on combining the AOA and TDOA equation sets into a single equation system.

3.3.3 Cramer Rao Lower Bound for AOA-TDOA Based Hybrid Source Localization

In this part the Cramer Rao Lower Bound (CRLB) is presented for 3D AOA-TDOA based hybrid source localization problem. The CRLB is found by inverting the Fisher Information Matrix (FIM). The lq^{th} block of the FIM is given by [49]

$$[\boldsymbol{FIM}(\boldsymbol{p})]_{lq} = E\left\{\frac{\partial}{\partial p_l}ln\big(f_{\widehat{\Psi}}(\widehat{\Psi}:p)\big)\frac{\partial}{\partial p_q}ln\big(f_{\widehat{\Psi}}(\widehat{\Psi}:p)\big)\right\} \tag{3.142}$$

where $\boldsymbol{p}_l$ is the lth element of the true target location vector $\boldsymbol{P}$; $f_{\widehat{\Psi}}(\widehat{\Psi}:p)$ is the likelihood function with respect to the true target position and $\boldsymbol{R}_{\boldsymbol{\Psi}}^{-1}$ is the inverse of the covariance of the angle and range difference measurements. The natural log-likelihood function can be written as

$$ln\big(f_{\widehat{\Psi}}(\widehat{\Psi}:p)\big) = \frac{1}{2}\big(\widehat{\boldsymbol{\Psi}} - \boldsymbol{\Psi}(\boldsymbol{p})\big)^T\boldsymbol{R}_{\boldsymbol{\Psi}}^{-1}\big(\widehat{\boldsymbol{\Psi}} - \boldsymbol{\Psi}(\boldsymbol{p})\big) + \gamma \tag{3.143}$$

where γ is constant term independent from the target position. The complete **FIM** can be written as

$$\boldsymbol{FIM}(\boldsymbol{p}) = \big(\nabla_p\boldsymbol{\Psi}(\boldsymbol{p})\big)^T\boldsymbol{R}_{\boldsymbol{\Psi}}^{-1}\big(\nabla_p\boldsymbol{\Psi}(\boldsymbol{p})\big) \tag{3.144}$$

The derivation starts with defining the operator ∇_p which represents the gradient vector

$$\nabla_p \Psi(p) = \left[\frac{\partial \Psi(p)}{\partial p_x} \quad \frac{\partial \Psi(p)}{\partial p_y} \quad \frac{\partial \Psi(p)}{\partial p_z} \right] \tag{3.145}$$

Under assuming azimuth and elevation measurements are independent from each other, the covariance of the angle measurements can be written as

$$R_\Psi = \begin{bmatrix} R_\theta & 0 & 0 \\ 0 & R_\phi & 0 \\ 0 & 0 & R_\tau \end{bmatrix} \tag{3.146}$$

where the LxL matrices R_θ and R_ϕ are the covariances of the azimuth and elevation measurements respectively. Moreover $(L-1)x(L-1)$ matrix R_τ represents the covariance of the range difference measurements. The covariance matrices of the azimuth, elevation and range difference measurements are presented in sections 3.1 and 3.2.

The $(3L-1)x1$ vector $\Psi(p)$ represents the true angles and range differences with respect to the true target position. This vector consists of two $Lx1$ vectors and one $(L-1)x1$ vector; $g_1(p)$, $g_2(p)$, $h(p)$ which represent the true azimuth, elevation angles and range differences respectively, i.e.,

$$\Psi(p) = [g_1^T(p) \quad g_2^T(p) \quad h^T(p)]^T \tag{3.147}$$

$$g_1(p) = [\theta_1, \ \theta_2, \dots, \theta_L]^T \tag{3.148}$$

$$g_2(p) = [\phi_1, \ \phi_2, \dots, \phi_L]^T \tag{3.149}$$

$$h(p) = c \left[\tau_{2,1}, \tau_{3,1}, \dots, \tau_{L,1} \right]^T \tag{3.150}$$

71

The expression $\nabla_p \Psi(p)$, can be represented in terms of the gradients of the true parameters as

$$\nabla_p \Psi(p) = \begin{bmatrix} \nabla_p g_1(p) \\ \nabla_p g_2(p) \\ \nabla_p h(p) \end{bmatrix} \tag{3.151}$$

The separated $(3L-1)x3$ matrix $\nabla_p \Psi(p)$ can be represented as

$$\nabla_p \Psi(p) = \begin{bmatrix} \dfrac{\partial g_1(p)}{\partial p_x} & \dfrac{\partial g_1(p)}{\partial p_y} & \dfrac{\partial g_1(p)}{\partial p_z} \\[2mm] \dfrac{\partial g_2(p)}{\partial p_x} & \dfrac{\partial g_2(p)}{\partial p_y} & \dfrac{\partial g_2(p)}{\partial p_z} \\[2mm] \dfrac{\partial h(p)}{\partial p_x} & \dfrac{\partial h(p)}{\partial p_y} & \dfrac{\partial h(p)}{\partial p_z} \end{bmatrix} \tag{3.152}$$

The sub-blocks of the matrix $\nabla_p \Psi(p)$ represent the partial derivate of the true parameters (azimuth and elevation angles, range differences) with respect to each coordinate of the true target position. The sub-block expressions have been presented in sections 3.1 and 3.2.

After constructing the matrix $\nabla_p \Psi(p)$ and calculating the complete FIM, CRLB matrix is written as

$$CRLB = (FIM)^{-1} \tag{3.153}$$

The $3x3$ **CRLB** matrix contains the axial minimum achievable variances on its diagonals.

$$diag(CRLB) = \left\{ \sigma_{P_x}^2, \sigma_{P_y}^2, \sigma_{P_z}^2 \right\} \tag{3.154}$$

The trace of the **CRLB** matrix gives the minimum achievable localization variance.

$$\sigma_P^2 = tr(CRLB) \tag{3.155}$$

CHAPTER 4

SINGLE STEP SOURCE LOCALIZATION

ALGORITHMS

In this chapter, single step source localization algorithms are investigated for different number of sources. The chapter starts with formulating the single step localization problem. After problem formulation, single step localization algorithms which are in maximum likelihood sense are presented. Two different algorithms are presented by Weiss and Amar for single and multiple sources [1, 45]. After presenting these algorithms, some novel high resolution and maximum likelihood approaches are introduced. Both of these algorithms use embedded AOA and TOA information of the received signals in the manifold model. In other words, these algorithms are designed to estimate the location of the source in a hybrid single step manner. The chapter ends by presenting the Cramer Rao Lower Bound expression for the single step source localization problem.

4.1 PROBLEM FORMULATION

Consider an emitting source and L sensor arrays, each one consisting of M elements. The vectors $\mathbf{p}$ and $\boldsymbol{p_l}$ denote the Cartesian coordinates of the transmitter and the lth array respectively. By assuming LOS (line-of-sight) propagation between the transmitter and the arrays, the signal observed by the lth sensor array is given by

$$y_l(t) = b_l \, \boldsymbol{a_l}(\boldsymbol{p}) \, s(t-\tau_l(\boldsymbol{p}) - t_0) + \, \boldsymbol{n_l}(t)$$

$$0 \le t \le T$$

(4.1)

where $\boldsymbol{y_l}(t)$ is a $Mx1$ vector, b_l is an unknown complex attenuation coefficient between the transmitter and the lth sensor array, $\boldsymbol{a_l}(\boldsymbol{p})$ is the $Mx1$ array steering vector of the lth array with respect to the transmitter location $\boldsymbol{p}$, $s(t)$ is the transmitted signal waveform, t_0 is the transmission time, $\tau_l(\boldsymbol{p})$ is the flight time of the signal between the array and transmitter and $\boldsymbol{n_l}(t)$ is the noise vector. After sampling the received signal (eqn. 4.2), DFT is taken (eqn. 4.3).

$$\boldsymbol{y_l}(\boldsymbol{n}) = [b_l \, \boldsymbol{a_l}(\boldsymbol{p}) \, s(t-\tau_l(\boldsymbol{p}) - t_0) + \, \boldsymbol{n_l}(t) \,]_{t=nT}$$

$$0 \le n < N_s$$

(4.2)

$$\boldsymbol{y_l}(\boldsymbol{k}) = b_l \, \boldsymbol{a_l}(\boldsymbol{p}) s \, (k) \, e^{-j.w_k.(\tau_l(\boldsymbol{p})+t_0)} + \, \boldsymbol{n_l}(\boldsymbol{k})$$

$$0 \le k < N_s; \; w_k = \frac{2\Pi \, k}{N_s \, T}$$

(4.3)

Note that the steering vector $\boldsymbol{a_l}(\boldsymbol{p})$ and the time of arrival $\tau_l(\boldsymbol{p})$ expressions contain the information about the location of the transmitter. The problem is finding the position of the source with the observed data directly, instead of the conventional two-step localization methods.

The problem formulation can easily be extended to multiple numbers of sources [1]. Consider Q emitting sources and L sensor arrays, each one consists of M elements. The vector $\boldsymbol{p_q}$ denotes the Cartesian coordinate of the qth transmitter. By previously mentioned assumptions, the signal observed by the lth sensor array is given by

$$\boldsymbol{y_l}(t) = \sum_{q=1}^{Q} b_{lq} \, \boldsymbol{a_l}(\boldsymbol{p_q}) \, s_q(t-\tau_l(\boldsymbol{p_q}) - t_q^0) + \, \boldsymbol{n_l}(t)$$

$$0 \le t \le T$$

(4.4)

where $\boldsymbol{y_l(t)}$ is a $Mx1$ vector, b_{lq} is an unknown complex attenuation coefficient between the qth transmitter and the lth sensor array, $\boldsymbol{a_l(p_q)}$ is the $Mx1$ array steering vector of the lth array with respect to the qth transmitter location $\boldsymbol{p_q}$, $s_q(t)$ is the transmitted signal waveform from the qth transmitter, t_q^0 is the transmission time, $\tau_l(\boldsymbol{p_q})$ is the flight time of the signal between the array and q^{th} transmitter and $\boldsymbol{n_l(t)}$ is the noise vector. The received signal partitioned into K sections each of length $T/K \gg max\{\tau_l(\boldsymbol{p_q})\}$. Actually the maximum realizable propagation time is the maximum propagation time between the receivers. For instance, if the largest distance between the sensor arrays is 50 km, then max $\{\tau_l(\boldsymbol{p_q})\}$ becomes 166 microseconds. Therefore 33.2 milliseconds for T/K period satisfy the requirement of 20 dB isolation ratio (" $\gg$ " represents 200 times for 20 dB isolation) between the sources [1, 59]. After sampling the received signal, DFT is taken for each section (eqn. 4.5).

$$\boldsymbol{y_l(w,k)} = \sum_{q=1}^{Q} [\, b_{lq} \, \boldsymbol{a_l(p_q)} \; s_q(w,k) \; e^{-j.\omega.(\tau_l(\boldsymbol{p_q})+t_q^0)} \,] + \boldsymbol{n_l(w,k)}$$

(4.5)

$$k=1, 2... K; \qquad w=1, 2... W; \qquad \omega = \frac{2\Pi\, w}{W\,(T/K)}$$

where $\boldsymbol{y_l(w,k)}$ is the wth Fourier coefficient of the kth section of the lth array corresponding to the frequency ω; $s_q(w,k)$ is the wth Fourier coefficient of the kth section of the qth signal waveform, $\boldsymbol{n_l(w,k)}$ is the wth Fourier coefficient of the kth section of the noise waveform at the lth array. For a simple representation, the vectors and scalars are rewritten as

$$\bar{s_q}(w,k) = s_q(w,k)\, e^{-j.\omega.t_q^0}$$

(4.6)

$$\bar{\boldsymbol{a}}_l(w, \boldsymbol{p_q}, \boldsymbol{b_{lq}}) = b_{lq} \boldsymbol{a_l(p_q)}\, e^{-j.\omega.\tau_l(\boldsymbol{p_q})}$$

(4.7)

It is obviously seen that all the information about the position of the transmitters are embedded into the expression $\bar{a}_l(w,\ p_q,\ b_{lq})$. In matrix notation, equations can be rewritten as

$$y_l(w,k) = A_l(w)\bar{s}(w,k) + n_l(w,k) \tag{4.8}$$

$$A_l(w) = \left[\bar{a}_l(w,p_1,b_{l1}), \bar{a}_l(w,p_2,b_{l2}), \dots, \bar{a}_l(w,p_Q,b_{lQ})\right] \tag{4.9}$$

$$\bar{s}(w,k) = [\ \bar{s}_1(w,k), \bar{s}_2(w,k), \dots, \bar{s}_Q(w,k)\ ]^T \tag{4.10}$$

Since the signal waveform vectors $\bar{s}(w,k)$ are the same for all sensors, the equations can be represented as

$$y(w,k) = A(w)\ \bar{s}(w,k) + n(w,k) \tag{4.11}$$

$$y(w,k) = [y_1^T(w,k), y_2^T(w,k), \dots, y_L^T(w,k)\ ]^T \tag{4.12}$$

$$n(w,k) = [n_1^T(w,k), n_2^T(w,k), \dots, n_L^T(w,k)\ ]^T \tag{4.13}$$

$$A(w) = [\ A_1^T(w), A_2^T(w), \dots, A_L^T(w)\ ]^T \tag{4.14}$$

Then autocorrelation matrix of each frequency bin can be written as

$$R(w) = E\{\ y(w,k)\ y^H(w,k)\ \} = A(w)\ R_s(w)\ A^H(w) + \sigma^2 I \tag{4.15}$$

$$R_s(w) = E\{\ \bar{s}(w,k)\ \bar{s}^H(w,k)\ \} \tag{4.16}$$

$$\sigma^2 \boldsymbol{I} = E\{\, \boldsymbol{n}(\boldsymbol{w}, \boldsymbol{k})\ \boldsymbol{n}^H(\boldsymbol{w}, \boldsymbol{k})\,\} \tag{4.17}$$

where the noise is assumed to be temporally and spatially white, uncorrelated between the frequency bins, uncorrelated with the signal waveforms and assumed to be zero mean with variance σ^2.

The problem is finding the locations of multiple number of sources from the observation autocorrelation matrices $\boldsymbol{R}(\boldsymbol{w})$. The AOA and TOA information of the sources are embedded in the array manifold expressions $\boldsymbol{A}(\boldsymbol{w})$, where the AOA information is the same for all frequency bins whereas TOA information changes.

4.2 SINGLE STEP SOURCE LOCALIZATION ALGORITHMS

In this part of the thesis, single step localization algorithms are presented. This part starts with presenting the Direct Position Determination Algorithms for single and multiple emitter cases, and then goes on with designing the conventional DOA estimation solutions for the multiple source localization problem. Multiple Signal Classification, Deterministic Maximum Likelihood and Stochastic Maximum Likelihood algorithms are modified for the single step passive multiple source localization problem. The sense of the modification is designing a centralized manifold model for the system, which is presented in detail in the relevant parts.

4.2.1 Direct Position Determination for Single Source

Various kinds of Direct Position Determination (DPD) algorithms were presented by Weiss et al. DPD algorithm is modified for different geometries (stationary, non-stationary) and modulation dependencies (modulation independent, OFDM) [1, 42-45].

For this algorithm the signal model given in (4.3) is used since there is only one source [45]. DPD algorithm is based on minimizing the cost function,

$$Q(\boldsymbol{p}) = \sum_{l=1}^{L} \sum_{k=0}^{N_s-1} \left\| \boldsymbol{y}_l(\boldsymbol{k}) - b_l\, \boldsymbol{a}_l(\boldsymbol{p})\, s(k)\, e^{-j.w_k.(\tau_l(\boldsymbol{p})+t_0)} \right\|_F^2 \tag{4.18}$$

where operator $\|.\|_F$ represents the Frobenius norm. By minimizing the cost function $Q(\boldsymbol{p})$ with respect to unknown attenuation coefficients b_l and without loss of generality assumptions

$$\|s_l\|^2=1; \ \|\boldsymbol{a}_l(\boldsymbol{p})\|^2=1; \ \forall l \tag{4.19}$$

DPD cost function for an unknown signal becomes,

$$\tilde{Q}(\boldsymbol{p}) = \lambda_{max}(\boldsymbol{D}) \tag{4.20}$$

where $\lambda_{max}(\boldsymbol{D})$ represents the largest eigenvalue of the matrix $\boldsymbol{D}$. The $N_s x N_s$ matrix $\boldsymbol{D}$ is defined as

$$\boldsymbol{D} = \boldsymbol{U}\boldsymbol{U}^H \tag{4.21}$$

$N_s x \ L$ matrix $\boldsymbol{U}$ consists of vectors which are calculated for each sensor array,

$$\boldsymbol{U} = [\ \boldsymbol{d_1}, \boldsymbol{d_2}, \ldots, \boldsymbol{d_L}] \tag{4.22}$$

Each $N_s x \ 1$ vector $\boldsymbol{d_l}$ contains information for each DFT coefficient as

$$\boldsymbol{d_l} = [\ d_l(0), d_l(1), \ldots, d_l(N_s - 1)\ ]^T \tag{4.23}$$

Actually this information is the correlation of the observed data with the array manifold,

$$d_l(k) = \ e^{-j.w_k.(\tau_l(\boldsymbol{p}))}\boldsymbol{a}_l^H(\boldsymbol{p})\boldsymbol{y}_l(k) \tag{4.24}$$

Dimensions of the matrix $\boldsymbol{U}$ are $N_s x \ L$, so $\boldsymbol{D}$ becomes $N_s x \ N_s$ matrix. Maximization of the cost function $\tilde{Q}(\boldsymbol{p})$ requires 2 dimensional search (or 3 dimensional search for 3D localization). Due to the large dimension cases (large number of snapshots) for matrix $\boldsymbol{D}$, $\boldsymbol{D}$ is replaced with LxL matrix $\tilde{\boldsymbol{D}}$. Then the cost function becomes,

$$\tilde{Q}(\boldsymbol{p}) = \lambda_{max}(\tilde{\boldsymbol{D}}) \tag{4.25}$$

$$\widetilde{D} = U^H U \qquad (4.26)$$

This result holds for an observation of the signal over time $N_s T$ seconds.

DPD Algorithm for Single Source:

1. After the observation period, obtain the snapshot vector $y_l(k)$ for each sensor array and for each DFT point.

2. Perform a grid search; in each search point
   i. Calculate the expressions $d_l(k)$, d_l and U with respect to the search point
   ii. By using expression U found in (i) obtain the expression $\widetilde{D}$
   iii. Calculate the largest eigenvalue of the matrix $\widetilde{D}$, and label it cost for the search point as $\widetilde{Q}(p)$

3. After performing the grid search, find the position estimate $\hat{p}$, which gives the maximum cost.

4.2.2 Direct Position Determination for Multiple Sources

As mentioned in the previous part, this algorithm is also presented by Weiss and Amar [1]. The algorithm uses signal subspace of the autocorrelation matrix of the observed waveforms. Similarly, the algorithm uses both the embedded AOA and TOA information of the multiple sources in one step. As *Single Source DPD* algorithm, *Multiple DPD* algorithm is frequency-bin dependent to use the TOA information. The cost function of the algorithm for a single source was presented in the previous part. In order to avoid the multiple dimensional search for each source, authors prefer to use MUSIC approach, in other words use the signal subspace of the autocorrelation matrix.

The received signal model for multiple sources is given in (4.5). The autocorrelation matrix can be written for each frequency bin as

$$R(w) = E\{ y(w,k)\, y^H(w,k) \} = A(w)\, R_s(w)\, A^H(w) + \sigma^2 I \qquad (4.27)$$

where $R_s(w)$ represents the signal covariance for each frequency bin w,

$$R_s(w) = E\{\, \bar{s}(w,k)\ \bar{s}^H(w,k)\,\} \tag{4.28}$$

$$k=1,\ 2\ ...\ K; \qquad w=1,\ 2\ ...\ W$$

Similarly, $\sigma^2 I$ represents the noise covariance for each frequency bin w,

$$\sigma^2 I = E\{\, n(w,k)\ n^H(w,k)\,\} \tag{4.29}$$

$$k=1,\ 2\ ...\ K; \qquad w=1,\ 2\ ...\ W$$

Again, sectioning in time domain is applied for isolation purposes [1, 59]. In other words, K number of snapshots are taken for each frequency bin. As indicated before, MUSIC based DPD approach uses the cost function,

$$F(p,b) = \sum_{w=1}^{W} \bar{a}^H(w,p,b)\, U_s(w)\, U_s^H(w)\, \bar{a}(w,p,b) \tag{4.30}$$

where $\bar{a}(w,p,b)$ represents the collection of the steering expressions of each sensor array

$$\bar{a}(w,p,b) = [\, \bar{a}_1^T(w,p,b_1), \bar{a}_2^T(w,p,b_2), \ldots, \bar{a}_L^T(w,p,b_L)]^T \tag{4.31}$$

$$b = [b_1, b_2, \ldots, b_L]^T \tag{4.32}$$

where $U_s(w)$ is $MLxQ$ matrix which consists of the eigenvectors of $R(w)$ corresponding to the Q largest eigenvalues. Also p and b represent the unknown position vector and the unknown complex attenuation coefficients between the arrays and this unknown source position respectively. Note that the manifold vector $\bar{a}(w,p,b)$ contains the L complex attenuation coefficients in addition to embedded AOA and TOA information respect to the unknown position. The extreme points of the cost function depend on all unknowns and require $2(L-1)+D$ dimensional search. To reduce the search dimension, authors present the manifold expression as

$$\bar{a}(w,p,b) = \Psi(w)\, H\, b \tag{4.33}$$

$$\Psi(w)$$
$$= diag \{ \ \boldsymbol{a}_1^T(\boldsymbol{p}) \ e^{-j.\omega.\tau_1(\boldsymbol{p})}, \ \ \boldsymbol{a}_2^T(\boldsymbol{p}) \ e^{-j.\omega.\tau_2(\boldsymbol{p})}, \dots, \ \ \boldsymbol{a}_L^T(\boldsymbol{p}) \ e^{-j.\omega.\tau_L(\boldsymbol{p})} \ \} \qquad (4.34)$$

$$\boldsymbol{H} = \boldsymbol{I}_L \ \otimes \ \mathbf{1}_M \qquad (4.35)$$

where $\boldsymbol{\Psi}(w)$ is the block diagonal matrix with elements consist of response manifold vectors of the sensor arrays, $\boldsymbol{I}_L$ is $L \ x \ L$ identity matrix, $\mathbf{1}_M$ is $M \ x \ 1$ vector consists of ones and $\otimes$ stands for Kronecker product. Substituting the mentioned new manifold representation in the original cost function (4.30) results with

$$F(\boldsymbol{p}, \boldsymbol{b}) = \ \boldsymbol{b}^H \boldsymbol{H}^H \left[\sum_{w=1}^{W} \boldsymbol{\Psi}^H(w) \ \boldsymbol{U}_s(w) \ \boldsymbol{U}_s^H(w) \ \boldsymbol{\Psi}(w) \right] \boldsymbol{H} \ \boldsymbol{b} \qquad (4.36)$$

The norm of $\boldsymbol{b}$ is assumed as $\boldsymbol{1}$ to obtain a unique solution. Consequently, for any position $\boldsymbol{p}$, the maximum point of the cost function $F(\boldsymbol{p}, \boldsymbol{b})$, corresponds to the maximum eigenvalue of the matrix $\boldsymbol{D}(\boldsymbol{p})$ defined as

$$\boldsymbol{D}(\boldsymbol{p}) = \ \boldsymbol{H}^H \left[\sum_{w=1}^{W} \boldsymbol{\Psi}^H(w) \ \boldsymbol{U}_s(w) \ \boldsymbol{U}_s^H(w) \ \boldsymbol{\Psi}(w) \right] \boldsymbol{H} \qquad (4.37)$$

Finally, the original cost function $F(\boldsymbol{p}, \boldsymbol{b})$ reduces to

$$F(\boldsymbol{p}) = \lambda_{max}\{ \ \boldsymbol{D}(\boldsymbol{p}) \ \} \qquad (4.38)$$

where $\lambda_{max}\{ \ \boldsymbol{D}(\boldsymbol{p}) \ \}$ represents the largest eigenvalue of the matrix $\boldsymbol{D}(\boldsymbol{p})$, which is a function of the observed data, in other words, function of the signal subspace of the auto-covariance matrix of the received data, and the manifold response of each sensor array with respect to the source located at location $\boldsymbol{p}$. The searching is required to achieve in D-dimensions (generally D=2, for 3D localization D=3).

An illustrative scenario is shown in Figure 4.1. In this scenario SNR is 0 dB and for each DFT bin 100 snapshots are used to calculate the cost function. Each sensor

array is equipped with a 5 element Uniform Linear Array (ULA). True target locations and the positions of the sensor arrays are labeled.
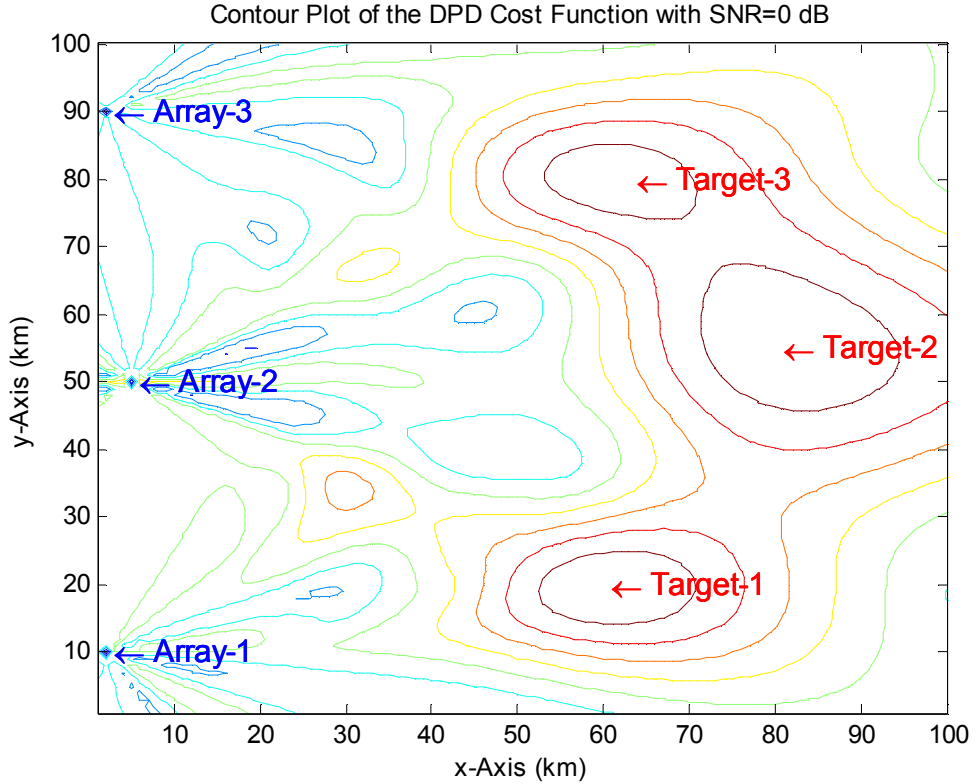
Figure 4.1: Contour Plot of the DPD Cost Function for 2D Scenario (SNR=0dB)

The cost function $F(p) = \lambda_{max}\{ D(p) \}$ has peaks near the target locations. The true target locations are labeled with the arrows; the peaks give the position estimates.

DPD Algorithm for Multiple Emitters:

1. After the observation period, obtain the snapshot vector $y(w, k)$ for each section k and frequency bin w.

2. Calculate the observation covariance matrix $R(w)$ for each frequency bin.

3. Obtain the matrix $U_s(w)$ by calculating the eigenvectors of $R(w)$ corresponding to the Q largest eigenvalues.

4. Perform a grid search; in each search point
   i. Calculate the expression $\boldsymbol{\Psi}(\boldsymbol{w})$ with respect to the search point
   ii. By using expression $\boldsymbol{\Psi}(\boldsymbol{w})$ found in (i) obtain the expression $\boldsymbol{D}(\boldsymbol{p})$
   iii. Calculate the largest eigenvalue of the matrix $\boldsymbol{D}(\boldsymbol{p})$, and label it cost for the search point as $F(\boldsymbol{p})$
5. After performing the grid search, find the position estimate $\hat{\boldsymbol{p}}$, which gives the maximum cost.

Weiss and Amar, analyzed the performance of the DPD algorithm in the presence of modeling errors such as multipath, mutual coupling and calibration errors in [48]. The DPD algorithm gives better location estimates than the conventional AOA based method for multiple emitters in the presence of mentioned model errors.

4.2.3 Direct Localization with Multiple Signal Classification

Certainly, Multiple Signal Classification (MUSIC) algorithm marks a new era in Direction-of-Arrival (DOA) estimation [60, 78]. As mentioned in the previous part, Weiss et al. uses an alternative MUSIC approach in single step multiple source localization problem. In conventional MUSIC approach, noise subspace of the total observation is used instead of using signal subspace of the observations. In other words, conventional MUSIC is applied to the multiple source localization problem with little modifications on array manifold expression. The array manifold and the observation autocorrelation matrix consequently signal and noise subspaces are modified by using all sensors of the separated sensor arrays. To merge the separated array manifolds by preventing spatial aliasing, the TOA information of each array is added to the conventional manifold expression. The resulting expression becomes,

$$\boldsymbol{A}(\boldsymbol{w}) = [a_{11}(w) \; a_{12}(w) \dots a_{1M}(w) \; a_{21}(w) \dots a_{lm}(w) \dots a_{LM}(w)]^T \qquad (4.39)$$

where $a_{lm}(w)$ represents the phase response of the mth sensor of the lth array with respect to the wth frequency bin.

$$a_{lm}(w)$$

$$= e^{-j.\frac{2\Pi}{W}\frac{w}{\left(\frac{T}{K}\right)}(\tau_l(p))} \, e^{-j\frac{2\Pi}{\lambda}\left(P_{lm_x}sin(\theta_l)cos(\phi_l)+P_{lm_y}cos(\theta_l)cos(\phi_l)+P_{lm_z}sin(\phi_l)\right)} \qquad (4.40)$$

$$w=1, 2... W$$

where P_{lm_x}, P_{lm_y} and P_{lm_z} are the x, y and z coordinates of the mth sensor of the lth array respectively. θ_l is the azimuth angle of the source signal to the lth array, whereas ϕ_l is the elevation angle. The angles θ_l and ϕ_l can be easily expressed with the vector coordinates of the lth array p_l, m^{th} sensor of lth array p_{lm} and the transmitter p.

$$a_{lm}(w) = e^{-j.\frac{2\Pi}{W}\frac{w}{\left(\frac{T}{K}\right)}\frac{\|P-P_l\|}{c}} \, e^{-j\frac{2\Pi}{\lambda}P_{lm}^T\frac{(P-P_l)}{\|P-P_l\|}} \qquad (4.41)$$

where the operator $\|.\|$ represents the Euclidian norm. The observation autocorrelation matrix given in (4.15) is rewritten

$$R(w) = E\{ y(w,k) \, y^H(w,k) \} = A(w) \, R_s(w) \, A^H(w) + \sigma^2 I \qquad (4.42)$$

where the signal and noise covariance matrices are defined as

$$R_s(w) = E\{ \bar{s}(w,k) \, \bar{s}^H(w,k) \}$$
$$\sigma^2 I = E\{ n(w,k) \, n^H(w,k) \} \qquad (4.43)$$
$$k=1, 2... K; \qquad w=1, 2... W;$$

As shown in the above expression, the rank of the part $A(w) \, R_s(w) \, A^H(w)$ is equal to the number of sources Q. Similarly the rank of the noise expression $\sigma^2 I$ is equal to the total number of sensors LM. Consequently the rank of the autocorrelation matrix is equal to LM. If the autocorrelation matrix is written in terms of its eigenvalues and eigenvectors,

$$R(w) = V \wedge V^H \qquad (4.44)$$

where $MLxML$ matrix $\wedge$ contains the eigenvalues of $R(w)$ on its diagonal entries,

$$\Lambda = diag\{ (\lambda_1 + \sigma^2), (\lambda_2 + \sigma^2), \dots, (\lambda_Q + \sigma^2), \sigma^2, \dots, \sigma^2 \} \tag{4.45}$$

$MLxML$ matrix V contains the eigenvectors of $R(w)$ on its columns,

$$V = [v_1, v_2, \dots, v_Q, v_{Q+1}, \dots, v_{ML}] \tag{4.46}$$

The signal and noise subspaces of the observation autocorrelation matrix can be defined as

$$S = [v_1, v_2, \dots, v_Q] \tag{4.47}$$

$$G = [v_{Q+1}, \dots, v_{ML}] \tag{4.48}$$

where $MLxQ$ matrix S contains the eigenvectors of the signal components, $MLx(ML - Q)$ matrix G contains the eigenvectors of the noise components. When the $R(w)$ expression is multiplied with noise subspace G,

$$R(w)\, G = \sigma^2 G = A(w)\, R_s(w)\, A^H(w)\, G + \sigma^2 G \tag{4.49}$$

Then, the representation reduces to

$$A(w)\, R_s(w)\, A^H(w)\, G = 0 \tag{4.50}$$

However the $A(w)\, R_s(w)$ part of the expression has a full column rank, so the $A^H(w)\, G$ part should be zero to satisfy the equation (4.50).

$$A^H(w)\, G = 0 \tag{4.51}$$

The true locations of the sources $\{p_i\}_{i=1}^{Q}$ are the only solutions of the equation,

$$A^H(w)\, G\, G^H A(w) = 0 \tag{4.52}$$

if $ML > Q$, in other words if the number of sources is less than the total number of sensors. Then the MUSIC spectrum can be written in terms of the source position as

$$F(\boldsymbol{p}) = \frac{1}{A^H(\boldsymbol{w}) \, \boldsymbol{G} \, \boldsymbol{G}^H A(\boldsymbol{w})} \tag{4.53}$$

Note that the manifold expression $A(\boldsymbol{w})$ highly depends on the source position $\boldsymbol{p}$. When the MUSIC spectrum is calculated for each position (grid search is performed), the peaks of the spectrum give the source location estimates. This fact can be written as

$$\hat{\boldsymbol{p}} = argmax_p \left\{ \frac{1}{A^H(\boldsymbol{w}) \, \boldsymbol{G} \, \boldsymbol{G}^H A(\boldsymbol{w})} \right\} \tag{4.54}$$

Similarly, the searching is required to achieve in D-dimensions (generally D=2, for 3D localization D=3).

An illustrative scenario is shown in Figure 4.2, for 2D scenario the MUSIC cost function $F(\boldsymbol{p})$ is calculated for each point. The scenario is exactly the same with the scenario used in DPD illustration (i.e. SNR=0 dB, 100 snapshots are used for each frequency bin, each sensor array is equipped with 5-element ULA, locations of the sensor arrays and the targets are the same).
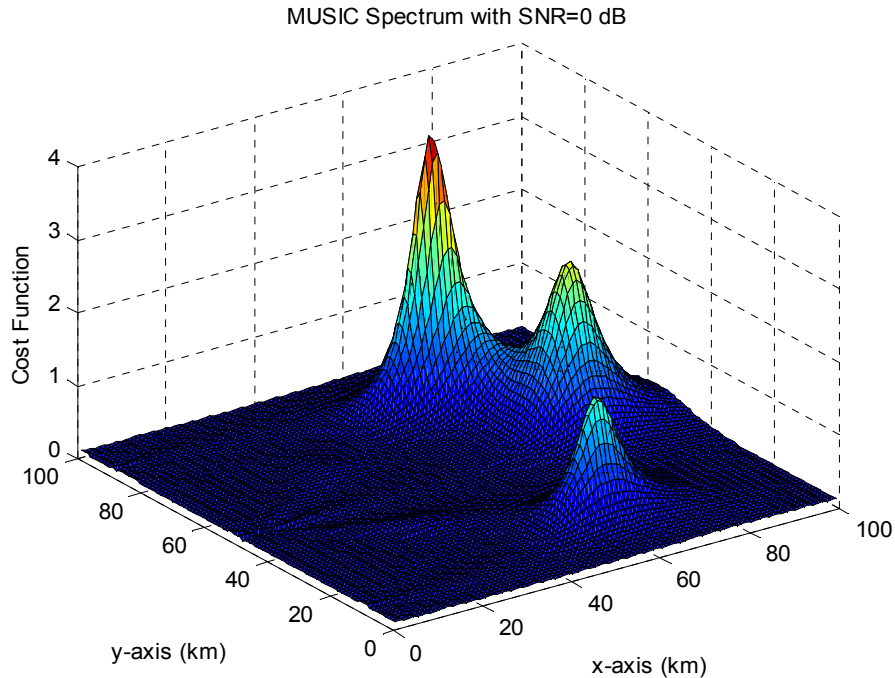
Figure 4.2: MUSIC Cost Function for 2D Scenario (SNR=0 dB)

As mentioned in the previous paragraphs, the peaks of the MUSIC spectrum give the location estimates of the emitters. MUSIC spectrum has sharper peaks than the DPD cost function. The contour plot of the MUSIC spectrum is shown in Figure 4.3. When the contour plots of the MUSIC and DPD cost functions are compared, it is obviously seen that MUSIC spectrum contains sharper peaks. The true target locations and the locations of the sensor arrays are labeled in the figure.
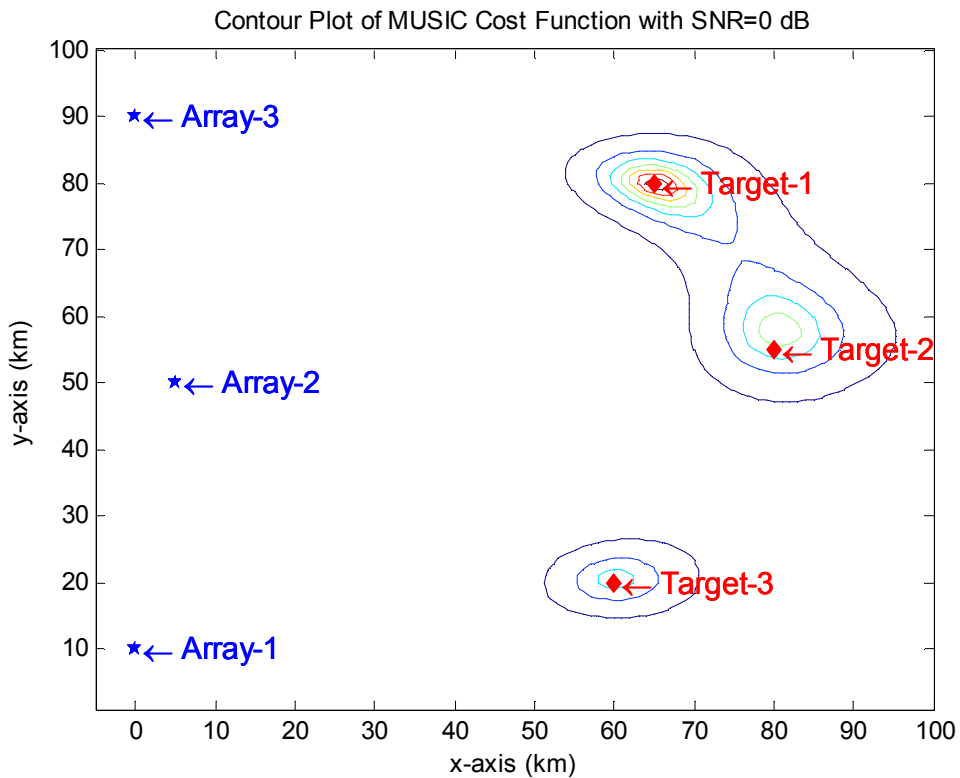
Figure 4.3: Contour Plot of the MUSIC Cost Function for 2D Scenario (SNR=0 dB)

Direct Localization with MUSIC Algorithm:

1. After the observation period, obtain the snapshot vector $y(w, k)$ for each section k and frequency bin w.
2. Calculate the observation covariance matrix $R(w)$ for each frequency bin.
3. Obtain the noise subspace matrix $G(w)$ by performing an eigen decomposition to $R(w)$

4. Perform a grid search; in each search point

    i.   Calculate the expression $A(w)$ with respect to the search point

    ii.   Calculate the MUSIC pseudo spectrum, and label it cost for the search point as $F(p)$

5. After performing the grid search, find the position estimate $\hat{p}$, which gives the maximum cost.

4.2.4 Direct Localization with Deterministic Maximum Likelihood for Multiple Sources

Deterministic Maximum Likelihood (DML) algorithm is widely used in Direction-of-Arrival (DOA) estimation. The DML algorithm was contributed to the literature by Schweppe to estimate the DOA of the multiple sources with a sensor array [59, 79-80].

In this part, DML expression used in DOA estimation problem is modified for the single step multiple source localization problem. In this algorithm, the noise is modeled as a stationary Gaussian white process. Moreover noise is assumed to be spatially and temporally white and circularly symmetric between the sensors and the frequency bins. Under these assumptions, noise can be written as

$$E\{n(w_a, k)\ n^H(w_b, l)\} = \sigma^2\ I\ \delta_{ab}\delta_{kl}$$
$$E\{n(w_a, k)\ n^T(w_b, l)\} = 0 \tag{4.55}$$

where δ represents Dirac -Delta function. The signal is also assumed to be circularly symmetric and temporally white Gaussian random process with mean $A(w)\bar{s}(w, k)$. The array output expression is written as

$$y(w, k) = A(w)\ \bar{s}(w, k) + n(w, k) \tag{4.56}$$

So the multivariate Probability Density Function (PDF) of the snapshot model can be presented as,

$$f_y(\mathbf{y}(\mathbf{w},\mathbf{k})) = \frac{1}{(\Pi\sigma^2)^{ML}} \; exp\left[\frac{-\|\mathbf{y}(\mathbf{w},\mathbf{k}) - \mathbf{A}(\mathbf{w})\,\bar{\mathbf{s}}(\mathbf{w},\mathbf{k})\|^2}{\sigma^2}\right] \tag{4.57}$$

Then, the likelihood function can be written as

$$L_{DML}(\mathbf{w},\mathbf{p},\bar{\mathbf{s}}(\mathbf{w},\mathbf{k}),\sigma^2)$$

$$= \prod_{k=1}^{K}(\Pi\sigma^2)^{-ML} \; exp\left[\frac{-\|\mathbf{y}(\mathbf{w},\mathbf{k}) - \mathbf{A}(\mathbf{w})\,\bar{\mathbf{s}}(\mathbf{w},\mathbf{k})\|^2}{\sigma^2}\right] \tag{4.58}$$

By taking the logarithm of both left and right sides, the negative log-likelihood function (normalized by the number of snapshots) becomes

$$l_{DML} = ML\,log(\sigma^2) + \frac{1}{K\sigma^2}\sum_{k=1}^{K}\|\mathbf{y}(\mathbf{w},\mathbf{k}) - \mathbf{A}(\mathbf{w})\,\bar{\mathbf{s}}(\mathbf{w},\mathbf{k})\|^2 \tag{4.59}$$

When the log-likelihood function is minimized for the noise variance σ^2 and the signal waveforms $\bar{\mathbf{s}}(\mathbf{w},\mathbf{k})$, these expressions can be written as,

$$\hat{\sigma}^2 = \frac{1}{ML}\,tr\{\Pi_A^{\perp}\,\hat{\mathbf{R}}_y(\mathbf{w})\} \tag{4.60}$$

$$\hat{\mathbf{s}}(\mathbf{w},\mathbf{k}) = \mathbf{A}^{\#}(\mathbf{w})\,\mathbf{y}(\mathbf{w},\mathbf{k}) \tag{4.61}$$

where $\hat{\mathbf{R}}_y(\mathbf{w})$ is the observation covariance matrix constructed by using all sensors as

$$\hat{\mathbf{R}}_y(\mathbf{w}) = \frac{1}{K}\sum_{k=1}^{K}\mathbf{y}(\mathbf{w},\mathbf{k})\,\mathbf{y}^H(\mathbf{w},\mathbf{k}) \tag{4.62}$$

and $\Pi_A^{\perp}$ represents the projector onto the noise subspace. The projector $\Pi_A^{\perp}$ can be calculated by using the projector onto the signal space. The expression $\Pi_A^{\perp}$ can be written as

$$\Pi_A^{\perp} = \mathbf{I} - \Pi_A \tag{4.63}$$

where the expression Π_A is the projector onto the signal subspace. $\boldsymbol{I}$ represents the identity matrix with dimension $LMxLM$. The projector onto the signal subspace can be calculated with the manifold expression as

$$\Pi_A = A(w)\, A^{\#}(w) \tag{4.64}$$

The expression $A^{\#}(w)$ is the pseudo-inverse of the manifold, which can be written as

$$A^{\#}(w) = [\, A^H(w)\, A(w)\,]^{-1}\, A^H(w) \tag{4.65}$$

Finally, by using the explicit minima for the noise variance and the signal waveforms, the position estimate can be written as

$$\hat{\boldsymbol{p}} = argmin_p\ \{\ tr\{\Pi_A^{\perp}\, \widehat{\boldsymbol{R}}_y(w)\}\ \} \tag{4.66}$$

The derivation of the expression is similar to the DML derivation used in DOA estimation [59]. The idea is, when the projector $\Pi_A^{\perp}$ removes all signal components, energy should be the smallest. After the grid search, Q (number of sources) lowest valleys give the source locations. Iterative techniques can be used to reduce the algorithmic complexity; however good initial position estimates are required to find the global minima and the other lowest $(Q - 1)$ valleys.

Direct Localization with DML Algorithm:

1. After the observation period, obtain the snapshot vector $\boldsymbol{y}(\boldsymbol{w}, \boldsymbol{k})$ for each section k and frequency bin w.
2. Calculate the observation covariance matrix $\boldsymbol{R}(\boldsymbol{w})$ for each frequency bin.
3. Perform a grid search; in each search point
    i.   Calculate the expression $\boldsymbol{A}(\boldsymbol{w})$ with respect to the search point
    ii. By using the expression $\boldsymbol{A}(\boldsymbol{w})$, calculate the projector onto the noise subspace $\Pi_A^{\perp}$
    iii. Calculate the expression $tr\{\Pi_A^{\perp}\, \widehat{\boldsymbol{R}}_y(\boldsymbol{w})\}$, and label it as the cost of the search point

4. After performing the grid search, find the position estimate $\widehat{\boldsymbol{p}}$, which gives the minimum cost.

4.2.5 Direct Localization with Stochastic Maximum Likelihood for Multiple Sources

The Stochastic Maximum Likelihood (SML) algorithm was introduced by Stoica to estimate the DOA of the multiple sources with a sensor array [81]. In this part, SML expression used in DOA estimation problem is modified for the single step multiple source localization problem. The proposed approach cannot be used for totally unknown signals, because the signal waveforms are modeled as unknown Gaussian random processes.

By ignoring the constant terms, negative log-likelihood function becomes,

$$\frac{1}{K}\sum_{k=1}^{K}\| \Pi_A^\perp \, \boldsymbol{y}(\boldsymbol{w}, \boldsymbol{k}) \|^2 = tr\{ \Pi_A^\perp \, \widehat{\boldsymbol{R}}_{\boldsymbol{y}}(\boldsymbol{w})\} \tag{4.67}$$

For fixed position vector $\boldsymbol{p}$, the log-likelihood function minimized with respect to the signal covariance $\boldsymbol{R}_s(\boldsymbol{w})$ and the noise variance σ^2. The resulting expressions for $\widehat{\boldsymbol{R}}_s(\boldsymbol{w})$ and $\widehat{\sigma}^2$ can be written as

$$\widehat{\boldsymbol{R}}_s(\boldsymbol{w}) = \boldsymbol{A}^\#(\boldsymbol{w})\big(\widehat{\boldsymbol{R}}_{\boldsymbol{y}} - \widehat{\sigma}_{SML}^2 \, \boldsymbol{I}\big)\big(\boldsymbol{A}^\#(\boldsymbol{w})\big)^H \tag{4.68}$$

$$\widehat{\sigma}_{SML}^2 = \frac{1}{ML - Q} \, tr\{ \Pi_A^\perp \, \widehat{\boldsymbol{R}}_{\boldsymbol{y}}(\boldsymbol{w})\} \tag{4.69}$$

where the observation covariance is calculated by using all snapshots from all sensors, as

$$\widehat{\boldsymbol{R}}_{\boldsymbol{y}} = \frac{1}{K}\sum_{k=1}^{K} \boldsymbol{y}(\boldsymbol{w}, \boldsymbol{k}) \, \boldsymbol{y}^H(\boldsymbol{w}, \boldsymbol{k}) \tag{4.70}$$

Then the source position is represented as

$$\widehat{\boldsymbol{p}} = argmin_p \left\{ log \left[det \left(\boldsymbol{A} \, \widehat{\boldsymbol{R}}_s(\boldsymbol{w}) \boldsymbol{A}^H + \hat{\sigma}_{SML}^2 \, \boldsymbol{I} \right) \right] \right\} \tag{4.71}$$

where the *det* represents the determinant of the inside. Similarly, for Q number of sources, Q lowest valleys give the source location estimates after the grid search.

Direct Localization with SML Algorithm:

1. After the observation period, obtain the snapshot vector $\boldsymbol{y}(\boldsymbol{w}, \boldsymbol{k})$ for each section k and frequency bin w.

2. Calculate the observation covariance matrix $\mathbf{R}(\mathbf{w})$ for each frequency bin.

3. Perform a grid search; in each search point
   i. Calculate the expression $\boldsymbol{A}(\boldsymbol{w})$ with respect to the search point
   ii. By using the expression $\boldsymbol{A}(\boldsymbol{w})$, calculate the projector onto the noise subspace $\Pi_A^\perp$
   iii. By using the expression $\Pi_A^\perp$, calculate $\hat{\sigma}_{SML}^2$
   iv. By using the expression $\boldsymbol{A}(\boldsymbol{w})$ and $\hat{\sigma}_{SML}^2$, calculate $\widehat{\boldsymbol{R}}_s(\boldsymbol{w})$
   v. Calculate the expression $log\left[det\left(\boldsymbol{A} \, \widehat{\boldsymbol{R}}_s(\boldsymbol{w}) \boldsymbol{A}^H + \hat{\sigma}_{SML}^2 \, \boldsymbol{I} \right) \right]$ and label it as the cost of the search point

4. After performing the grid search, find the position estimate $\widehat{\boldsymbol{p}}$, which gives the minimum cost.

4.3 CRAMER RAO LOWER BOUND FOR SINGLE STEP SOURCE LOCALIZATION

In this part, Cramer Rao Lower Bound (CRLB) expression for the single step multiple source localization problem is presented. In the simulations, accuracies of the various single step position estimators are compared with the lower bound. The CRLB defines the limits of the estimators, that is no estimator can perform better than this bound. The noise and the measurement errors are the main sources of error. Measurement errors are systematic and unique to each implementation. The Cramer Rao Lower Bound for *Single Step Source Localization* problem was derived and presented by Weiss [41]. As mentioned in the *"Problem Formulation"* part, the

unknowns are the locations of the sources, complex attenuation coefficients between the sources and the sensor arrays and the signal waveforms of the sources. These unknowns are mathematically represented as,

$$P = [p_1, p_2, \dots, p_Q] \tag{4.72}$$

$$B = [b_1, b_2, \dots, b_Q] \tag{4.73}$$

$$b_q = [b_{1,q}, b_{2,q}, \dots, b_{L,q}]^T \tag{4.74}$$

where Q is the number of sources, L is the number of sensor arrays, p_q is the $Dx1$ vector representing the Cartesian coordinates of the qth source, $b_{l,q}$ is the complex attenuation coefficient between the qth source and the lth sensor array. Moreover, there is no prior knowledge about the Q number of different signal waveforms. The **CRLB** matrix is equal to the inverse of the Fisher Information Matrix (**FIM**). The **FIM** consists of different blocks each contains information about different unknowns. For zero mean Gaussian signals, the blocks of the FIM are represented as,

$$FIM_{ij} = tr \left\{ R_y^{-1} \frac{\partial R_y}{\partial \theta_i} R_y^{-1} \frac{\partial R_y}{\partial \theta_j} \right\} \tag{4.75}$$

where R_y is the autocorrelation matrix constructed by using all sensors. R_y can be represented as,

$$R_y = A \wedge A^H + \sigma^2 I \tag{4.76}$$

A is the $MLxQ$ manifold matrix and contains the phase response of each sensor with respect to the each source, $\wedge$ is the QxQ autocorrelation matrix of the signal waveforms.

As mentioned, the complete **FIM** consists of different blocks with respect to the unknown parameters, namely, signal waveforms, real and imaginary parts of the complex attenuation coefficients and the source positions. The complete FIM consists of 16 different blocks for this problem. The structure of the complete FIM is shown below.

$$FIM = \begin{bmatrix} FIM_{\Lambda\Lambda} & FIM_{\Lambda\bar{B}} & FIM_{\Lambda\tilde{B}} & FIM_{\Lambda P} \\ FIM_{\bar{B}\Lambda} & FIM_{\bar{B}\bar{B}} & FIM_{\bar{B}\tilde{B}} & FIM_{\bar{B}P} \\ FIM_{\tilde{B}\Lambda} & FIM_{\tilde{B}\bar{B}} & FIM_{\tilde{B}\tilde{B}} & FIM_{\tilde{B}P} \\ FIM_{P\Lambda} & FIM_{P\bar{B}} & FIM_{P\tilde{B}} & FIM_{PP} \end{bmatrix} \tag{4.77}$$

By using the fact,

$$FIM_{ij} = FIM_{ji}^{H} \tag{4.78}$$

the off-diagonal blocks are represented for only the upper triangular part of the **FIM**.

In Appendix A, the FIM block representations are directly given. The derivations of the FIM blocks are given in [41]. The derivative of the manifold matrix A with respect to the source position is required to calculate all of the **FIM** blocks. In Appendix B, derivative of the manifold matrix is presented. By constructing the complete **FIM**, **CRLB** matrix can be calculated as

$$CRLB = (FIM)^{-1} \tag{4.79}$$

The diagonal entries of the **CRLB** matrix give the lower bounds for the estimation variances of the unknown parameters. By considering the structures of the **FIM** blocks, block diagonals of the **CRLB** matrix can be expressed as

94

$$CRLB = \begin{bmatrix} CRLB_{\wedge\wedge} & & & \\ & CRLB_{\bar{B}\bar{B}} & & \\ & & CRLB_{\tilde{B}\tilde{B}} & \\ & & & CRLB_{PP} \end{bmatrix} \tag{4.80}$$

The block associated with the source position variances is the rightmost lowest block of the matrix $CRLB$. The size of the block $CRLB_{PP}$ is $3Qx3Q$ for 3D localization problem. The block $CRLB_{PP}$ contains the achievable minimum axial variances for each emitter on its diagonals.

$$CRLB_{PP} = diag(\sigma_{p_{1,x}}^2, \sigma_{p_{1,y}}^2, \sigma_{p_{1,z}}^2 \dots, \sigma_{p_{Q,x}}^2, \sigma_{p_{Q,y}}^2, \sigma_{p_{Q,z}}^2) \tag{4.81}$$

By selecting the diagonal entries of the matrix $CRLB_{PP}$ the lower variances of the positions of the emitters can be calculated.

4.4 CONCLUSION

In this chapter, the single step source localization problem is formulized for single and multiple number of emitters. As seen from the formulation, the received signal model contains both AOA and TOA information. A criterion for the observation time is given for multiple localization problem for isolation purposes between the targets. Moreover the criterion for sectioning in the observation period is presented.

Secondly, the Direct Position Determination (DPD) algorithms are presented for single source and multiple source cases. New direct localization approaches are derived for 3D localization such as Direct Localization with Multiple Signal Classification (MUSIC), Direct Localization with Deterministic Maximum Likelihood (DML) and Direct Localization with Stochastic Maximum Likelihood (SML). The cost functions of some of the methods are compared in 2D scenarios for easier illustration of the concept.

Finally, the Cramer Rao Lower Bound expression derived by Weiss is given for single step multiple source localization problem. The **FIM** block representations

(derived by Weiss in [41]) are given in Appendix A. Moreover, derivative of the manifold matrix A with respect to the true source positions is required to calculate all of the **FIM** blocks. The derivation of the derivative of the manifold matrix is performed in this thesis and presented in Appendix B. As mentioned before, the CRLB consists of different blocks with respect to the unknown parameters, namely, signal waveforms, real and imaginary parts of the complex attenuation coefficients and the positions of the emitters. The CRLB expression contains minimum achievable variances of the unknowns.

CHAPTER 5

SIMULATIONS

The performances of the AOA based ML and LS, TDOA based ML and LS, AOA-TDOA based hybrid ML, single step based DPD, MUSIC, DML and SML location estimation algorithms are compared under various cases. In each comparison, related CRLB expressions are calculated to investigate the performance of the algorithms with the achievable ultimate performance.

The simulations are presented in two parts. In the first part, individual comparisons of the algorithms are presented. In other words, AOA based methods, TDOA based methods and single step based methods are investigated individually under the single source case. AOA-TDOA based hybrid ML method is compared with the AOA and TDOA based methods in order to see the performance improvement. The performances are evaluated by comparing the azimuth & elevation deviations and TOA deviations for conventional methods. These deviation values chosen to represent the error statistics are consistent with the literature [7, 12, 27, 49]. However the performances of the single step methods are evaluated by comparing the SNR of the observed signal and number of snapshots used for location estimation. Lastly the geometrical dependencies of the conventional methods and the single step methods are investigated by comparing the CRLB expressions with fixed statistical errors. In other words, the angle, time deviations, SNR values are fixed for the methods; and CRLB expressions are compared by changing the target and sensor geometries to investigate the performance deviations with respect to the geometrical effects.

In the second part of the simulations, the performance of the single step and AOA based ML methods are compared under multiple emitter case. The performance comparisons are evaluated by changing the SNR values and the number of snapshots. Moreover resolvability analyses are performed to investigate the capabilities of the methods under various geometrical deployments.

Each point of the simulation plots is the result of 100 Monte-Carlo experiments, if it is not indicated.

The accuracy measure in the simulations is the Root-Mean-Square (RMS) of the position error. The RMS error can be defined as

$$RMS = \sqrt{\frac{1}{N_{MC}} \sum_{i=1}^{N_{MC}} \left\| \boldsymbol{P} - \widehat{\boldsymbol{P}}_i \right\|^2} \tag{5.1}$$

where $\boldsymbol{P}$ is the emitter location, $\widehat{\boldsymbol{P}}_i$ is the ith emitter location estimate and N_{MC} is the number of Monte-Carlo experiments. When the performance comparisons have been performed under multiple number of emitters, the RMS of the whole system is used for evaluation. The RMS expression can be simply written as

$$RMS = \sqrt{\frac{1}{N_{MC}Q} \sum_{i=1}^{N_{MC}} \sum_{q=1}^{Q} \left\| \boldsymbol{P}_q - \widehat{\boldsymbol{P}}_{qi} \right\|^2} \tag{5.2}$$

where Q represents the total number of emitters, $\boldsymbol{P}_q$ is the location of the qth emitter and $\widehat{\boldsymbol{P}}_{qi}$ is the ith emitter location estimate for the qth source.

In the simulations, additive zero-mean white Gaussian noise waveforms are used. The snapshot model for multiple emitter scenario is given in equation (4.4). In the simulations, complex attenuation coefficients b_{lq} equal to 1 for all sensor arrays and the emitters. Then the SNR expression can be written as

$$SNR = 10log_{10}\left(\frac{\sigma_{s_q}^2}{\sigma_{n_l}^2}\right)$$

$$\sigma_{s_q}^2 = \sigma_s^2, \qquad \forall q \qquad\qquad (5.3)$$

$$\sigma_{n_l}^2 = \sigma_n^2, \qquad \forall l$$

5.1 INDIVIDUAL COMPARISON OF THE ALGORITHMS UNDER SINGLE SOURCE CASE

5.1.1 Comparison of AOA Based Localization Techniques

As a first simulation, the planar deployment is chosen for the sensor arrays. Sensor arrays are located at the corners of a 100km x 100km square, and the Cartesian coordinate of the emitter is (150, 150, 30).
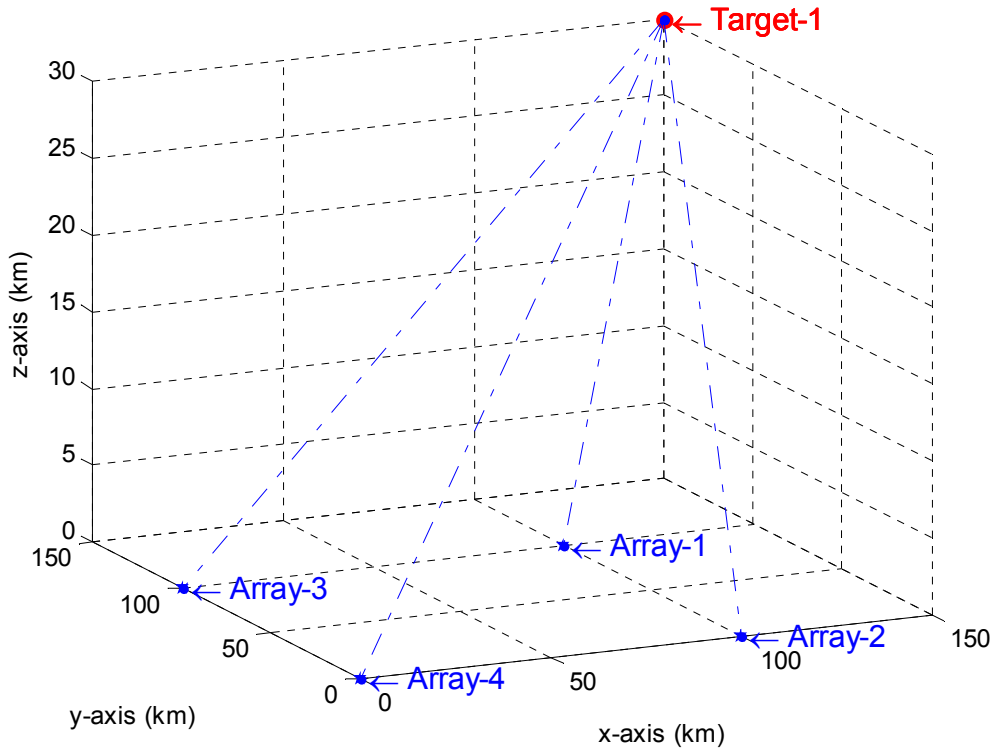
Figure 5.1: Sensor Array and Target Locations for AOA Based Localization Scenario
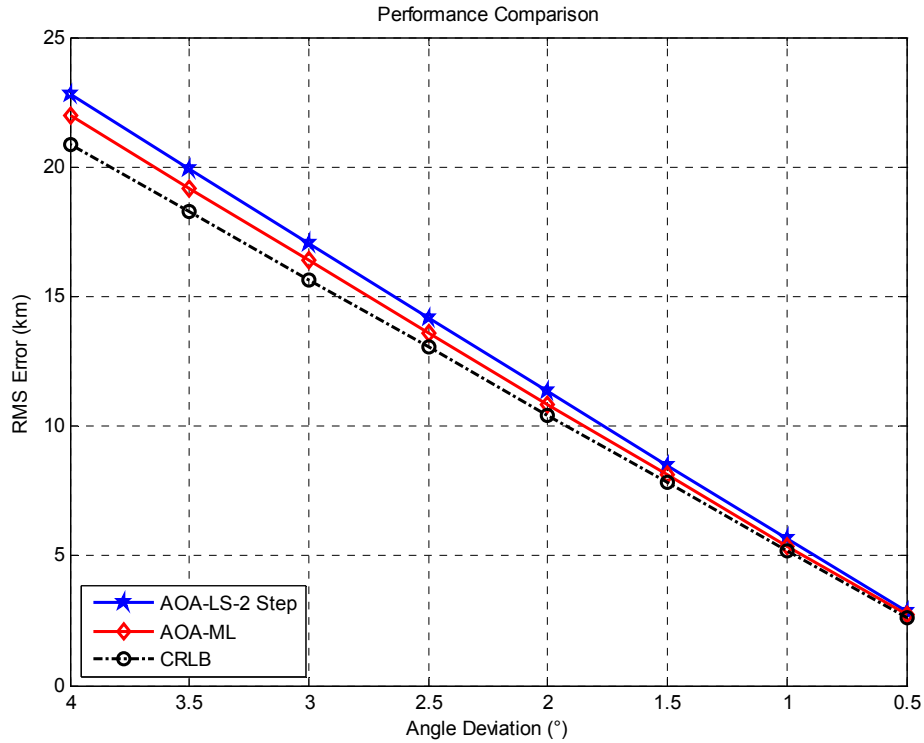
Figure 5.2: 3D Performance Comparison of AOA Based Algorithms where $\sigma_\theta = \sigma_\phi$

First, the performance of the AOA based localization algorithms are compared with the Cramer Rao Lower Bound (CRLB) for various azimuth and elevation deviations. In the simulation, azimuth and elevation deviations are equal in each step and the deviations are changing between 0.5° and 4°.

In the simulations, first LS location estimation is computed, and then this LS estimate is taken as initial location for the ML algorithm. An iterative grid search (20km x 20 km x 20km) is performed near the LS estimate and the point which gives the minimum cost is labeled as location ML estimate.

The algorithms (ML and LS) show good performances with respect to the CRLB. However when the geometric scenario shown in Figure 5.1 is considered, it is obvious that AOA based localization is successful (can be considered as localization errors lower than 5-7 km) for angle deviations lower than 1.5° or 1°. Moreover, it is seen from Figure 5.2 that this claim is supported by the CRLB.
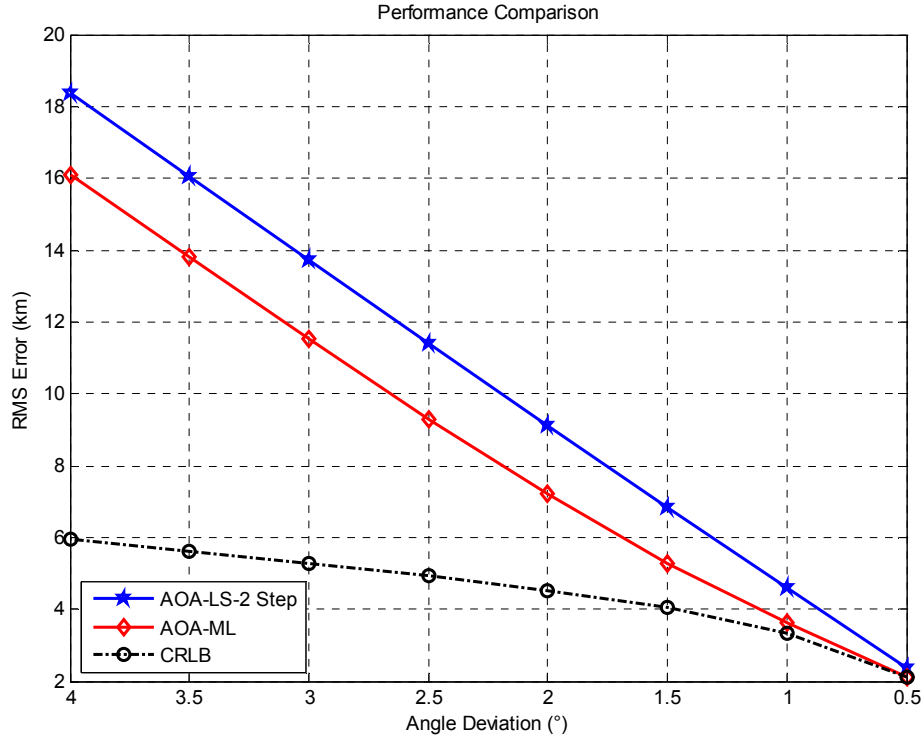
Figure 5.3: 3D Performance Comparison of AOA Based Algorithms with Fixed Elevation Deviation $\sigma_\phi = 1°$

To see the effects of the individual angle deviations, two different simulations have been done. First, elevation deviation is fixed at 1° for all cases and azimuth deviation varies between 4° and 0.5° for all sensor arrays. It is seen from Figure 5.3 that the performance of the LS algorithm degrades for higher azimuth deviations. Hence the ML performance degrades since the grid search is performed near LS estimate. Secondly azimuth deviation is fixed to 1° for all cases and elevation deviation varies between 4° and 0.5°. As seen from Figure 5.4, methods have good performances with respect to the CRLB. A geometrical illustration of this problem is given in Chapter-3. By changing angle deviations, the shapes of the elliptic cones are changed. Moreover by changing sensor array- target geometry, the volume which is the intersection of the elliptic cones lies from sensor array to the target location changes. The degradation on the performance is not specific for the azimuth or elevation deviation. It is specific for the array-target geometry, which is tried to be illustrated with the Error Ellipse concept given in Chapter-2. In other

words, the degradation in azimuth is due to the planar deployment of the arrays as in Figure 5.1.
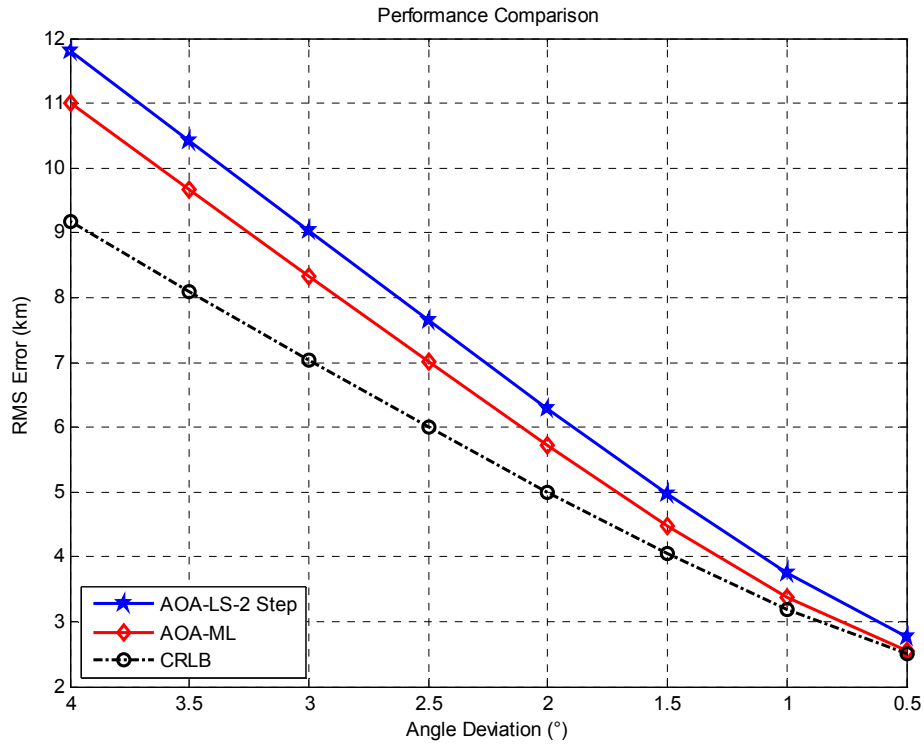
Figure 5.4: 3D Performance Comparison of AOA Based Algorithms with Fixed Azimuth Deviation $\sigma_\theta = 1°$

5.1.2 Comparison of TDOA Based Localization Techniques

For TDOA based localization, a fifth sensor is used for in addition to the planar deployment used for AOA based localization. The additional sensor is located at the point (0, 50, 5). The reason of using an additional sensor is due to the TDOA based LS algorithm which is presented in Chapter-3. As mentioned in the related section, for 3D LS localization at least five sensors are needed due to the linearization. Other sensors are located at the corners of a 100km x 100km square, and the Cartesian coordinate of the emitter is (150, 200, 20). The locations of the sensors (arrays with one element) and the emitter are shown in Figure 5.5.

The aim of the geometrical scenario given in Figure 5.5 is to investigate the performance of the algorithm under non-optimum sensor geometry. As mentioned

in section 3.2, platonic sensor deployment is optimum for TDOA based source localization for single emitter case.
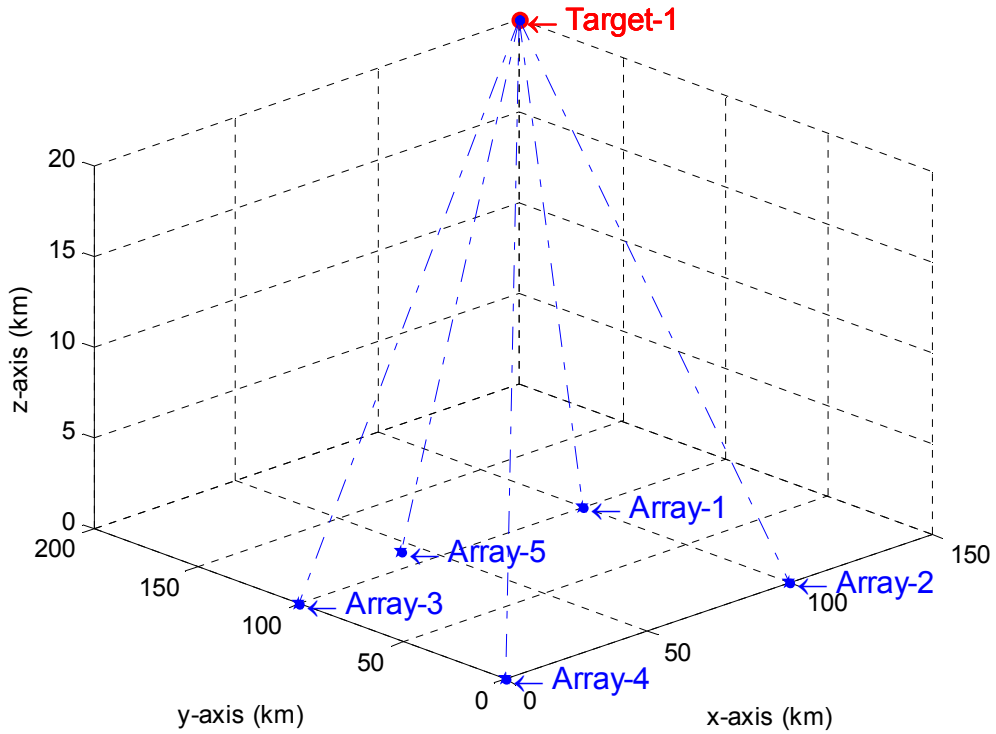
Figure 5.5: Sensor and Target Locations for TDOA Based Localization Scenario

In the simulation, Time-of-Arrival (TOA) deviations are changing between 0.8 μsec to 0.1 μsec. Similarly, ML method searches the grid with minimum cost near LS estimate. As shown in Figure 5.6, the performance of the LS algorithm degrades with respect to the ML method and the CRLB.

The TOA deviations can be easily expressed as Range-of-Arrival (ROA) deviations. The ROA deviations vary between 240m and 30m. Consequently, the Time-Difference-of-Arrival (TDOA) and Range-Difference-of-Arrival (RDOA) deviations varies between 1.6μsec to 0.2μsec and 480m to 60m, respectively.

The CRLB presented in Figure 5.6 shows that the achievable RMS of the localization approximately varies between 5km to 500m. By considering CRLB and the RDOA deviations, the effect of the sensor geometry is obvious. The

performance of the TDOA based localization algorithms is highly dependent on the sensor-target geometry, which is investigated in the further simulations.
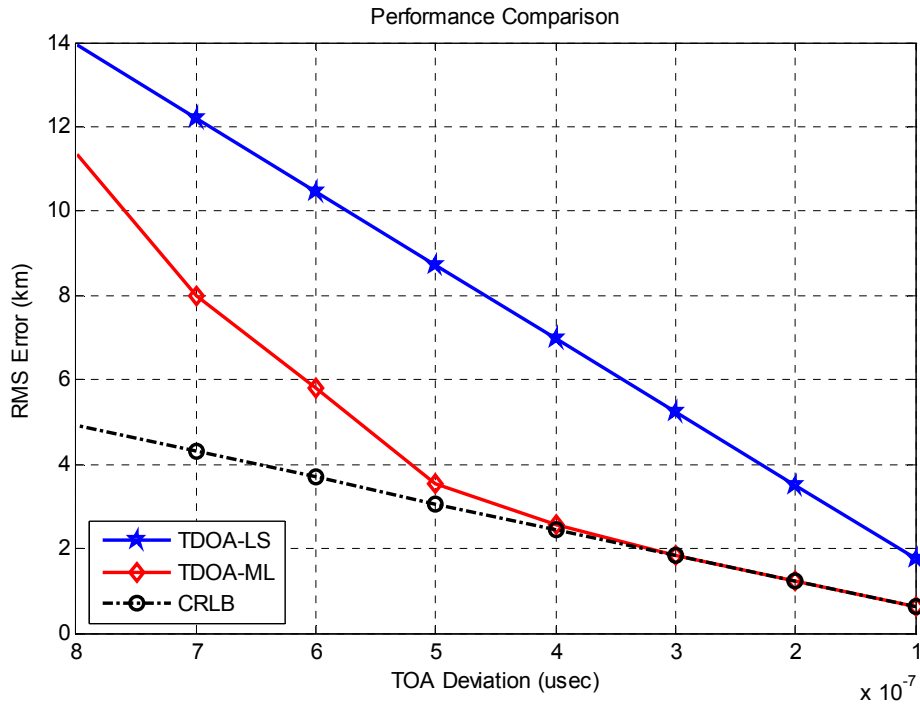
Figure 5.6: Performance Comparison of TDOA Based Algorithms for Different TOA Deviations σ_τ

5.1.3 Comparison of Hybrid Based Localization with the AOA and TDOA Based Methods

As mentioned in Chapter-3, the target location can be estimated by combining the AOA and TDOA measurements. The performance of the hybrid method is investigated with the AOA based and TDOA based methods. Optimum sensor array geometry is used to see the effect of the measurement merging. In other words, since TDOA based localization highly depends on the geometry, optimum sensor array deployment is used to investigate the hybrid performance.

The Cartesian locations of the sensor arrays (0 0 0; 0 0 20; 7.0711 7.0711 10; -7.0711 7.0711 10; 7.0711 -7.0711 10; -7.0711 -7.0711 10) are selected in such a manner that generates optimum octahedron deployment. Cartesian coordinate of the

emitter is (15, 40, 15). The locations of the sensor arrays and the emitter are shown in Figure 5.7.

In the simulations, various conventional two step algorithms, moreover the lower bounds are investigated; namely, for AOA based algorithms ML and LS techniques, for TDOA based localization ML and LS methods, lastly ML for hybrid based localization. Different CRLBs are compared with the performance of the algorithms such as CRLB of AOA based localization, CRLB of TDOA based localization and CRLB for AOA-TDOA based hybrid localization. These CRLB expressions have been derived in Chapter-3.
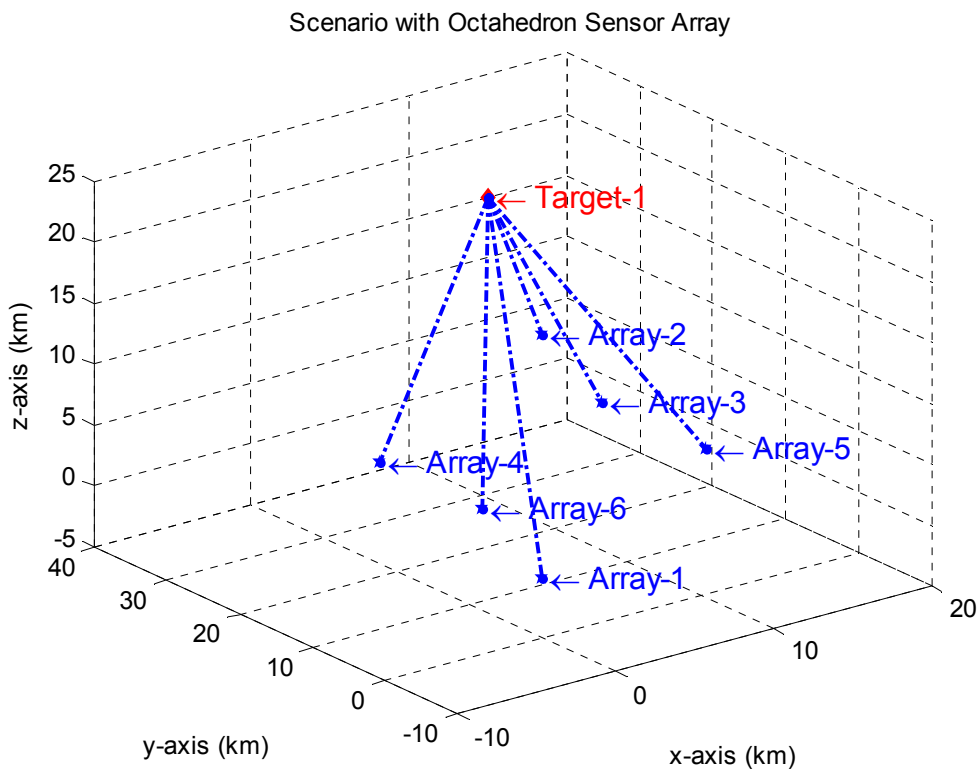
Figure 5.7: Locations of the Octahedron Sensor Array and the Emitter

In the first simulation, azimuth and elevation deviations are equal in each step and the deviations are changing between 0.5° and 4°. Moreover TOA deviation varies between 0.8 μsec to 0.1 μsec. For hybrid ML algorithm, both angle and TOA

deviations varies in each step and these deviations are labeled at the upper and lower x-axes of the performance plot seen in Figure 5.8.

When the performance plot is investigated, it is seen that the AOA based algorithms have better performance than TDOA based localization techniques. The reason of this situation is directly relevant with the selected angle and TOA deviations. The performance of the hybrid algorithm is better than both AOA based and TDOA based localization methods.
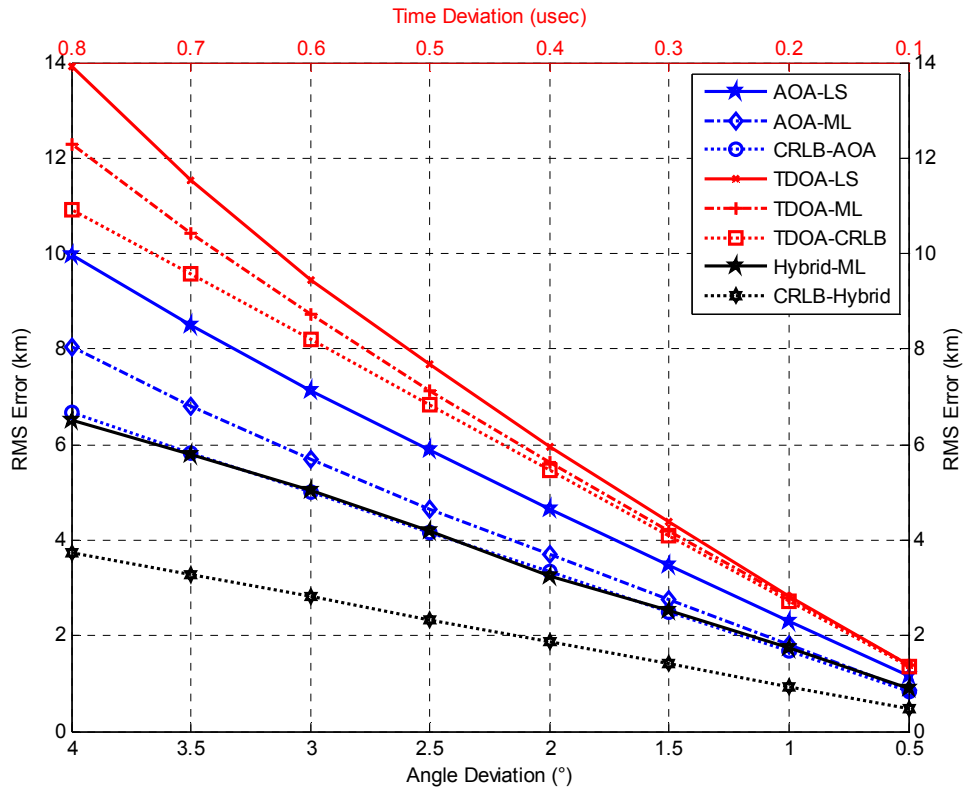
Figure 5.8: 3D Performance Comparison of Conventional Two Step Algorithms for Different Angle Deviations $\sigma_\theta = \sigma_\phi$ and TOA Deviations σ_τ

Actually, the aim of this simulation is to show the performance improvement by merging the AOA and TDOA measurements for hybrid localization.

As seen from Figure 5.8, the ML algorithm gives better performance than LS algorithms for AOA and TDOA based localization. Moreover the Hybrid ML

algorithm outperforms both AOA and TDOA based ML methods. By combining the independent angle and TDOA measurements, minimum achievable RMS error value, namely, CRLB, becomes lower than the CRLB of AOA based localization and CRLB of TDOA based localization in hybrid processing. However, it is obviously seen that the performance improvement in AOA-TDOA Hybrid method does not seem very important at low angle deviations with respect to the other methods.
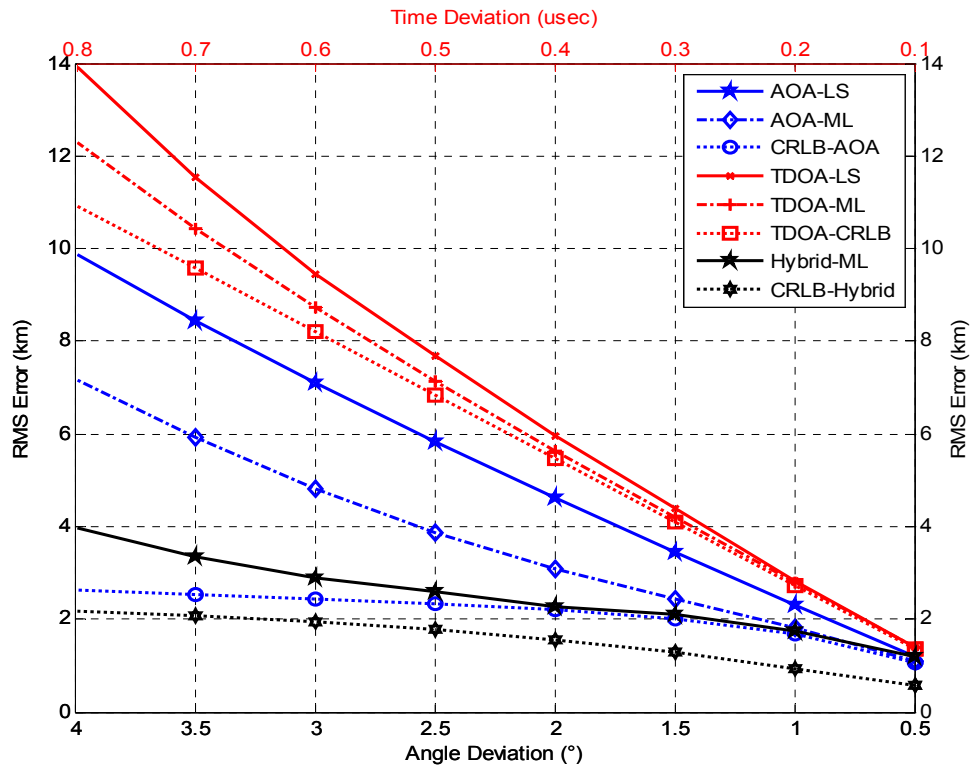
Figure 5.9: Performance Comparison of Conventional Two Step Algorithms for Different Azimuth Deviations σ_θ and TOA Deviations σ_τ with fixed Elevation Deviation $\sigma_\phi = 1°$

As a second simulation, the elevation deviation is fixed to 1°, and azimuth deviation is changing between 0.5° and 4°. Moreover TOA deviation varies between 0.8 µsec to 0.1 µsec. As seen in Figure 5.9, TDOA based localization algorithms and the CRLB of TDOA based localization stay the same with the previous simulation since the TOA deviations are the same. The performance of the AOA based LS algorithm

degrades with respect to the AOA based CRLB. The performance of AOA based ML algorithm and hybrid based ML algorithm become better with fixed elevation deviation.

The CRLBs for hybrid and AOA based localization become lower for higher azimuth deviation values with respect to the previous analysis.
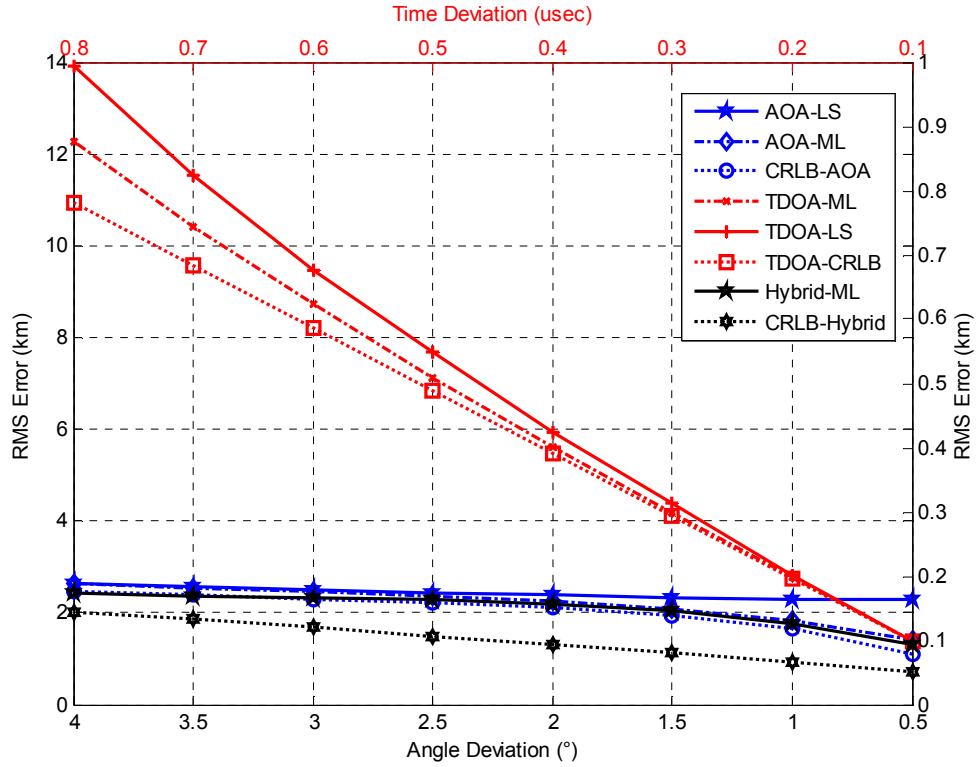
Figure 5.10: 3D Performance Comparison of Conventional Two Step Algorithms for Different Elevation Deviations σ_ϕ and TOA Deviations σ_τ with fixed Azimuth Deviation $\sigma_\theta = 1°$

As a third simulation, the azimuth deviation is fixed to 1°, and the elevation deviation is changing between 0.5° and 4°. Moreover TOA deviation varies between 0.8 μsec to 0.1 μsec. As seen in Figure 5.10, TDOA based localization algorithms and the CRLB of TDOA based localization stay the same with the previous simulations since the TOA deviations are the same. The performances of AOA based ML algorithm and hybrid based ML algorithm become better with fixed azimuth deviation.

The CRLBs for hybrid and AOA based localization become lower for higher azimuth deviation values with respect to the previous analysis.

The performance of the AOA based LS algorithm becomes better with respect to the AOA based CRLB. However the performance of the AOA based LS method seems like not changing with the elevation deviation in Figure 5.10. For closer investigation the performance plot is zoomed near the relevant region as shown in Figure 5.11.
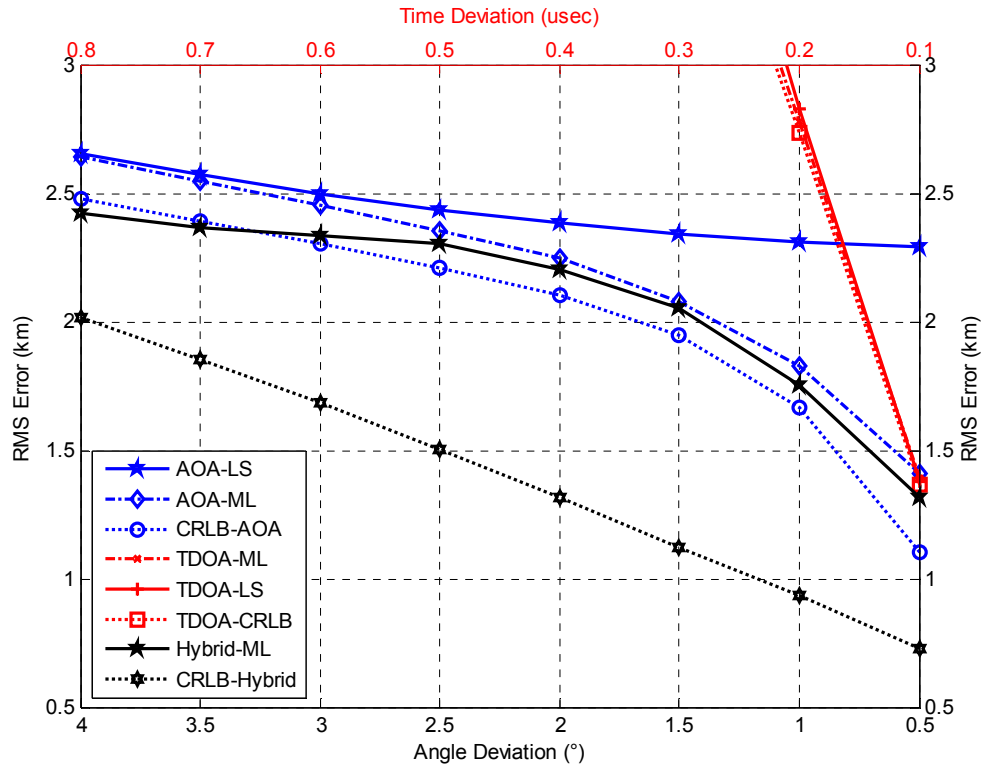
Figure 5.11: 3D Performance Comparison of Conventional Two Step Algorithms for Different σ_ϕ and σ_τ with $\sigma_\theta = 1°$; (Zoomed)

When closer investigation is performed, it is seen from Figure 5.11 that the performance of the AOA based LS method improves slightly with a decreasing elevation deviation.

As a last simulation for conventional two step algorithms, azimuth and elevation deviations are equal in each step and the deviations are changing between 0.5° and 4°. Moreover TOA deviation is fixed to 0.5 µsec, which means 150m ROA deviation.

As shown in Figure 5.12, the performance of the hybrid based ML algorithm and the relevant CRLB are affected from the fixed TOA deviation. The performances of the Hybrid and AOA based methods become similar at low angle deviations due to the fixed TOA deviation. It is obviously shown that previous linear characteristics (see Figure 5.8) of the performance of the Hybrid method and Hybrid CRLB become corrupted with fixing the TOA deviation.
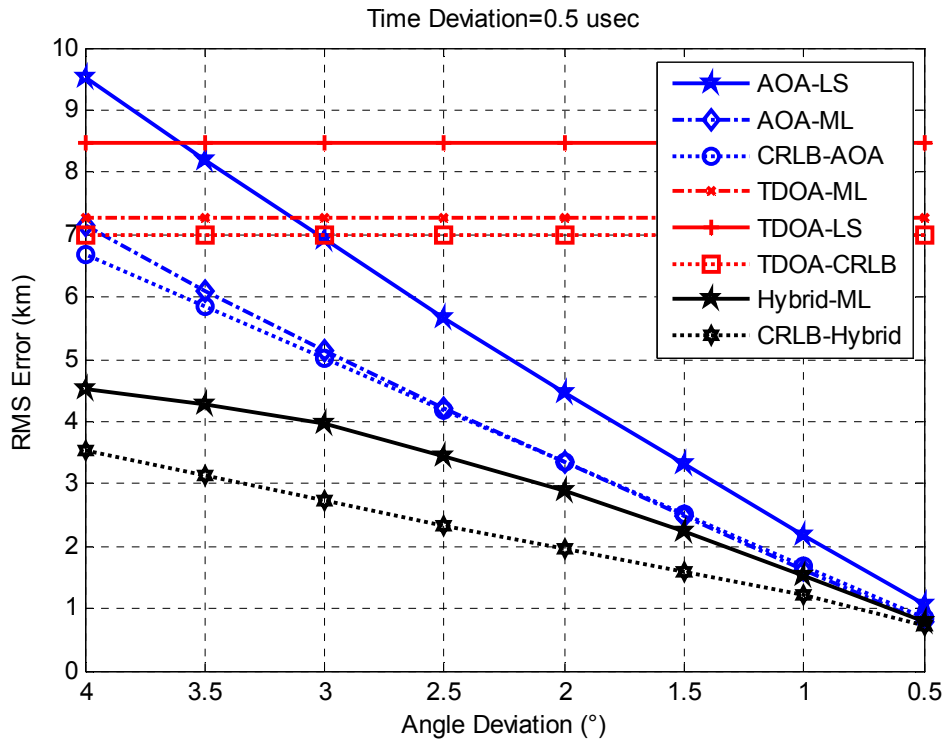

Figure 5.12: 3D Performance Comparison of Conventional Two Step Algorithms for Different Angle Deviations σ_θ and σ_ϕ with fixed TOA Deviation $\sigma_\tau = 0.5 \ \mu sec$

5.1.4 Comparison of Single Step Localization Techniques

By using the same octahedron geometry, the 3D performances of the single step algorithms are investigated.

In the single step performance comparison simulations, 5-element Uniform Linear Array (ULA) with $0.5 \ \lambda$ sensor separation is used in each sensor array, where λ is

the wavelength. Only one frequency bin is used to estimate the target location, and 100 snapshots are calculated for this frequency bin.

After generating the snapshot model for each sensor, additive white Gaussian (AWG) noise is added to the observation with various SNR values. The noise is independent from the signal waveform and the independent between the sensors.

The single step algorithms are Direct Position Determination, MUSIC, DML and SML methods which are presented in sections 4.2.2, 4.2.3, 4.2.4 and 4.2.5 respectively. Moreover the performances of the algorithms are compared with the CRLB of single step source localization which is given in section 4.3. In the simulation, 100 experiments have been performed for each SNR value.

Actually, it is a fact that 2D AOA estimation cannot be performed with a ULA since the θ and ϕ separation cannot be solved with phase difference measurements in one dimension. However, by using TOA information which is embedded in the gross manifold model, this problem is solved. This is another advantage of the single step methods tried to be illustrated in Figure 5.13.
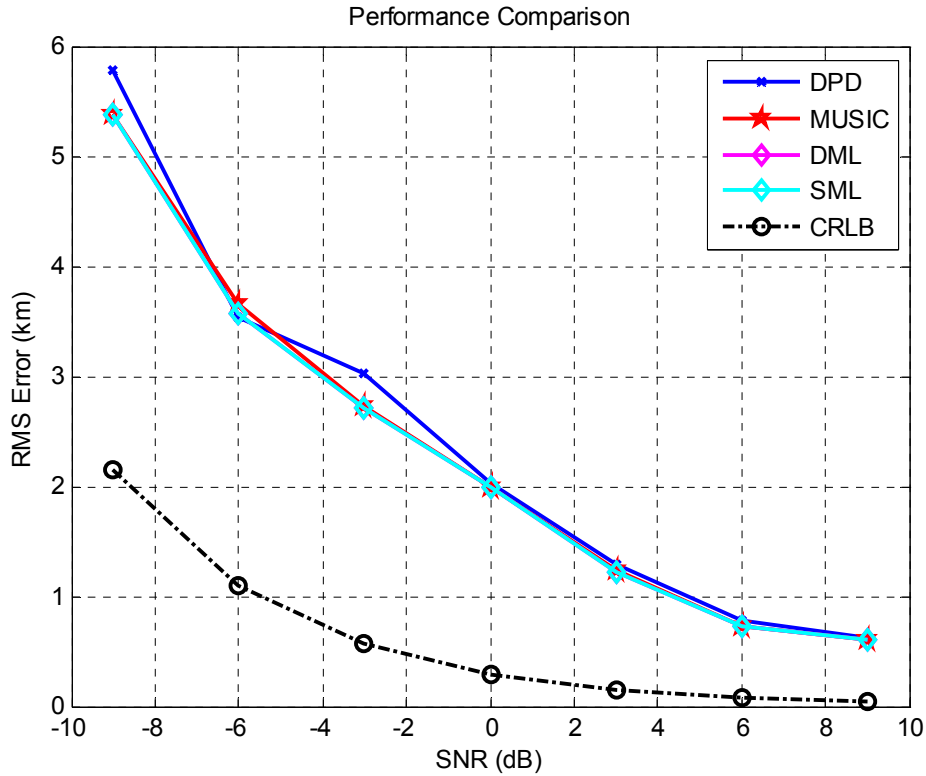
Figure 5.13: 3D Performance Comparison of Single Step Algorithms for Different SNR Values

The SNR value varies between -9 dB to 9 dB with 3 dB steps. It is seen from the above figure that all of the algorithms are working in low SNR values, which cannot be performed with conventional two step techniques. The main source of this performance improvement is on the array gain. In other words, in the observation period, the signal components of the observations are added since the signal components observed by the sensors are coherent, whereas noise components cannot be added since the noise is independent between the sensors.

As seen from Figure 5.13, the performances of the algorithms seem to be the same. However, the RMS errors of the algorithms are higher than the CRLB of single step localization, which means that all algorithms still are not efficient localization approaches.

As a second simulation for single step algorithms, the effect of snapshot number is investigated. The snapshot number logarithmically varies between 64 and 1024. The snapshots numbers are [64, 128, 256, 512, 1024].
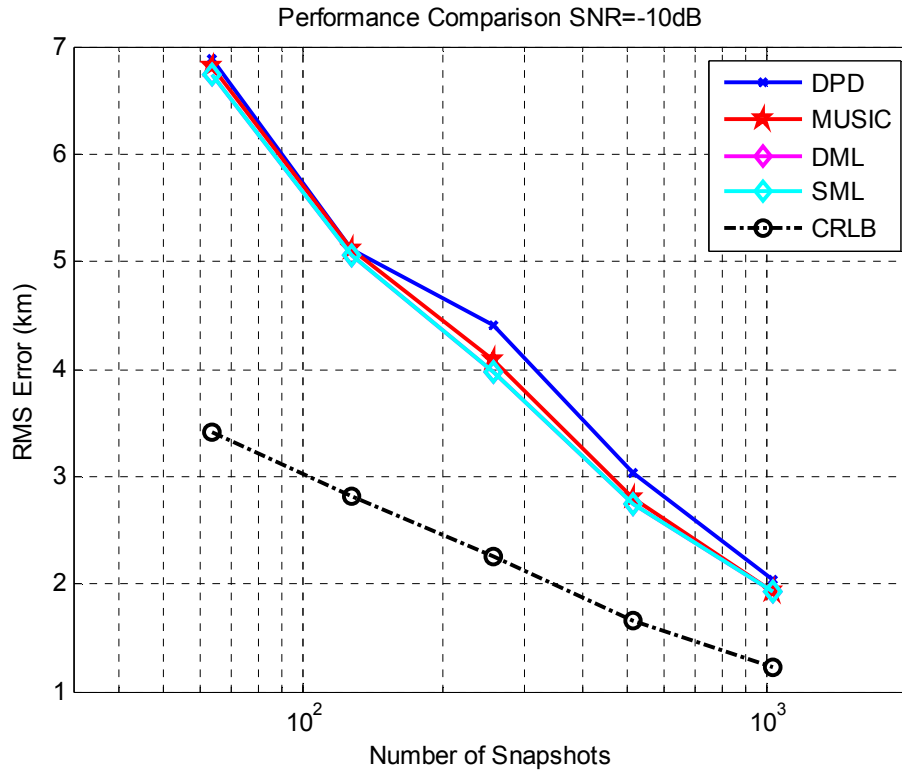
Figure 5.14: 3D Performance Comparison of Single Step Algorithms for different number of snapshots with -10 dB SNR value

When the snapshot number is changing, SNR value is fixed to -10 dB in all sensor arrays. It is seen from Figure 5.14 that, MUSIC, DML and SML give little bit accurate target location estimates than DPD in high number of snapshots.

Note that in these single step simulations 6 sensor arrays (ULA) with each of 5 elements are used. That means observations are collected via 30 independent channels, which is the main source of the performance improved of single step algorithms. However, more fair simulations are performed in section 5.2 to show that the single step algorithms outperform conventional two step algorithms.

5.1.5 Geometrical Effects on the Localization Methods

In this part of the simulations, the geometrical effects on the source location problem are investigated. It is known that the performance of the TDOA based algorithms highly depends on the sensor-target geometry. Moreover, the performances of the AOA based algorithms are affected with the array-target geometry, which is tried to be illustrated in section 3.1.4 by defining and giving different error ellipses.

In this part, mainly two different geometrical effects are illustrated. In the first simulation step, the coordinate of the first sensor array varied, whereas in the second simulation step, the target coordinate is varied in each Cartesian dimension.

In the first simulation the sensor arrays are located at (0 0 Z; 7.0711 7.0711 0; -7.0711 7.0711 0; 7.0711 -7.0711 0; -7.0711 -7.0711 0) such as a pyramid deployment.
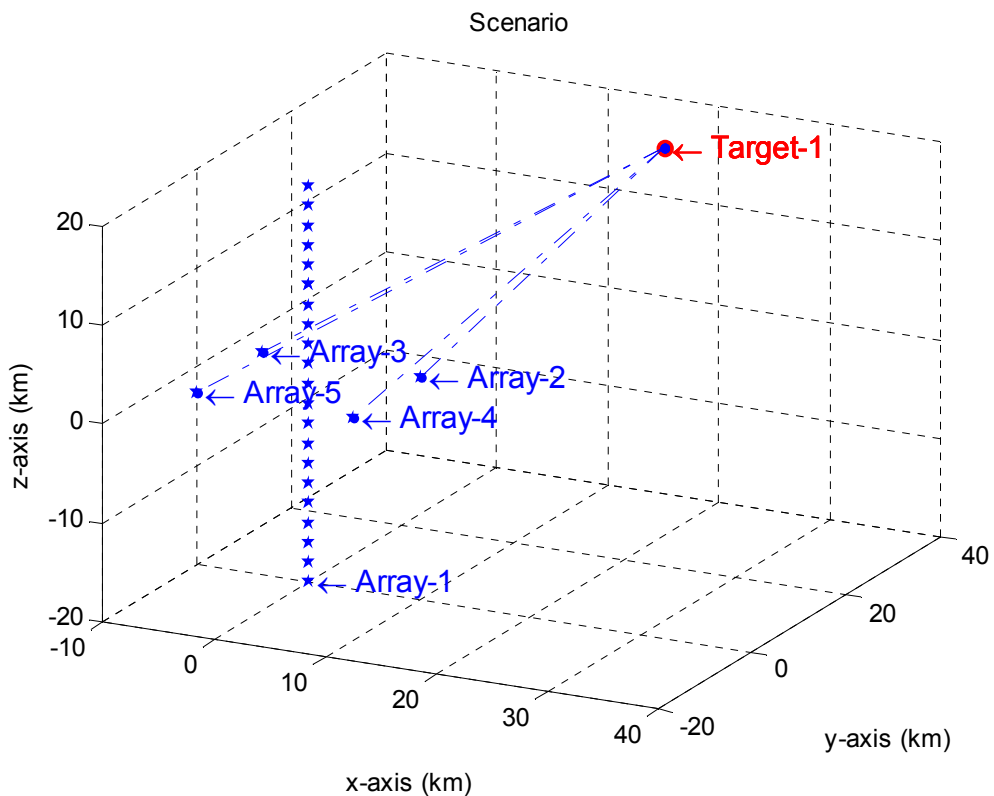
Figure 5.15: Geometrical Scenario: Effect of Sensor Array Location

Moreover the target is located at (15, 40, 15). The z-coordinate of the first array varies between 20 and -20 with 2km steps. The geometrical scenario is shown in Figure 5.15. The aim is to see the effects of planar or near planar sensor array deployment on the performances of the methods. In these simulations (geometrical effects) only the CRLBs are compared to see the geometrical effects on minimum achievable RMS errors, in other words, to see the geometrical effects on parameter estimation and source location with pre-measured parameters.
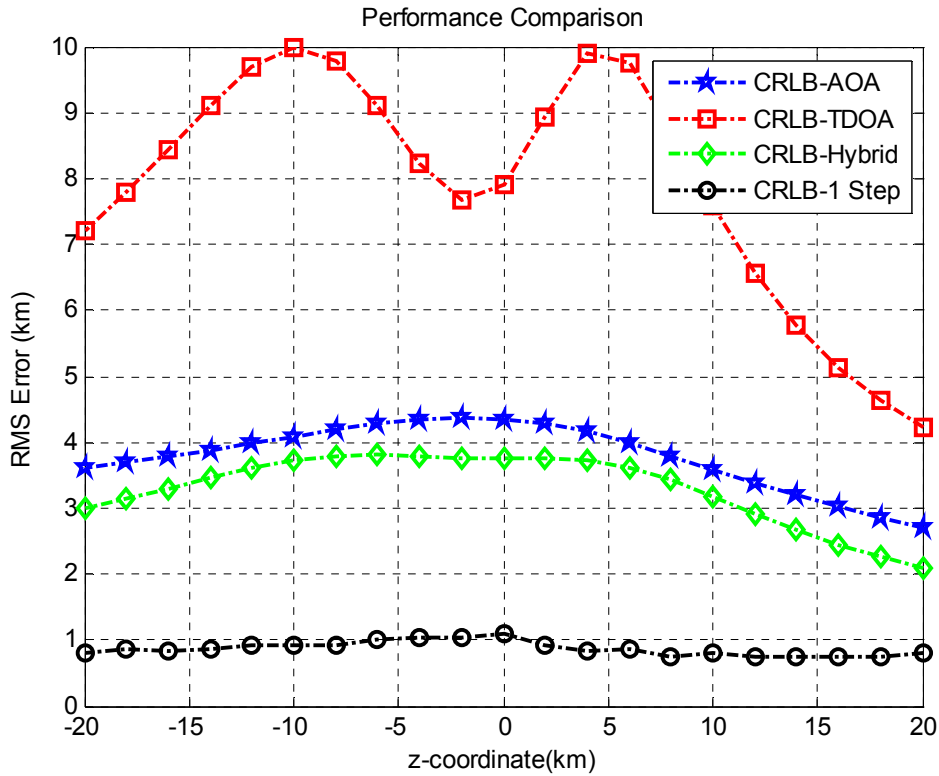
Figure 5.16: Comparison of Lower Bounds for Changing Sensor Array Location

When the z-coordinate of the first sensor array varies between 20 and -20, the azimuth and elevation deviations are fixed to 2°, the TOA deviation is fixed to 0.4 µsec and the SNR is fixed to 0 dB for CRLB calculations. CRLB values for AOA based localization, TDOA based localization, AOA-TDOA based hybrid localization and the single step localization are calculated for each geometric scenario. For single step localization, in each sensor array 5 element ULA is used. Moreover 100 snapshots are taken from each sensor for only one frequency bin.

It is obvious from Figure 5.16 that, all of the lower bounds are affected from the varying sensor array coordinate. However, TDOA based lower bound is more affected than the others. The reason of the fluctuating response in TDOA based localization is due to the parameter estimation performed between separate sensors. In AOA based localization angle measurements are independent between the sensor arrays, whereas, TDOA is calculated via correlating the observations taken from separate sensors. When the TDOA values between the sensor arrays become closer, the lower bound becomes higher. It is seen from Figure 5.16 that hybrid based lower bound gives a response better than the AOA and TDOA based lower bounds. Hybrid based lower bound becomes constant between the z-coordinate values -10 and 5. Finally, it is obvious that single step based lower bound is the least dependent on the array deployment geometry.
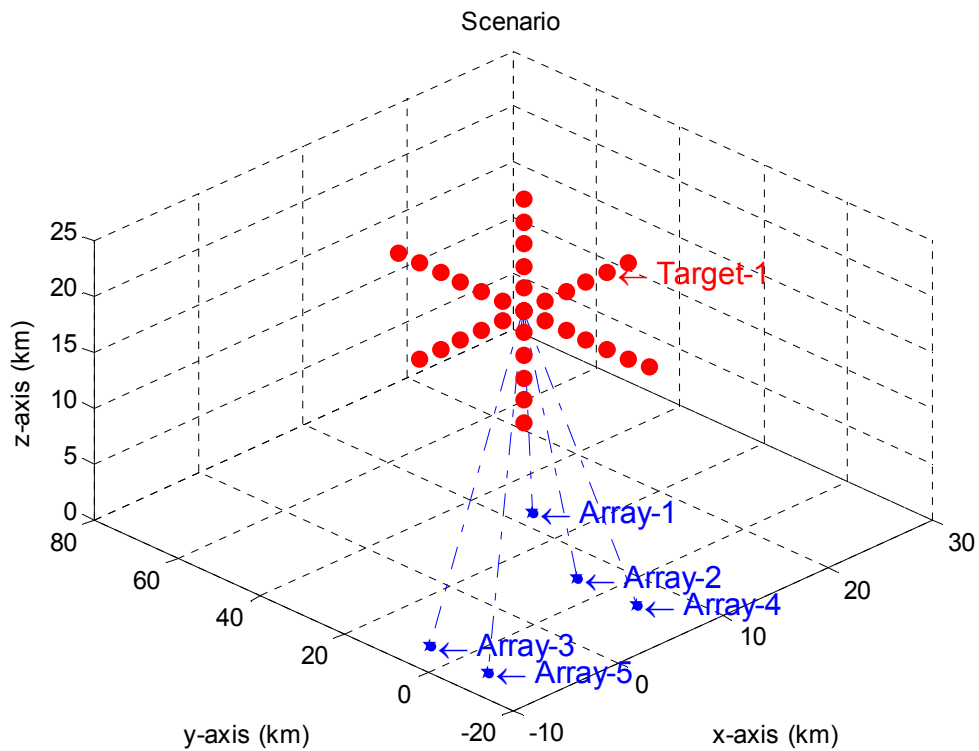
Figure 5.17: Geometrical Scenario: Effect of Target Location

As a second simulation to see the geometrical effects on the performance, the coordinates of the sensor arrays are fixed to (0 0 10; 7.0711 7.0711 0; -7.0711

7.0711 0; 7.0711 -7.0711 0; -7.0711 -7.0711 0) and the target coordinate is changing near the same target coordinate mentioned in the previous simulations. The axial coordinates of the target is varied in each step of this simulation. The x and z coordinates of the target varies between 5 to 25 with 2km steps, whereas the y coordinate varies between 10 to 70 with 5 km steps. The geometrical scenario is illustrated in Figure 5.17.

Deviations of the parameters, namely, azimuth, elevation and TOA deviations are the same with the previous simulations ($\sigma_\theta = \sigma_\phi = 2°$ and $\sigma_\tau = 0.4\,\mu sec$). Moreover all of the parameters are the same for the single step localization (5-element ULA, SNR=0dB, Number of Snapshots=100).

First, the effect of the x-coordinate of the target is investigated. 1000 experiments have been performed for each geometrical scenario.
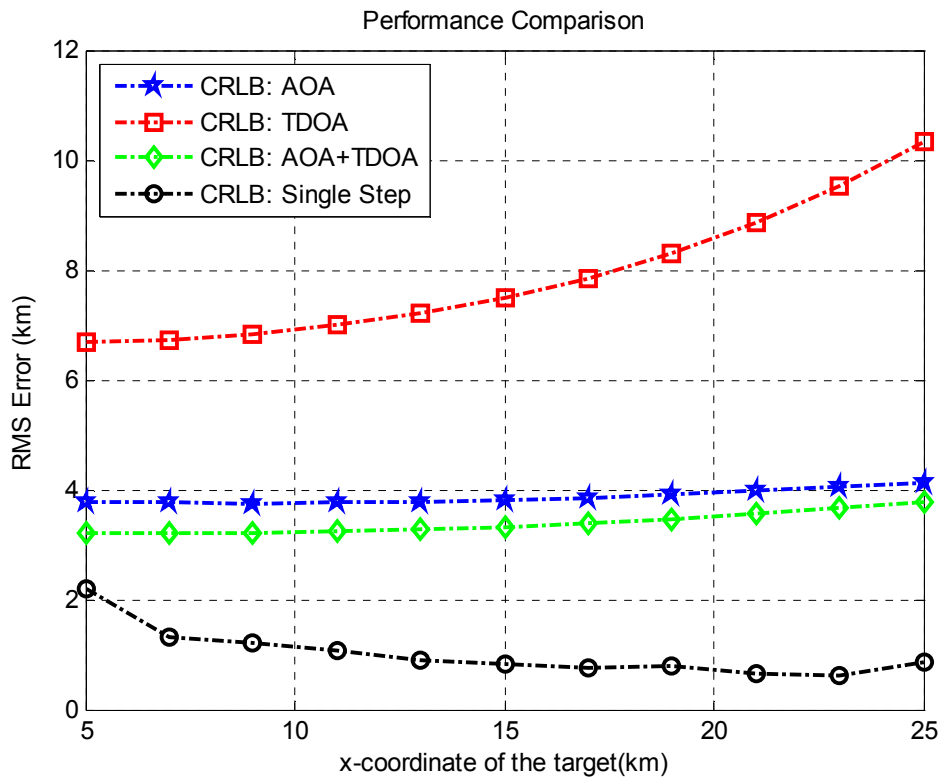
Figure 5.18: Comparison of Lower Bounds for Changing x-Coordinate of the Target

In the simulation shown in Figure 5.18, it is shown that AOA based lower bound is the least dependent on this situation. TDOA based lower bound becomes higher with an increasing x-coordinate of the target since the TDOA values measured between the sensors become closer to each other.
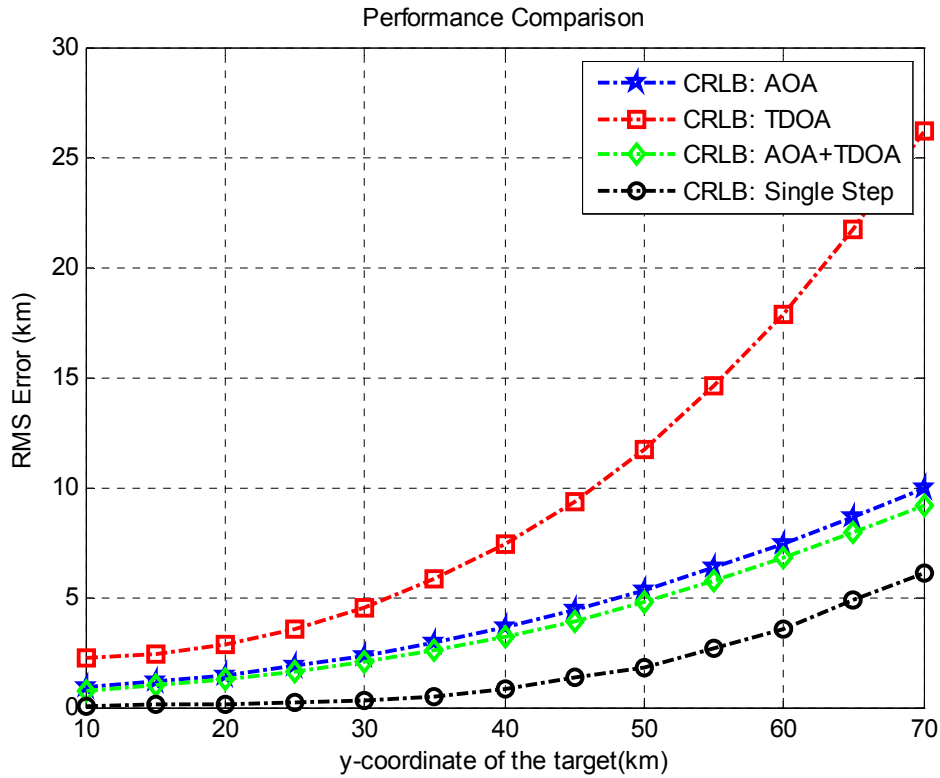
Figure 5.19: Comparison of Lower Bounds for Changing y-Coordinate of the Target

Second, the effect of the y-coordinate of the target is investigated. It is shown from Figure 5.19 that, all of the lower bounds are affected with the varying y-coordinate of the target. The effects of geometrical deployment on AOA based localization is mentioned in section 3.1.4. The effect of deployment geometry on TDOA based localization is shown in previous simulations. In this simulation, it is shown that the lower bound for single step localization is affected with the target coordinate.

Finally, the effect of the z-coordinate of the target is investigated. This investigation is presented in Figure 5.20.
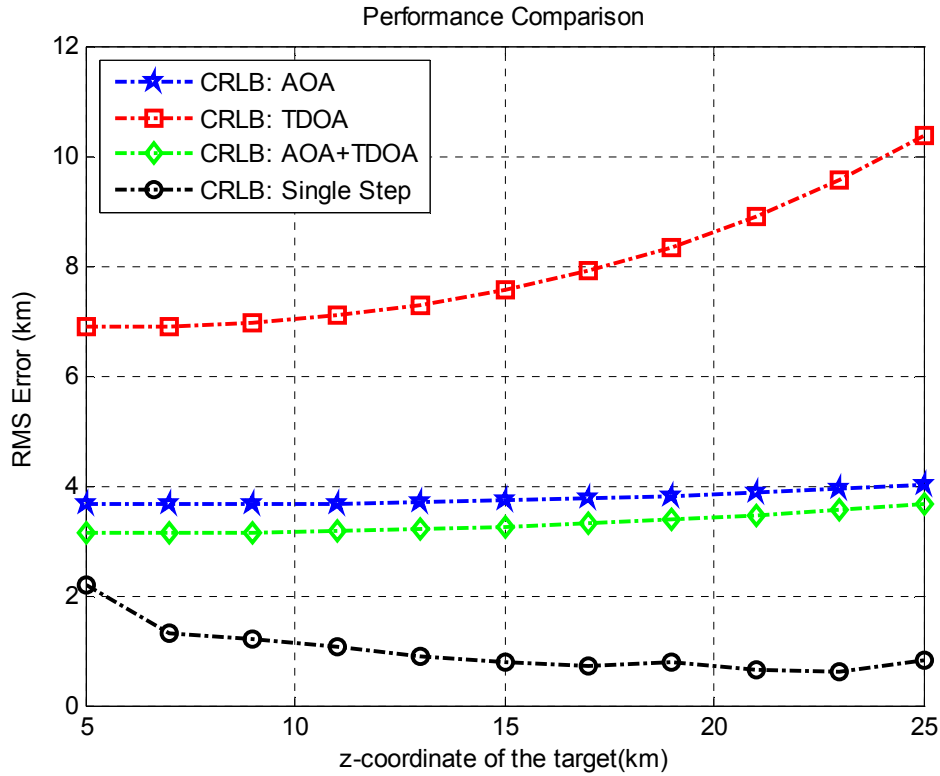
Figure 5.20: Comparison of Lower Bounds for Changing z-Coordinate of the Target

It is shown that AOA based lower bound is the least dependent on varying z-coordinate of the target. TDOA based lower bound becomes higher with an increasing z-coordinate of the target since the TDOA values measured between the sensors become closer to each other. Moreover, lower bound for the single step localization becomes higher for low values of the target's z-coordinate.

5.2 COMPARISON OF THE ALGORITHMS UNDER MULTIPLE SOURCES CASE

In this part of the simulations, fair comparison between the single step localization methods and the conventional two step methods are presented. Simulations are performed in 2D geometry since single step algorithms are computationally very costly.

DPD, Direct Localization with MUSIC, DML and SML techniques are single step localization techniques, whereas AOA ML estimation with Brute Force Data

119

Association algorithm (BFA) is used as a two step localization method. TDOA based localization hence hybrid based techniques are not investigated in multiple emitters case, since TDOA cannot be measured for completely continuous multiple emitters.

In the simulations, 5-element Uniform Linear Array (ULA) with 0.5 λ sensor separation is used in each sensor array. Two sources are modeled as emitting independent signal waveforms. Only one frequency bin is used to estimate the target location, and N (mentioned in the simulations) number of snapshots are calculated for this frequency bin. After generating the snapshot model for each sensor, additive white Gaussian (AWG) noise is added to the observation with various SNR values. The noise is independent from the signal waveforms and independent between the sensors. In each simulation, 150 experiments have been performed.

Root-MUSIC algorithm is used to estimate the AOA values (for two emitters) in each sensor array. After performing AOA measurements, BFA is used to associate the AOA values for each emitter. By obtaining the associated AOA sets, AOA based ML localization algorithm is used to estimate the target locations.

As mentioned in the previous simulations, target coordinates are estimated directly by the single step algorithms.

Moreover, both AOA based and single step localization lower bounds are compared with each simulation.

The simulations consist of three main parts. The first two parts are performed to investigate the geometrical effects on the methods, whereas the last part is performed to investigate the resolvability skills of the algorithms.

5.2.1 Comparison of the Algorithms under Optimum Geometry

Optimum deployment scenarios for AOA based localization are investigated in section 3.1.4 by illustrating error ellipses. As seen from the mentioned analyses, the major and minor radiuses of the error ellipse become smaller when the target is surrounded by the sensor arrays.

In the simulations, 4 sensor arrays (ULA with 5 element) and 2 sources are used. The Cartesian coordinates of the targets are (30, 50) and (70, 50), whereas the positions of the sensor arrays are (-5 -5; -5 105; 105 -5; 105 105). The deployment scenario is shown in Figure 5.21.
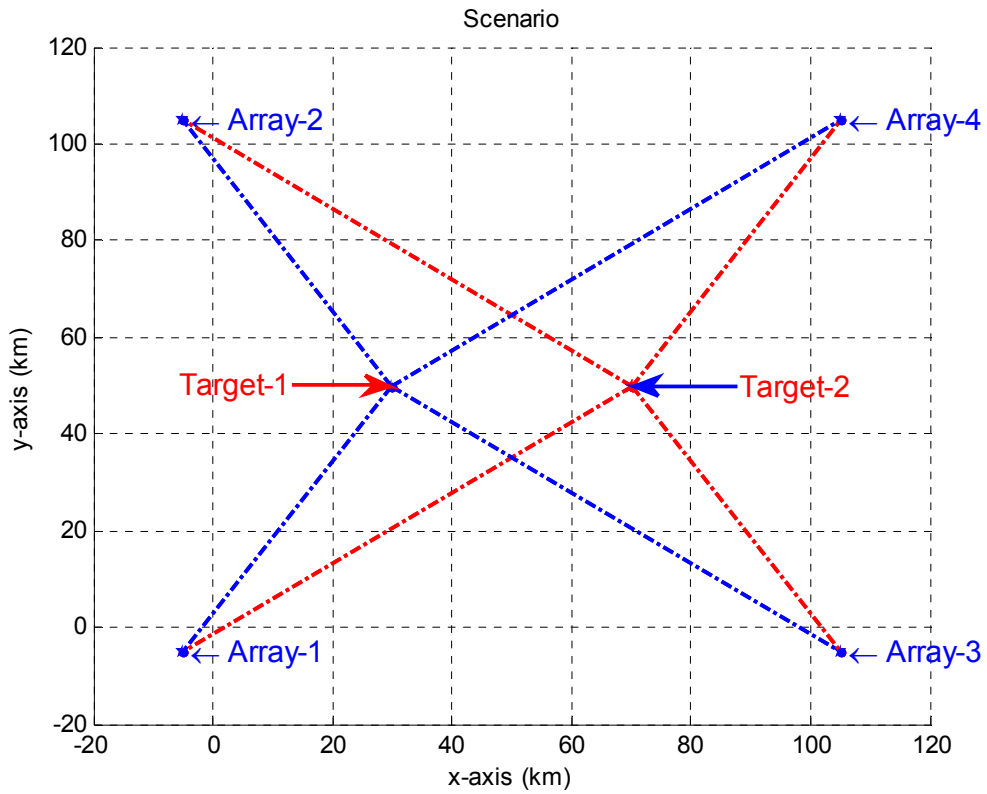
Figure 5.21: Multiple Source Scenario-1: Locations of Sensor Arrays and the Emitters

The number of snapshots are fixed to 100 for only one frequency bin. The first analysis is performed with varying SNR values between -9 to 9 dB with 3 dB steps. The result of this simulation is shown in Figure 5.22. AOA based ML localization technique gives efficient estimation response when it is compared with the AOA based CRLB.
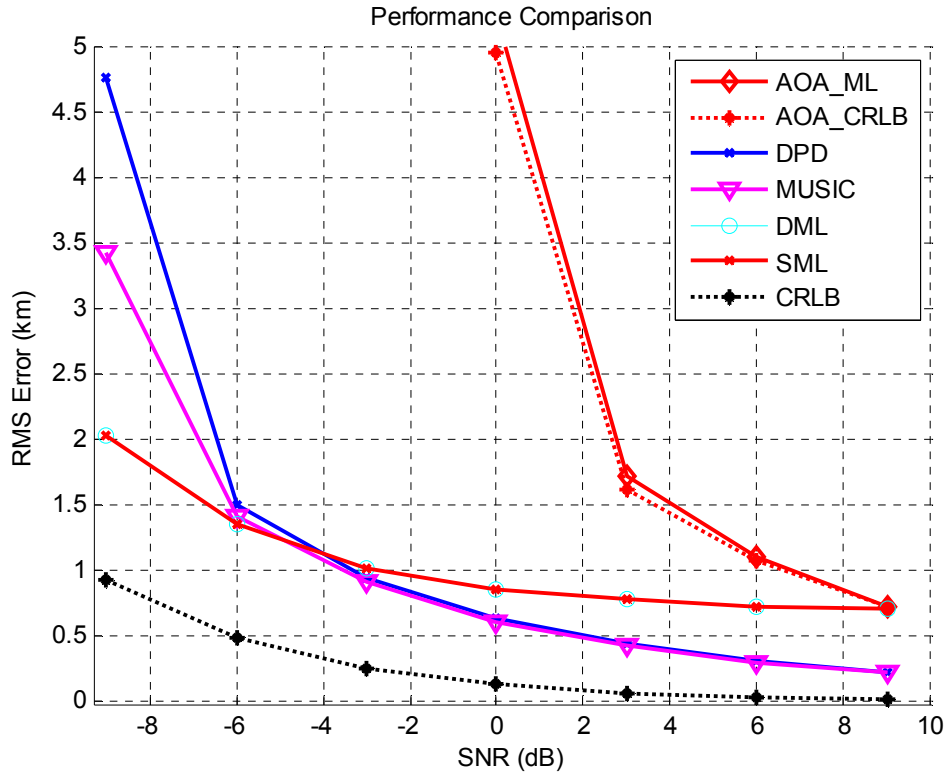
Figure 5.22: Performance Comparison of the Techniques with changing SNR value for Multiple Source Scenario-1

The single step algorithms outperform the conventional AOA based localization technique. Moreover the single step performances are much lower than the minimum achievable AOA based localization error. The DML and SML algorithms give the best performances in low SNR values, however at high SNR the performances of the algorithms degrade with respect to those of MUSIC and DPD methods. Lastly, it can be seen that MUSIC outperforms the DPD at low SNR values with the given number of snapshots (100).

The second analysis is performed by varying the number of snapshot values (64, 128, 256, 512, 1024) for different SNR values such as -10 dB and 0 dB. The performance comparison of the algorithms with SNR value fixed to -10 dB is shown in Figure 5.23. AOA based method and the CRLB are not shown in the figure, since AOA based localization does not work in such low SNR value. It is seen that when the number of snapshots is 64 (with RMSEs of 10km), none of the

algorithms perform source localization. By increasing the number of snapshots, algorithms start to work, and become closer to the lower bound.
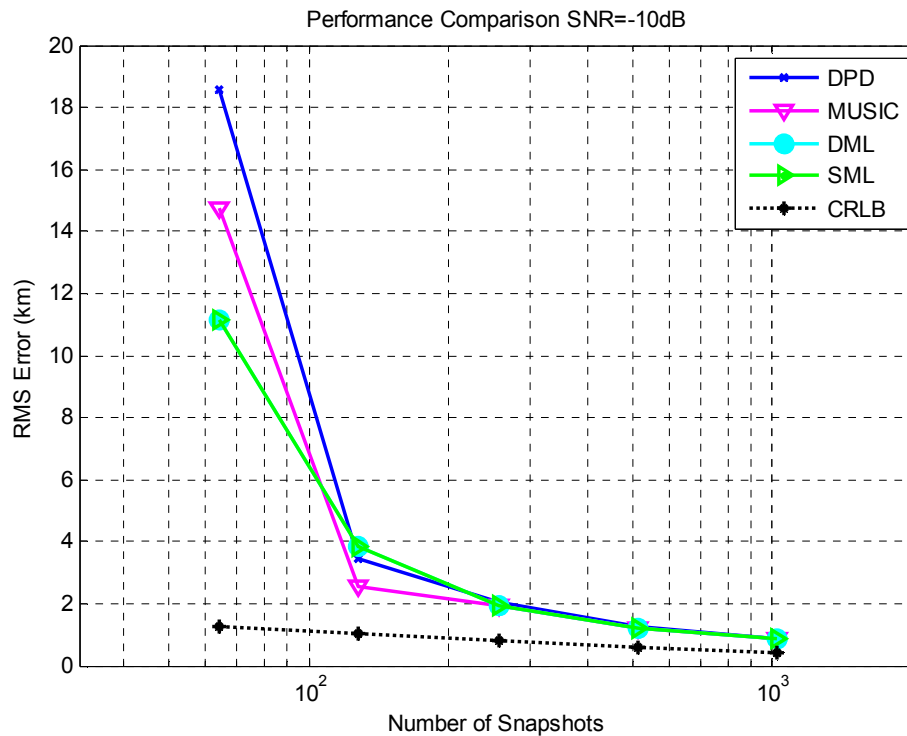
Figure 5.23: Performance Comparison of the Techniques with Changing Number of Snapshots and fixed -10 dB SNR value for Multiple Source Scenario-1

Finally, when the number of snapshots region between 128-1024, MUSIC outperforms all of the algorithms, which is a result of using noise space in source localization.

When SNR value is fixed to 0 dB, the performance comparison of the algorithms with varying number of snapshots is shown in Figure 5.24. It is seen that AOA based localization starts to work with relative high SNR for high number of snapshots, however, there is still a large difference with the performance of the single step algorithms. It is seen that MUSIC algorithm is better than DPD at 0 dB SNR.

As mentioned in the previous simulations performed in 3D geometry, the reason of the performance improvement observed in single step processing is due to the array gain. 20 different sensors are used to estimate the target locations directly in single

step methods, whereas 5 sensors are used to estimate 2 AOA values (2 azimuth angles for 2 sources, see Figure 5.21) in each sensor array for AOA based ML localization.
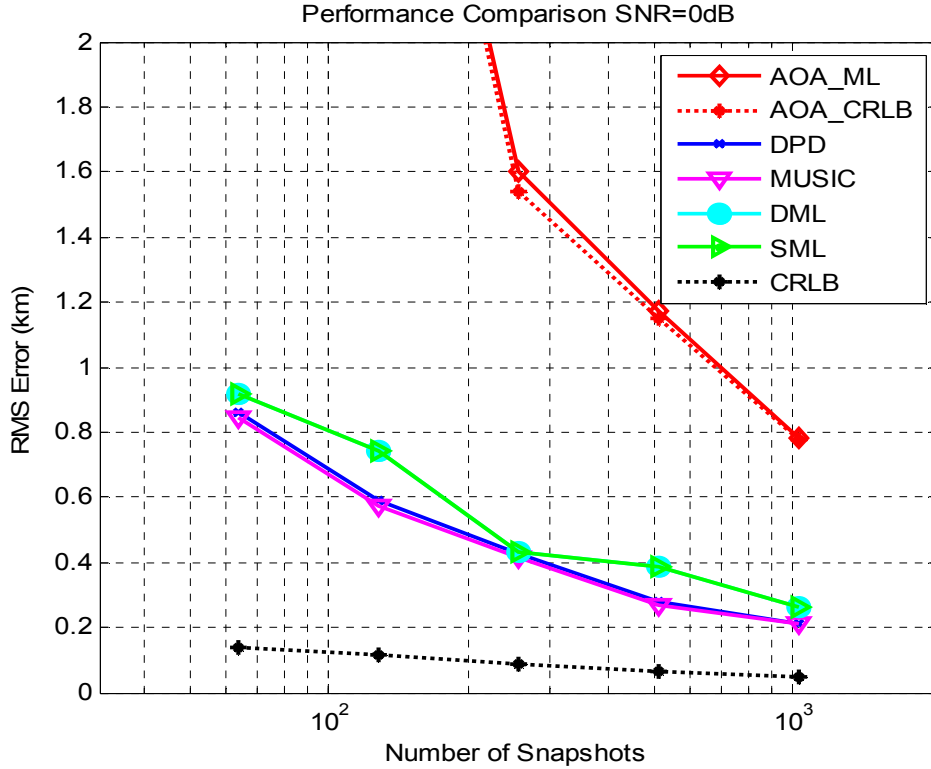
Figure 5.24: Performance Comparison of the Techniques with Changing Number of Snapshots and fixed 0 dB SNR value for Multiple Source Scenario-1

5.2.2 Comparison of the Algorithms under Practical Geometry

In the previous part, performance comparison between the single step and two step localization methods are tried to be investigated under optimum deployment geometry for two step localization with varying parameters. However, practical deployments may not be realized as an optimum deployment in tactical Electronic Warfare (EW) scenarios. Consequently, in this part of the simulations, similar performance comparisons are performed in more practical deployments.

In the simulations, 3 sensor arrays (ULA with 5 element) and 2 sources are used. The Cartesian target locations are (10, 60) and (90, 60), whereas the positions of the sensor arrays (10 5; 50 15; 90 5). The deployment scenario is shown in Figure 5.25.
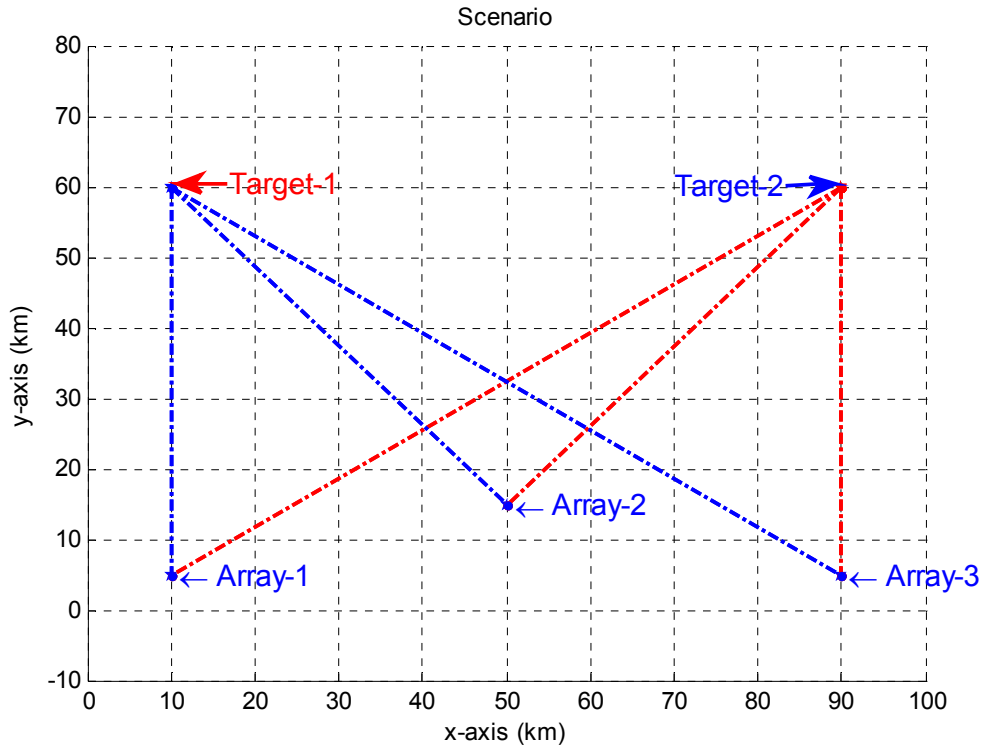

Figure 5.25: Multiple Source Scenario-2: Locations of Sensor Arrays and the Emitters

The number of snapshots are fixed to 100 for only one frequency bin. The first analysis is performed by varying SNR values between -9 to 9 dB with 3 dB steps. The result of this simulation is shown in Figure 5.26. AOA based ML localization technique gives efficient estimation response when it is compared with the AOA based CRLB. However, when it is compared with the previous simulation geometry, AOA performance becomes better. The reason of this situation is the relative angle separation between the targets relative to the sensor arrays. In other words, in the previous simulation geometry, the targets are angularly close to each other and Root-MUSIC algorithm cannot resolve the AOAs of the targets. But, in these simulations, angle separation is wide enough for Root MUSIC algorithm as seen from geometrical scenario given in Figure 5.25. Extensive resolvability

analyses are presented in section 5.3 for both optimum and practical deployment geometries.
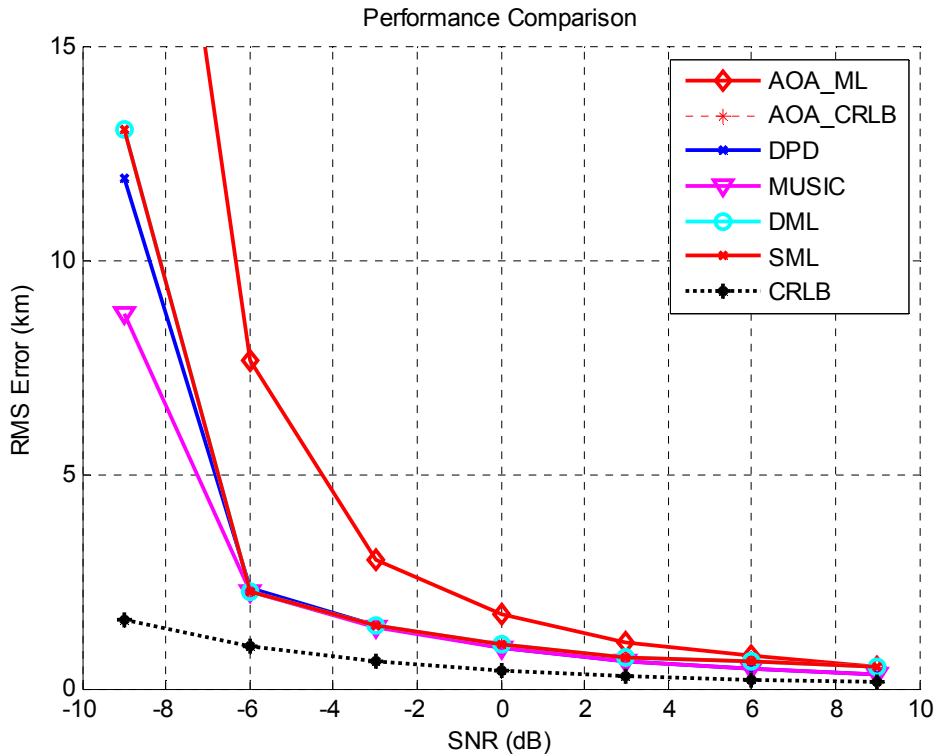
Figure 5.26: Performance Comparison of the Techniques with Changing SNR value for Multiple Source Scenario-2

In the simulation shown in Figure 5.26, it is obviously seen that, single step algorithms give better performance than AOA based ML localization technique as expected. MUSIC algorithm gives the best performance at the low SNR values.

The second analysis is performed by varying the number of snapshot values (64, 128, 256, 512, 1024) for different SNR values such as -10 dB and 0 dB. The performance comparison of the algorithms with SNR value fixed to -10 dB is shown in Figure 5.27. It is seen that none of the algorithms can estimate the source locations at low number of snapshots. Relative to other methods, MUSIC method gives the best performance. However it is still not efficient when it is compared with the single step CRLB. Moreover, by increasing the number of snapshots, algorithms start to work, and become closer to the lower bound.
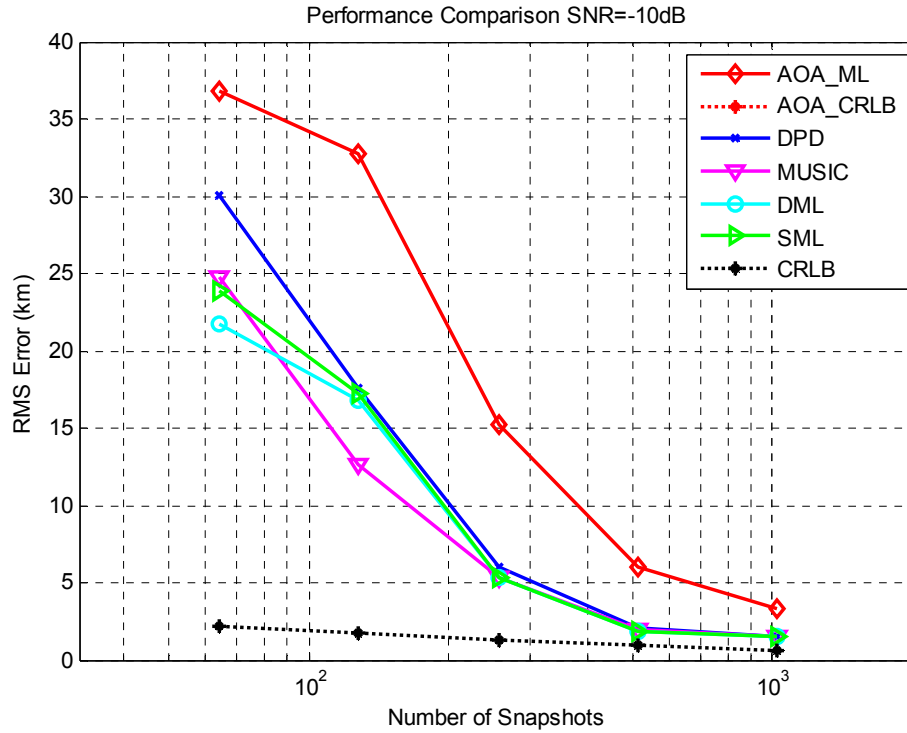
Figure 5.27: Performance Comparison of the Techniques with Changing Number of Snapshots and fixed -10 dB SNR value for Multiple Source Scenario-2

When the SNR value fixed to 0 dB, the performance comparison of the algorithms by varying the number of snapshots is shown in Figure 5.28. It is seen that AOA based localization starts to work closer to the single step methods for $SNR = 0\ dB$. It is seen that MUSIC algorithm is better than DPD at 0 dB SNR and DPD and MUSIC methods are better than SML and DML techniques.

When the results are compared with the optimum and practical deployment geometries, it is seen that the single step methods perform better and the CRLB is lower in the optimum deployment scenario. For the practical deployment given in Figure 5.25, CRLB for the single step algorithms goes higher whereas the AOA based algorithm is less affected in comparison.
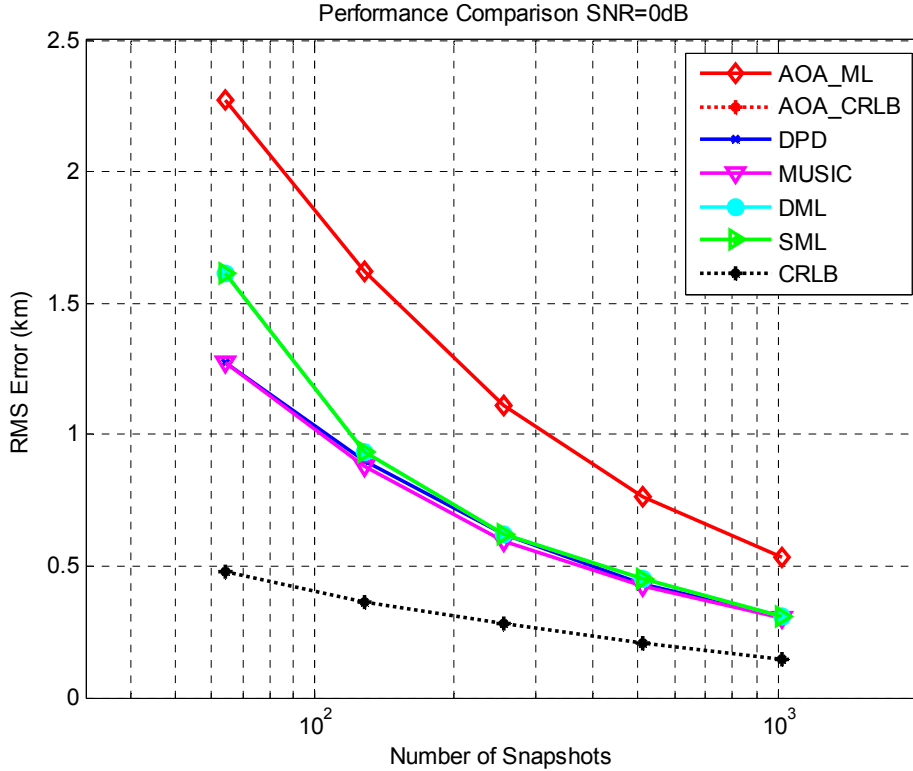
Figure 5.28: Performance Comparison of the Techniques with Changing Number of Snapshots and fixed 0 dB SNR value for Multiple Source Scenario-2

5.2.3 Comparison of the Resolvability Skills of the Algorithms

In this part of the simulations, resolvability capabilities of the single step and two step localization methods are investigated. The simulations are performed for both practical and optimum deployment geometries mentioned in the previous sections.

First, resolvability is analyzed for optimum deployment scenario. The coordinate of the first target is (50, 50) and the coordinate of the second target is (x, 50). The x-coordinates of the second target are (20, 30, 35, 41, 44, 47, 53, 56, 59, 65, 70, 80). The resolvability skills are compared only for changing x-coordinate of the target, since the array deployment has a square shape. In the simulations, 4 sensor arrays (ULA with 5 element) are used. The Cartesian coordinates of the sensor arrays are

(-5 -5; -5 105; 105 -5; 105 105) which is the same as the previous optimum
deployment. The deployment scenario is shown in Figure 5.29.
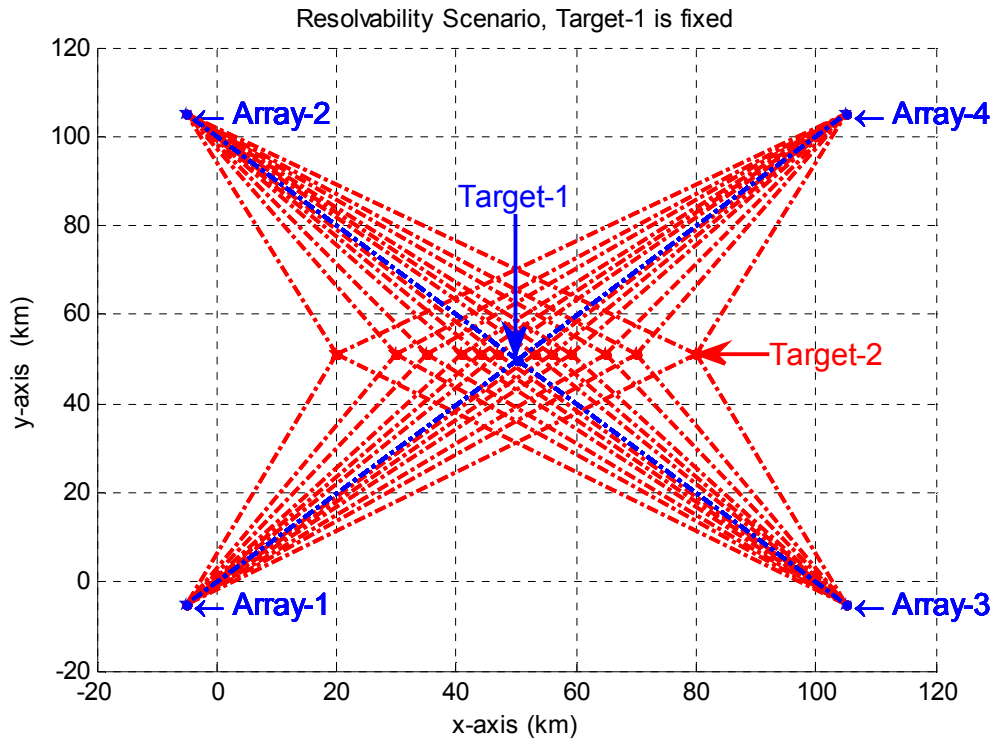
Figure 5.29: Resolvability Analysis for Multiple Source Scenario-1: Target-1 is
fixed and x-Coordinate of the Target-2 is changing

In the simulations, 100 snapshots are used for only one frequency bin, and SNR
value is fixed to 20 dB to investigate the resolvability capabilities of the algorithms
when the targets are close to each other. 150 experiments are performed for each x-
coordinate of the second target.

The resolvability performances of the methods are shown in Figure 5.30. When the
performance of the AOA based ML method is investigated, it is shown that the
algorithm cannot resolve the targets, when the separation between the targets is
lower than 6 km. In other words, when the x-coordinate of the target is 47 or 53,
AOA based ML method has a RMS error around 7 km which is approximately
twice the separation distance.
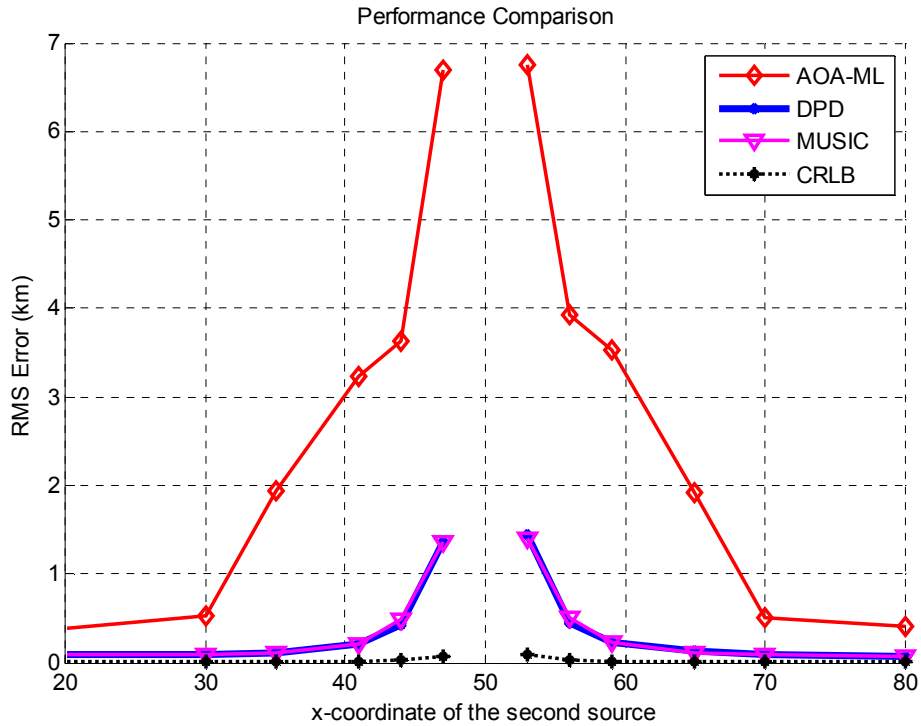
Figure 5.30: Comparison of the Resolvability Performances of the Algorithm with 20 dB SNR value

In the optimum deployment scenario, the performance degradation of the AOA based localization method is due to the insufficiency of the Root-MUSIC algorithm in resolving the closely located emitters. Improvement of localization performance for AOA based location estimation with optimum deployment is presented in Section 3.1.4 with error ellipses.

The second analysis is performed with using the practical deployment mentioned in the previous section. Two different simulations are performed with the practical scenario; both x and y coordinates of the target are varying in the analysis.

The sensor arrays are deployed as mentioned in the previous section, which is considered to be practical deployment. The coordinates of the sensor arrays are (10 5; 50 15; 90 5) and the first target coordinate is fixed to (60, 90). Structure of the sensor arrays (ULA with 5 element), number of snapshots and the SNR value are the same with the previous resolvability analyses for optimum deployment scenario.
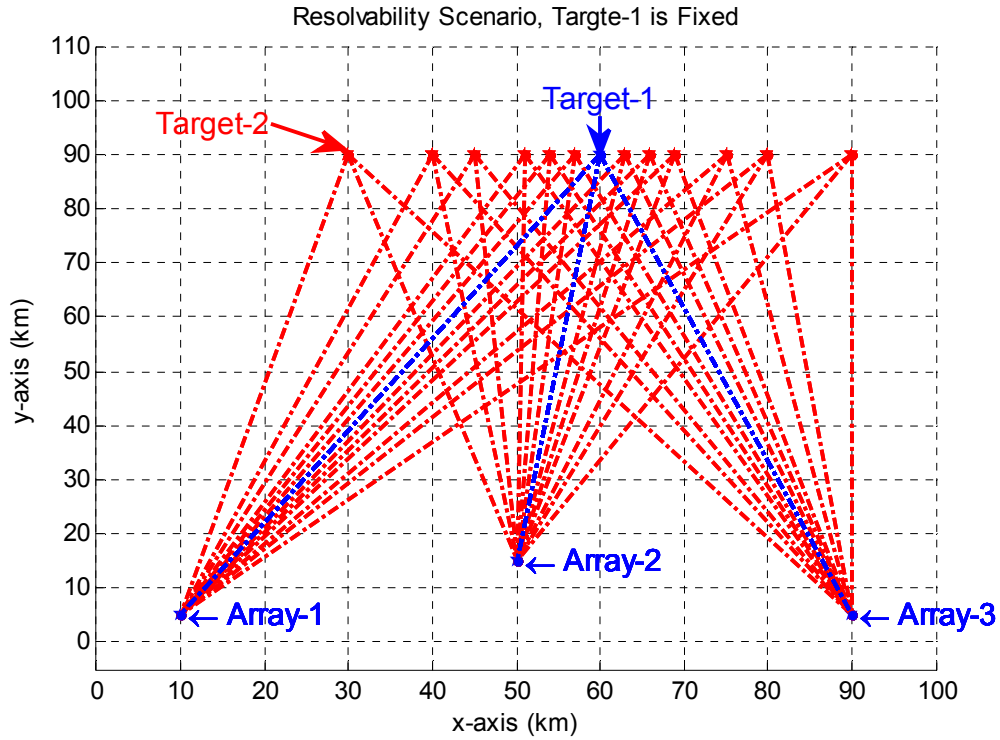
Figure 5.31: Resolvability Analysis for Multiple Source Scenario-2: Target-1 is fixed and x-Coordinate of the Target-2 is changing

As a first investigation, the x-coordinate of the second target is varied between 30 and 90, and the y-coordinate of the second target is 90. The x-coordinate values used in RMSE calculations are (30, 40, 45, 51, 54, 57, 63, 66, 69, 75, 80, 90). The deployment scenario is shown in Figure 5.31.

The resolvability performances of the methods are shown in Figure 5.32. It is shown that AOA based localization performance is improved with respect to the optimum deployment due to the wide angular separation between the targets. In other words, the practical array-target deployment is worse than the optimum deployment for AOA based localization, whereas the practical deployment is better than the optimum deployment for AOA measurement. By combining the two steps, the performance of the conventional method is improved. When the performance of the single step algorithms is investigated, it is shown that algorithms perfectly resolve the emitter when the separation between the emitters are higher than 9 km.

By decreasing the separation distance, algorithms become worse with respect to the single step CRLB.
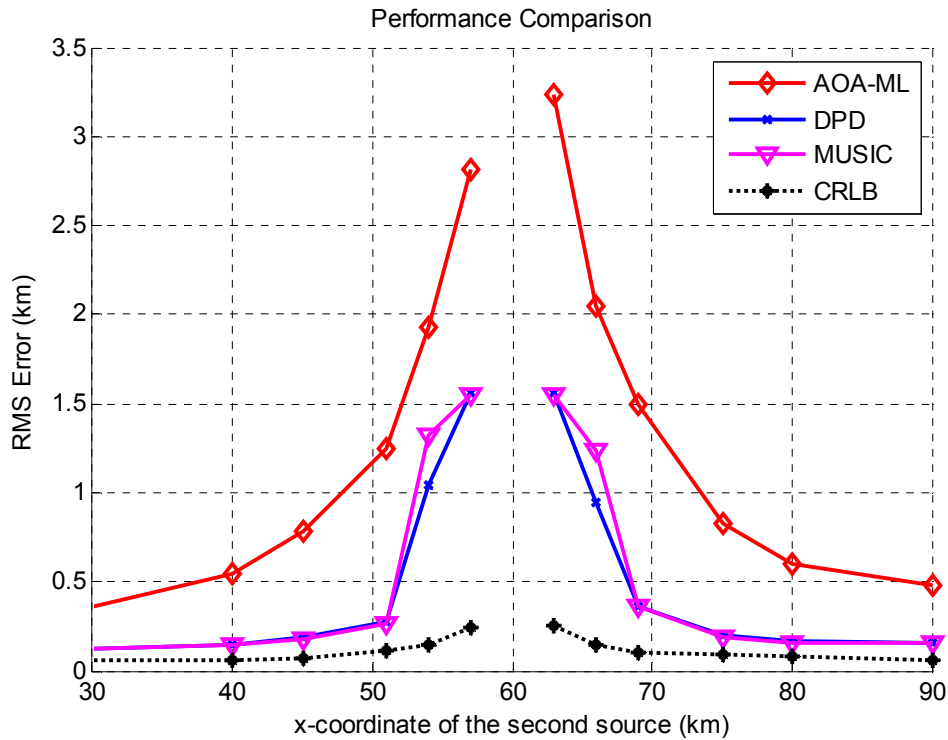
Figure 5.32: Comparison of the Resolvability Performances of the Algorithms with 20 dB SNR value

As a second investigation, the y-coordinate of the second target is varied between 20 and 80. The x-coordinate of the second target is fixed to 60 and the y-coordinate values used in RMSE calculations are (20, 30, 35, 40, 41, 44, 47, 53, 56, 59, 65, 70, 80). The deployment scenario is shown in Figure 5.33. All other parameters such as sensor arrays (ULA with 5 element), number of snapshots and the SNR value are the same with the previous resolvability analysis.

The resolvability performances of the methods are shown in Figure 5.34. It is shown that AOA based localization performance is improved with respect to the optimum deployment due to the wide angular separation between the targets. When the performances of the single step algorithms are investigated, it is shown that algorithms perfectly resolve the emitter when the separation between the emitters are higher than 9 km.
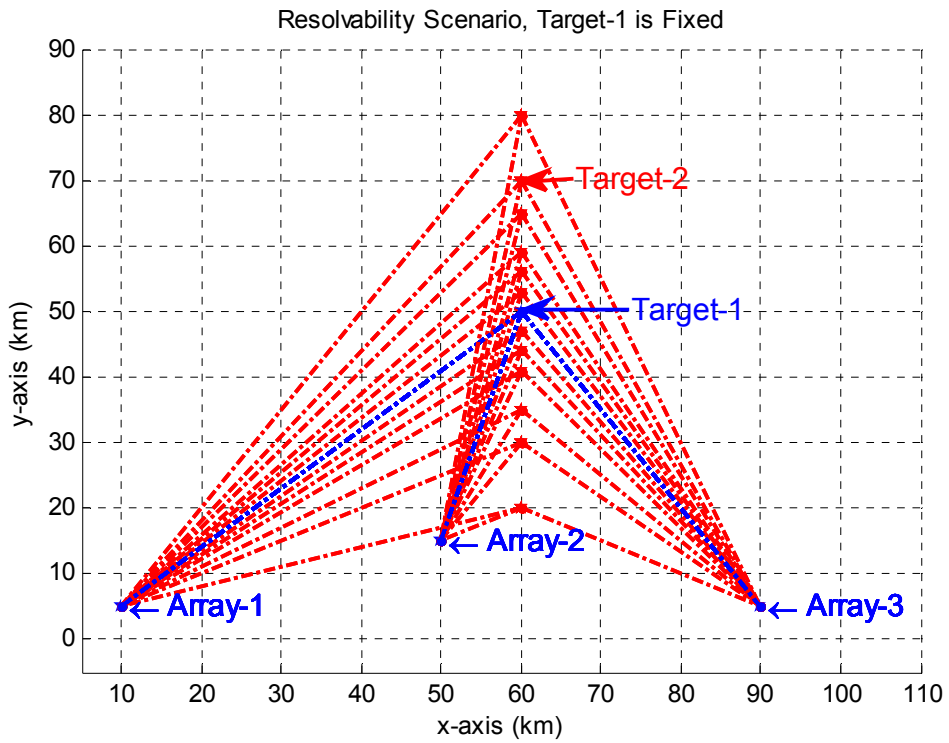
Figure 5.33: Resolvability Analysis for Multiple Source Scenario-2: Target-1 is
fixed and y-Coordinate of the Target-2 is changing

By decreasing the separation distance, algorithms become worse with respect to the
single step CRLB.

Moreover, the AOA based localization and single step localization methods show
approximately the same performance when the emitters are close to each other.
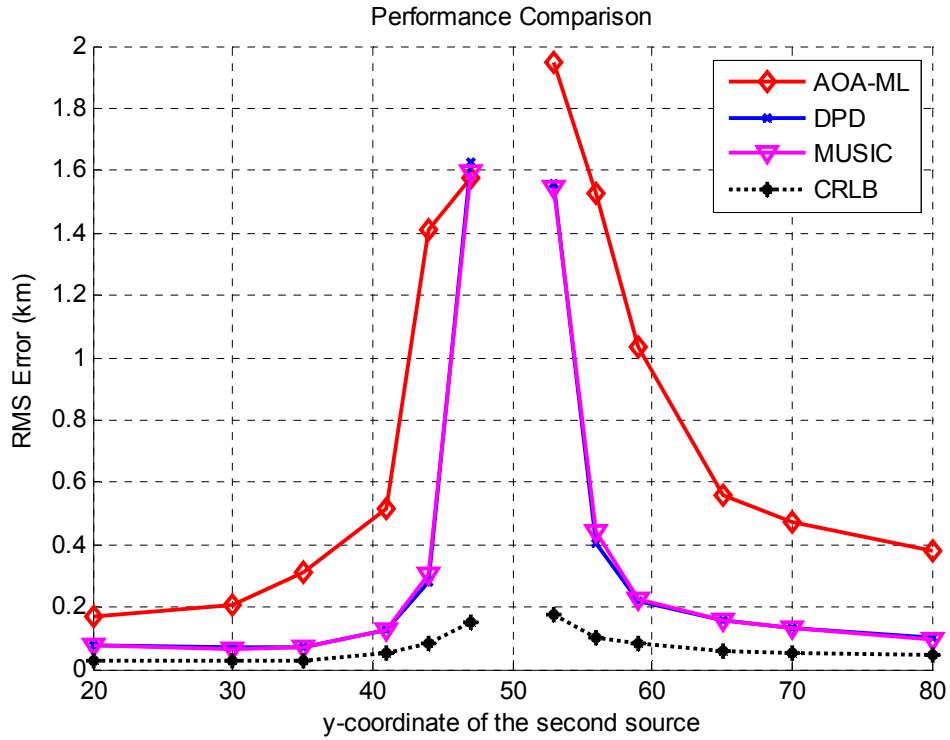
Figure 5.34: Comparison of the Resolvability Performances of the Algorithms with 20 dB SNR value

5.3 EVALUATION OF THE SIMULATIONS

Simulations have been done in two parts. In the first part of the simulations, individual comparison of the classical two step and single step methods are investigated under the single emitter case. Moreover geometrical effects on the performance of the algorithms are compared with varying target and sensor coordinates. In the second part, the performance of the AOA based localization method (with Brute Force data association algorithm) and the single step algorithms are investigated under the multiple source case.

In the second part of the simulations, it is shown that the AOA based ML algorithm gives near the performance of an efficient estimator. However, in some parts of the first section, AOA based ML is not capable so much. The main reason of this situation is that, ML location estimate is found from the search point that gives the

minimum cost in the 20x20x20 km^3 volume around the LS estimate. The same reason is valid for the performance degradation of the TDOA based ML method. It is seen from the simulations that, the performances of both AOA and TDOA based LS methods depend on the target-sensor geometry. The performance improvement is observed by using the AOA and TDOA measurements jointly. Due to combining the different equation sets with different independent error statistics, the performance improvement is observed.

The single step methods give better performances; especially, Direct Localization (DL) with MUSIC method gives at least the same performance with the Direct Position Determination (DPD) in all of the simulations. As mentioned in Chapter-4, DPD method needs eigen-decomposition in each grid search, however MUSIC method does not. It is obviously seen that MUSIC method is less complex than the DPD method. DL with Deterministic ML (DML) and DL with Stochastic ML (SML) methods give good performances at low SNR values, however with an increasing SNR, the performance of the algorithms become similar with the conventional methods. Moreover, the geometrical effects on the performance of the techniques are investigated. In the mentioned simulations, CRLB expressions of the AOA based, TDOA based, AOA-TDOA based hybrid and single step methods are compared. In other words, by comparing achievable ultimate performances, the geometrical effects on the methods examined clearly. It is shown from the simulations that the localization accuracy of the TDOA based methods highly depends on the target-sensor geometry. The performance of the TDOA based methods suddenly degrades with small geometrical differences. AOA based localization methods also depend on the deployment geometry, which is presented by performing various simulations based on error ellipse forms in Chapter-3. However, AOA based methods are not dependent on geometry as TDOA based methods. Moreover, hybrid methods give a better performance than the TDOA and AOA based methods. Finally it can be said that single step methods are most robust to the geometrical effects.

In the second part of the simulations, the performances of the AOA based method and single step methods are compared under the multiple source case. Two different

deployment geometries are used to investigate the performances of the methods under the optimum and practical deployment scenarios. It is shown by the simulations that the performance of the single step methods outperforms the classical AOA based localization method in all deployment cases. When, the performances of the algorithms are compared with varying number of snapshots, the single step methods give better results as expected. Finally resolvability skills of the techniques are investigated. It is shown from the simulations that the single step methods have better resolvability capabilities than the conventional AOA based method. Actually, this result is not surprising due to the dimensions of the observation covariance matrices used in AOA based methods and single step methods. In AOA based methods L different MxM covariance matrices are used for AOA measurements, however in single step methods $LMxLM$ covariance matrix is used for location estimation, where L is the number of sensor arrays each has M sensors. In AOA based methods, the overall system can resolve $(M-1)$ emitters; however in single step methods $(LM-1)$ emitters can be resolved due to the larger covariance matrix.

CHAPTER 6

CONCLUSIONS

The main focus of this thesis is the 3D location estimation of the unknown emitters with stationary target-sensor deployment. The approaches developed to solve this problem can be separated into two parts. The first group can be considered as a conventional approach and called as the two step localization. In the first step, position related parameters such as AOA and TDOA are estimated; and in the second step, location of the emitter is estimated by collecting the pre-measured location related parameters from distributed stations. However, the location estimation problem can be solved directly, which is called as single step localization. In single step localization concept, the location of the emitter is estimated directly by collecting the observations from the spatially distributed stations. The practical implementations of the single step methods seem feasible with developing communication technologies. In this work, both of these concepts are presented and investigated in detail.

First, conventional methods such as AOA based, TDOA based and AOA-TDOA based hybrid algorithms are presented. 3D ML and LS based methods are given for the conventional methods. Since CRLB expressions, ML and LS localization approaches are given for 2D geometry in the literature; various 3D expressions are derived and presented in this work. Namely, 3D CRLB expressions and 3D ML localization approaches for AOA based and AOA-TDOA based hybrid methods; 3D LS expressions for AOA based methods are derived and presented in this thesis. Error ellipse expressions, which can be considered as a performance criterion for AOA based methods, are presented and various simulations have been performed to

express the geometrical dependencies of the AOA based techniques for both 2D and 3D geometrical scenarios. It is shown by the simulations that the localization accuracy improves when the target is surrounded by the sensor arrays. Moreover the need of data association for AOA based localization methods for multiple emitter cases is presented and expressed with illustrations. Brute Force method [52] which is proposed for data association is discussed.

Single step localization methods found in the literature are presented such as DPD methods for single source and multiple sources. Moreover, three different single step location estimation methods are proposed using the philosophy of high resolution and ML Direction Finding (DF) techniques. Proposed Direct Localization (DL) with Multiple Signal Classification (MUSIC), DL with Deterministic Maximum Likelihood (DML) and DL with Stochastic Maximum Likelihood (SML) approaches are presented and explained.

Specific CRLB expressions for AOA based, TDOA based, AOA-TDOA based hybrid and single step localization approaches are derived and presented for investigating the ultimate achievable performance.

Various simulations are performed and evaluated. Individual comparisons of the methods are done. The performances are evaluated by comparing the azimuth and elevation deviations and TOA deviations for the conventional methods. In the simulations, ML methods give better performance than the LS techniques for AOA based and TDOA based localization methods as expected. However ML methods do not achieve the best performance in these simulations since the MLE is found by searching the grid point with minimum cost near the LS location estimate. The performances of the single step methods are evaluated by comparing the SNR values and the number of snapshots observed for single step methods. Using simulations, it is shown that the performance of the single step algorithms is good even at the -10 dB SNR values with comparable number of snapshots (~100). DPD and MUSIC methods give approximately the same performance in various simulations. As presented in the detailed algorithmic expressions, DPD method needs eigen-decomposition in each grid search; however DL with MUSIC method does not. It is shown that algorithmic complexity of the proposed MUSIC method is

less than that of the DPD method. DL with DML and DL with SML methods give good performances at low SNR values, however with an increasing SNR, the performances of the algorithms become similar with the conventional methods. One drawback of the DML and SML methods can be briefly explained as the need of the multidimensional search for the multiple emitter cases. However, there is no need to increase the search dimension in DPD and MUSIC methods due to multiple source scenarios. Furthermore, geometrical effects on the performance of the localization methods are investigated. It is shown that the localization accuracy of the TDOA based methods highly depends on the target-sensor geometry. The performance of the TDOA based methods degrades with small geometrical differences. As seen from the simulations, it can be said that single step methods are more robust to the geometrical effects. However, the single step methods are algorithmically more complex than the conventional methods.

In the second part of the simulations, performances of the methods are compared under the multiple source case with different geometrical deployments such as optimum and practical deployment scenarios. AOA based ML localization algorithm is used together with Root MUSIC AOA estimation method and Brute Force data association technique as a conventional two step algorithm. DPD and MUSIC methods are used for single step methods. In the simulations, it is shown that the single step methods outperform the conventional two step method under various cases such as varying SNR values and number of snapshot values. Moreover resolvability capabilities of the methods are compared. In the simulations, the coordinate of the first emitter is fixed and the position of the second emitter is varied near the first one. It is shown that the resolvability of the single step methods is better than that of the classic method. Actually, this result is not surprising due to the dimensions of the covariance matrices used in AOA based methods and the single step methods. In AOA based methods L different MxM covariance matrices are used for AOA measurements, however in single step methods $LMxLM$ covariance matrix is used for location estimation, where L is the number of sensor arrays each has M sensors. In AOA based methods, the overall system can resolve $(M-1)$ emitters; however in single step methods $(LM-1)$ emitters can be

resolved due to the gross covariance matrix. The performance improvement of the centralized processing in the localization problem can be explained by the observation covariance dimensions. The main source of this performance improvement directly depends on the array gain. In other words, in the observation period the signal components of the observations are added since the signal components observed by the sensors are coherent. However noise components cannot be added since the noise is independent between the sensors.

The advantages of the single step methods over the conventional methods under multiple emitter case can be summarized as follows:

- Performance improvement due to the centralized processing

- No need of data association algorithm for multiple source case

- Can use ULA for 3D localization

However, the main disadvantage of the single step methods is that they are computationally very expensive compared to the conventional methods. Furthermore, in single step techniques the communication load between the sensor arrays and the processing center is higher than that of the conventional approaches.

Many of conventional two step source localization methods contributed to the literature for single emitter scenarios. However, for multiple emitter scenarios, data association of pre-measured position related parameters (i.e. AOAs) with respect to each emitter should be performed. As future work, conventional two step localization algorithms for multiple emitters, which do not need data association, may be investigated. In this thesis, source localization problem is investigated for stationary emitter-sensor deployment. Conventional two step and single step localization methods for "moving sensor-stationary target", "stationary sensor-moving target", "moving sensor-moving target" scenarios can be studied. Finally, closed form solutions of single step source localization problem may be investigated as future work for both stationary and non-stationary deployment scenarios.

REFERENCES

[1]. Amar, A and Weiss, A.J., "Direct Position Determination of Multiple radio Signals", IEEE International Conference on Acoustics, Speech and Signal Processing 2004 Proceedings ICASSP '04, Volume: 2, 17-21 May 2004, pp. ii-81-4 vol.2

[2]. Stansfield, R. G., "Statistical Theory of DF Fixing", Journal of IEE 14, Part IIIA, 15, 1947, pp. 762-770

[3]. Ancker, C.J. "Airborne Direction Finding – Theory of Navigation Errors", IRE Transactions on Aeronautical and Navigational Electronics, Volume: 5, 1958, pp. 199–210

[4]. Poirot, J. L. and McWilliams G. V., "Application of Linear Statistical Models to Radar Location Techniques", IEEE Transaction on Aerospace and Electronic Systems, Volume: AES-10, November 1974, pp. 830–834

[5]. Torrieri, D.J., "Statistical Theory of Passive Location Systems", IEEE Transactions on Aerospace and Electronic Systems, Volume: 20 (2), 1984, pp. 183–197

[6]. Foy, W.H., "Position-Location Solutions by Taylor-Series Estimation", IEEE Transaction on Aerospace and Electronic Systems, Volume: AES-12 (2), 1976, pp. 187–194

[7]. Gavish, M. and Weiss, A.J., "Performance Analysis of Bearing Only Target Location Algorithms, IEEE Transactions on Aerospace and Electronic Systems, Volume: 28 (3), 1992, pp. 817–828

[8]. Poirot, J. L. and Smith M. S., "Moving Emitter Classification", IEEE Transaction on Aerospace and Electronic Systems, Volume: 12 (2), March 1976, pp. 255-269

[9]. Brown, R. M., "Emitter Location using Bearing Measurements from a Moving Platform", Naval Research Laboratory, Washington DC, NRL Report No: 8483, June 1981

[10]. Pages-Zamora, A., Vidal, J. and Brooks, D., "Closed-Form Solution for Positioning Based on Angle of Arrival Measurements", PIMRC 2002

[11]. Rao, K. D. and Reddy D. C., "A New Method for Finding Electromagnetic Emitter Location", IEEE Transaction on Aerospace and Electronic Systems, Volume: 30 (4), October 1994, pp. 1081-1085

[12]. Urruela, A, Pages-Zamora and A; Riba, J., "Divide-and Conquer Based Closed-form Position Estimation for AOA and TDOA Measurements", IEEE Acoustics, Speech and Signal Processing 2006 Proceedings, ICASSP 2006, Volume: 4, 14-19 May 2006, pp. IV-IV

[13]. Poisel, R.A., "Electronic Warfare Target Location Methods", Artech House, Norwood MA, 2005

[14]. Poisel, R.A., "Introduction to Communication Electronic Warfare Systems", Artech House, Norwood MA, 2002

[15]. Gavish, M. and Fogel, E., "Effect of Bias on Bearing Only Target Location", IEEE Transaction on Aerospace and Electronic Systems, Volume: 26 (1), January 1990, pp. 22-26

[16]. McCabe, H. and Al-Samara M., "Application of Sensor Fusion Algorithm to Nonlinear Data Containing Non-Stationary, Multiplicative Noise of Unknown Distribution", Proceedings of the 33rd Conference on Decision and Control, Florida, December 1994, pp. 1205-1206

[17]. Manolakis, D.E. and Cox, M.E., "Effect in Range Difference Position Estimation Due to Stations' Position Errors", IEEE Transaction on Aerospace and Electronic Systems, Volume: 34 (1), January 1998, pp. 328-334

[18]. Stein, S., "Algorithms for Ambiguity Functions Processing", IEEE Transactions on Acoustics, Speech, And Signal Processing, Volume: ASSP-29 (3), June 1981, pp. 588-599

[19]. Gezici, S., Tian, Z., Giannakis, G.B., Kobayashi, H., Molisch, A.F., Poor, H.V. and Sahinoglu, Z., "Localization via Ultra-Wideband Radios: A Look at Positioning Aspects for Future Sensor Networks", IEEE Signal Processing Magazine, Volume: 22 (4), 2005, pp. 70–84

[20]. Gustafsson, F. and Gunnarsson, F., "Mobile Positioning Using Wireless Networks: Possibilities and Fundamental Limitations Based on Available Wireless Network Measurements", IEEE Signal Processing Magazine, Volume: 22 (4), 2005, pp. 41–53

[21]. Sayed, A.H., Tarighat, A. and Khajehnouri, N., "Network-Based Wireless Location: Challenges Faced in Developing Techniques for Accurate Wireless Location Information", IEEE Signal Processing Magazine, Volume: 22 (4), 2005, pp. 24–40

[22]. Sun, G., Chen, J., Gou, W. and Liu, K.J.R., "Signal Processing Techniques in Network-Aided Positioning: A Survey of State-of-the-Art Positioning Designs", IEEE Signal Processing Magazine, Volume: 22 (4), 2005, pp. 12–23

[23]. Zagami, J.M., Parl, S.A., Bussgang, J.J. and Melillo, K.D., "Providing Universal Location Services using a Wireless E911 Location Network", IEEE Communications Magazine, Volume: 36 (4), 1998, pp. 66–71

[24]. Fang B.T., "Simple Solutions for Hyperbolic and Related Position Fixes", IEEE Transactions on Aerospace and Electronic Systems, Volume: 26 (5), 1990, pp. 748–753

[25]. Smith, J. and Abel J., "The Spherical Interpolation Method of Source Localization, IEEE Journal of Oceanic Engineering, Volume: 12 (1), 1987, pp. 246–252

[26]. Abel, J.S., "A Divide and Conquer Approach to Least-Squares Estimation", IEEE Transactions on Aerospace and Electronic Systems, Volume: 26 (2), 1990, pp. 423–427

[27]. Chan, Y.T. and Ho, K.C., "A Simple and Efficient Estimator for Hyperbolic Location", IEEE Transactions on Signal Processing, Volume: 42 (8), 1994, pp. 1905–1915

[28]. Mao, G., Fidan, B., and Anderson, B.D.O., "Wireless Sensor Network Localization Techniques", The International Journal of Computer and Telecommunications Networking, Volume: 51 (10), July 2007, pp. 2529-2553

[29]. Doğançay K., "Emitter Localization using Clustering-Based Bearing Association", IEEE Transactions on Aerospace and Electronic Systems, Volume: 41 (2), 2005, pp. 525–536

[30]. Drake S. and Doğançay K., "Geolocation by Time Difference of Arrival Using Hyperbolic Asymptotes", IEEE International Conference on Acoustics, Speech, and Signal Processing, Volume: 2, 2004, pp. ii-361-4

[31]. Shen, G., Zetik, R. and Thoma R. S., "Performance Comparison of TOA and TDOA Based Location Estimation Algorithms in LOS Environment", IEEE Proceedings of the 5th Workshop on Positioning, Navigation and Communication 2008, WPNC'08, Volume:1, March 2008, pp.71-78

[32]. Bard, J. D. and Ham, F. M., "Time Difference of Arrival Dilution of Precision and Applications", IEEE Transactions on Signal Processing, Volume: 47 (2), February 1999, pp. 521-523

[33]. Koorapaty, H., Grubeck, H. and Cedervall, M., "Effect of Biased Measurement Errors on Accuracy of Position Location Methods", IEEE GLOBECOM'98, Volume: 3, November 1998, pp. 1497-1502

[34]. Hall D.L., "Mathematical Techniques in Multisensor Data Fusion", Artech House Publishers, 2004

[35]. Yang, C., Huang, Y. and Zhu, X., "Hybrid TDOA/AOA Method for Indoor Positioning Systems", Seminar on Location Technologies 2007, The Institution of Engineering and Technology, Volume: 1, December 2007, pp. 1-5

[36]. Nur-A-Alam, M. and Haque, M.M., "A Least Square Approach for TDOA/AOA Wireless Location WCDMA System", Proceedings of 11th International Conference on Computer and Information Technology, ICCT'08, Volume: 1, December 2008, pp. 686-690

[37]. Lachapelle, G., Klukas, R. and Ma, C., "An Enhanced Two-Step Least Squared Approach for TDOA/AOA Wireless Location", IEEE International Conference on Communications, ICC'03, Volume: 2, May 2003, pp. 987-991

[38]. Abdul-Latif, O., Shepherd, P. and Pennock S., "TDOA/AOA Data Fusion for Enhancing Positioning in an Ultra Wideband System", IEEE International Conference on Signal Processing and Communications, ICSPC'07, Volume: 1, November 2007, pp. 1531-1534

[39]. Zhuang, W. and Cong, L., "Hybrid TDOA/AOA Mobile User Location for Wideband CDMA Cellular Systems", IEEE Transactions on Wireless Communications, Volume: 1 (3), July 2002, pp. 439-447

[40]. Chen, H. Y. and Chou, T. Y., "Hybrid TDOA/AOA Mobile User Location with Artificial Neural Networks", IEEE International Conference on Networking, Sensing and Control, ICNSC '08, Volume: 1, April 2008, pp. 847-852

[41]. Weiss, A.J., "Direct Position Determination of Multiple Radio Signals", EURASIP Journal on Applied Signal Processing 2005

[42]. Amar, A. and Weiss, A.J., "Optimal Radio Emitter Location Based on the Doppler Effect", 5th Sensor Array and Multichannel Signal Processing Workshop Proceedings 2008, 21-23 July 2008, pp. 54-57

[43]. Bar-Shalom, O. and Weiss, A.J., "Efficient Direct Position Determination of Orthogonal Frequency Division Multiplexing Signals", IET Radar, Sonar & Navigation, Volume: 3 (2), April 2009, pp. 101-111

[44]. Bar-Shalom, O. and Weiss, A.J., "Direct Position Determination using MIMO Radar", IEEE 25th Convention of Electrical and Electronics Engineers in Israel 2008, 3-5 December 2008, pp. 575-579

[45]. Weiss, A.J., "Direct Position Determination of Narrowband Radio Frequency Transmitters", IEEE Signal Processing Letters, Volume: 11 (5), May 2004, pp. 513-516

[46]. Amar, A. and Weiss, A.J., "Advances in Direct Position Determination", Sensor Array and Multichannel Signal Processing Workshop Proceedings 2004, 18-21 July 2004, pp. 584-588

[47]. Amar, A. and Weiss, A.J., "On Unique Passive Geolocation of Multiple Radio-Frequency Emitters", 8th International Symposium on Signal Processing and Its Applications 2005 Proceedings, Volume: 2, 28-31 August 2005, pp. 911-914

[48]. Amar, A. and Weiss, A.J., "Analysis of Direct Position Determination Approach in the Presence of Model Errors", 13th Workshop on Statistical Signal Processing 2005, 17-20 July 2005, pp. 521-524

[49]. Bishop, A. N., Fidan, B., Doğançay, K., Anderson, B. D. O. and Pathriana P. N., "Exploiting Geometry for Improved Hybrid AOA/TDOA-Based Localization", Signal Processing, Volume: 88 (7) , July 2008, pp. 1775-1791

[50]. Paradowski, L. R., "Microwave Emitter Position Location: Present and Future", 12th International Conference on Microwaves and Radar, MIKON '98, Volume: 4, May 1998, pp. 97-116

[51]. Tuncer, E. and Friedlander B., "Classical and Modern Direction of Arrival Estimation", Academic Press, 2009

[52]. Reed, J.D., da Silva, C.R.C.M. and Buehrer, R.M., "Multiple-Source Localization using Line-of-Bearing Measurements: Approaches to the Data Association Problem", IEEE Military Communication Conference 2008 (MILCOM '08), 16-19 November 2008, pp. 1-7

[53]. Bergamo, P. and Mazzini, G., "Localization in Sensor Networks with Fading and Mobility", The 13th IEEE International Symposium on Personal, Indoor and Mobile Radio Communications, Volume: 2, 2002, pp. 750–754

[54]. Elnahrawy, E., Li, X. and Martin, R., "The Limits of Localization Using Signal Strength: A Comparative Study", First Annual IEEE Conference on Sensor and Ad-Hoc Communications and Networks, 2004, pp. 406–414

[55]. Elnahrawy, E., Madigan, D., Martin, R., Ju, W.H., Krishnan, P. and Krishnakumar, A., "Bayesian Indoor Positioning Systems", IEEE INFOCOM 2005, Volume: 2, 2005, pp. 1217–1227

[56]. Niculescu, D. and Nath, B., "Localized Positioning in Ad Hoc Networks", IEEE International Workshop on Sensor Network Protocols and Applications, 2003, pp. 42–50

[57]. Patwari, N., Hero, A., Perkins, M., Correal, N. and O'Dea, R., "Relative Location Estimation in Wireless Sensor Networks, IEEE Transactions on Signal Processing, Volume: 51 (8), 2003, pp. 2137–2148

[58]. Levanon, N., "Interferometry Against Differential Doppler, Performance Comparison of Two Emitter Location Airborne Systems", IEE Proceedings, Volume: 136 (2), April 1989, pp. 70-74

[59]. Trees, H. L. V., "Optimum Array Processing: Part IV—Detection, Estimation, and Modulation Theory" John Wiley & Sons, 2002

[60]. Schmidt, R.O., Multiple emitter location and signal parameter estimation, In: Proc. RADC Spectral Estimation Workshop, 1979

[61]. Roy, R. and Kailath, T., "ESPRIT: Estimation of Signal Parameters via Rotational Invariance Techniques", IEEE Transactions on Acoustics, Speech, and Signal Processing, Volume: 37 (7), 1989, pp. 984–995

[62]. Paulraj, A., Roy, R. and Kailath, T., "A Subspace Rotation Approach to Signal Parameter Estimation", Proceedings of the IEEE, Volume: 74 (7), 1986, pp. 1044–1046

[63]. Kumaresan, R. and Tufts, D.W., "Estimating the Angles of Arrival of Multiple Plane Waves", IEEE Transactions on Aerospace and Electronic Systems, Volume: AES-19, 1983, pp. 134–139

[64]. Barabell, A., "Improving the Resolution Performance of Eigenstructure-Based Direction-Finding Algorithms", IEEE International Conference on Acoustics, Speech, and Signal Processing, Volume: 8, 1983, pp. 336–339

[65]. Friedlander, B. and Weiss, A.J, "On the Cramer-Rao Bound for Direction Finding of Correlated Signals", IEEE Transactions on Signal Processing, Volume: 41 (1), January 1993, pp. 495-499

[66]. Jenkins, H.H., Small Aperture Radio Direction Finding, Norwood, MA, Artech House, 1991

[67]. Gardner, W.A., "Simplification of MUSIC and ESPRIT by Exploitation of Cyclostationarity", Proceedings of IEEE, Volume: 76 (7), July 1988, pp. 845-847

[68]. Knapp, C.H. and Carter, G.C., "Generalized Correlation Method for Estimation of Time Delay", IEEE Transactions on Acoustics, Speech, And Signal Processing, Volume: ASSP-24 (4), August 1976, pp. 320-327

[69]. Manabe, T. and Takai, H., "Superresolution of Multipath Delay Profiles Measured by PN Correlation Method", IEEE Transactions on Antennas and Propagation, Volume: 40 (5), May 1992, pp. 500–509

[70]. Pallas, M.A. and Jourdain G., "Active High Resolution Time Delay Estimation for Large BT Signals, IEEE Transactions on Signal Processing, Volume: 39 (4), April 1991, pp. 781–787

[71]. Bouchereau, F., Brady, D. and Lanzl, C., "Multipath Delay Estimation using a Superresolution PN-Correlation Method", IEEE Transactions on Signal Processing, Volume: 49 (5), May 2001, pp. 938–949

[72]. Martin, R.K., Yan, C. and Fan, H.H., "Bounds on Distributed TDOA-Based Localization of OFDM Sources", IEEE International Conference on Acoustics, Speech and Signal Processing Proceedings, 2009, pp. 2289-2292

[73]. Yang, B. and Scheuing, J., "Cramer-Rao Bound and Optimum Sensor Array for Source Localization from Time Differences of Arrival", IEEE

International Conference on Acoustics, Speech and Signal Processing Proceedings, Volume: 4, 18-23 March 2005, pp. 961-964

[74]. Gustafsson, F. and Gunnarsson, F., "Particle Filters for Positioning in Wireless Networks", EUSIPCO, Toulouse, September 2002

[75]. Bard, J.D. and Ham, F.M., "An Algebraic Solution to the Time Difference of Arrival Equations", Proceedings of the IEEE South East Conference, April 1996

[76]. Mellen, G.M., "Closed-Form Solution for Determining Emitter Location Using Time Difference of Arrival Measurements", IEEE Transactions on Aerospace and Electronic Systems, Volume: 39 (3), July 2003, p. 1056-1058

[77]. Gustafsson, F. and Gunnarsson, F., "Positioning Using Time Difference of Arrival Measurements", IEEE International Conference on Acoustics, Speech and Signal Processing Proceedings, Hongkong, PRC, 2003

[78]. Schmidt, R.O., "A Signal Subspace Approach to Multiple Emitter Location and Spectral Estimation", Ph.D. Dissertation, Stanford University, California, 1981

[79]. Ziskind and Wax, M., "Maximum Likelihood Localization of Multiple Sources by Alternating Projection", IEEE International Conference on Acoustics, Speech and Signal Processing Proceedings, Volume: ASSP-36, October 1988, pp. 1553-1560

[80]. Schweppe, F., "Sensor Array Data Processing for Multiple Signal Sources", IEEE Transactions on Information Theory, Volume: IT-4, March 1968, pp. 294-305

[81]. Stoica, P. and Nehorai, A., "On the Concentrated Stochastic Likelihood Function in Array Signal Processing", Circuits, Systems and Signal Processing, Volume: 14, 1995, pp. 669-674

[82]. Cramer, H., Mathematical Methods of Statistics, Princeton University Press, 1946

APPENDIX A

FIM BLOCK REPRESANTATIONS FOR SINGLE STEP MULTIPLE SOURCE LOCALIZATION PROBLEM

In this part, direct representations for all FIM blocks are given for single step source localization problem. The derivations of the FIM blocks are given in [41]. As mentioned in *Section 4.1*, the unknowns for the single step localization problem are the locations of the sources, complex attenuation coefficients between the sources and the sensor arrays and the signal waveforms of the sources. The complete FIM consists of 16 different blocks for this problem. The structure of the complete FIM is shown below.

$$FIM = \begin{bmatrix} FIM_{\wedge\wedge} & FIM_{\wedge\overline{B}} & FIM_{\wedge\widetilde{B}} & FIM_{\wedge P} \\ FIM_{\overline{B}\wedge} & FIM_{\overline{B}\overline{B}} & FIM_{\overline{B}\widetilde{B}} & FIM_{\overline{B}P} \\ FIM_{\widetilde{B}\wedge} & FIM_{\widetilde{B}\overline{B}} & FIM_{\widetilde{B}\widetilde{B}} & FIM_{\widetilde{B}P} \\ FIM_{P\wedge} & FIM_{P\overline{B}} & FIM_{P\widetilde{B}} & FIM_{PP} \end{bmatrix} \quad (A.1)$$

By using the fact,

$$FIM_{ij} = FIM_{ji}^{H} \quad (A.2)$$

the off-diagonal blocks are represented for only the upper triangular part of the **FIM**.

The block related to the unknown signal waveforms can be presented as

$$FIM_{\wedge\wedge} = \left(A^H R_y^{-1} A\right) \odot \left(A^H R_y^{-1} A\right)^* \tag{A.3}$$

where the operator $\odot$ represents the Schur-Hadamard product (element-wise product). The gross manifold matrix expression A can be written in terms of the manifold expression for each sensor array as

$$A = [\, A_1^T, A_2^T, \dots, A_L^T \,]^T \tag{A.4}$$

For each sensor array, the individual manifold expressions can be written in terms of each emitter as

$$A_l = \left[\bar{a}_l(p_1, b_{l1}), \bar{a}_l(p_2, b_{l2}), \dots, \bar{a}_l(\, p_Q, b_{lQ})\right] \tag{A.5}$$

Finally, the column vector component of the manifold expression A_l can be separated into manifold vector, complex attenuation coefficient and TOA expression as

$$\bar{a}_l(p_q, b_{lq}) = b_{lq} a_l(p_q)\, e^{-j.\omega.\tau_l(p_q)} \tag{A.6}$$

The $\bar{a}_l(p_q, b_{lq})$ expression is $Mx1$ vector, which contains the response of each sensor in the lth sensor array with respect to the qth emitter.

The second block of the **FIM** is constructed due to the real parts of the complex attenuation coefficients.

$$\begin{aligned} FIM_{\bar{B}_m \bar{B}_l} = 2Re\Big\{&\left(\wedge A^H R_y^{-1} \bar{C}_l\right) \odot \left(\bar{C}_m^H R_y^{-1} A \wedge\right)^* \\ &+ \left(\bar{C}_m^H R_y^{-1} \bar{C}_l\right) \odot \left(\wedge A^H R_y^{-1} A \wedge\right)^*\Big\} \end{aligned} \tag{A.7}$$

where $\bar{C}_n$ represents the partial derivatives of the manifold matrix with respect to the real parts of the related complex attenuation coefficients. The mathematical structure of the matrix $\bar{C}_n$ is shown below.

$$\bar{C}_n = \left[\frac{\partial a_1}{\partial \bar{b}_{n1}}, \frac{\partial a_2}{\partial \bar{b}_{n2}}, \dots, \frac{\partial a_Q}{\partial \bar{b}_{nQ}}\right] \tag{A.8}$$

where a_q represents the qth column of the manifold matrix A.

Due to the mathematical similarity with the other **FIM** blocks, the block is rewritten as

$$FIM_{\bar{B}_m \bar{B}_l} = 2Re\left\{(A_1^H \bar{C}_l) \odot (\bar{C}_m^H A_1)^* + (\bar{C}_m^H R_y^{-1} \bar{C}_l) \odot A_2^*\right\} \tag{A.9}$$

where the expressions A_1 and A_2 are defined as

$$A_1 \triangleq R_y^{-1} A \wedge \tag{A.10}$$

$$A_2 \triangleq \wedge A^H R_y^{-1} A \wedge \tag{A.11}$$

By using similar derivations, the blocks $FIM_{\bar{B}_m \tilde{B}_l}$, $FIM_{\tilde{B}_m \tilde{B}_l}$ can be written as

$$FIM_{\bar{B}_m \tilde{B}_l} = 2Re\left\{(A_1^H \tilde{C}_l) \odot (\bar{C}_m^H A_1)^* + (\bar{C}_m^H R_y^{-1} \tilde{C}_l) \odot A_2^*\right\} \tag{A.12}$$

$$FIM_{\tilde{B}_m \tilde{B}_l} = 2Re\left\{(A_1^H \tilde{C}_l) \odot (\tilde{C}_m^H A_1)^* + (\tilde{C}_m^H R_y^{-1} \tilde{C}_l) \odot A_2^*\right\} \tag{A.13}$$

where $\tilde{C}_n$ represents the partial derivatives of the manifold matrix with respect to the imaginary parts of the related complex attenuation coefficients. The structure of the matrix $\tilde{C}_n$ is shown below.

$$\tilde{C}_n = \left[\frac{\partial a_1}{\partial \tilde{b}_{n1}}, \frac{\partial a_2}{\partial \tilde{b}_{n2}}, \dots, \frac{\partial a_Q}{\partial \tilde{b}_{nQ}}\right] \tag{A.14}$$

Similar to the attenuation coefficient related **FIM** blocks, **FIM** block associated with the unknown source positions can be written as

$$FIM_{P_m P_l} = 2Re\left\{(A_1^H D_l) \odot (D_m^H A_1)^* + (D_m^H R_y^{-1} D_l) \odot A_2^*\right\} \tag{A.15}$$

where D_n consists of the partial derivatives of the manifold matrix with respect to each Cartesian coordinate of the related source position. The structure of the matrix D_n is given as,

$$D_n = \left[\frac{\partial a_1}{\partial p_{n1}}, \frac{\partial a_2}{\partial p_{n2}}, \dots, \frac{\partial a_Q}{\partial p_{nQ}}\right] \tag{A.16}$$

where p_{nq} is the nth & q^{th} entry of the matrix P, given in equation (4.72). The FIM blocks related with the source positions and the complex attenuation coefficients (real and imaginary parts) are presented as

$$FIM_{P_m\bar{B}_l} = 2Re\left\{\left(A_1^H\overline{C}_l\right) \odot \left(D_m^H A_1\right)^* + \left(D_m^H R_y^{-1}\overline{C}_l\right) \odot A_2^*\right\} \tag{A.17}$$

$$FIM_{P_m\tilde{B}_l} = 2Re\left\{\left(A_1^H\widetilde{C}_l\right) \odot \left(D_m^H A_1\right)^* + \left(D_m^H R_y^{-1}\widetilde{C}_l\right) \odot A_2^*\right\} \tag{A.18}$$

Finally, the **FIM** block can be written as

$$FIM_{\wedge\bar{B}_m} = 2Re\left\{\left(A^H R_y^{-1}A \wedge\right)^* \odot \left(A^H R_y^{-1}\overline{C}_m\right)\right\} \tag{A.19}$$

which can be written in terms of the previously defined similar expressions A_1 and A_2 as

$$FIM_{\wedge\bar{B}_m} = 2Re\left\{(A^H A_1)^* \odot \left(A^H R_y^{-1}\overline{C}_m\right)\right\} \tag{A.20}$$

Similarly, the block related with the signals waveforms and the imaginary part of the complex attenuation coefficients can be presented as

$$FIM_{\wedge\tilde{B}_l} = 2Re\left\{(A^H A_1)^* \odot \left(A^H R_y^{-1}\widetilde{C}_m\right)\right\} \tag{A.21}$$

As seen from the previous derivations, the **FIM** block related to the signal waveforms and the source position can be written as

$$FIM_{\wedge p_m} = 2Re\left\{(A^H A_1)^* \odot \left(A^H R_y^{-1}D_m\right)\right\} \tag{A.22}$$

Finally, all of the blocks of the **FIM** have been represented. By constructing the complete **FIM**, **CRLB** matrix can be calculated as

$$CRLB = (FIM)^{-1} \tag{A.23}$$

APPENDIX B

D MATRIX REPRESANTATION FOR SINGLE STEP MULTIPLE SOURCE LOCALIZATION CRLB EXPRESSION

D_n consists of the partial derivatives of the manifold matrix with respect to each Cartesian coordinate of the related source position. The structure of the matrix D_n is given as

$$D_n = \left[\frac{\partial a_1}{\partial p_{n1}}, \frac{\partial a_2}{\partial p_{n2}}, \dots, \frac{\partial a_Q}{\partial p_{nQ}} \right] \tag{B.1}$$

where p_{nq} is the nth & q^{th} entry of the matrix P

$$P = [p_1, p_2, \dots, p_Q] \tag{B.2}$$

where Q is the number of sources, p_q is the $Dx1$ vector representing the Cartesian coordinates of the qth source. Each entry of the $LMx1$ vector a_q can be written as

$$a_{q_{lm}}$$
$$= b_{lq} \, e^{-j \cdot \frac{2\Pi}{W} \frac{w}{\left(\frac{T}{K}\right)} \left(\tau_l(p_q) \right)} \, e^{-j \frac{2\Pi}{\lambda} \left(P_{lm_x} sin(\theta_{lq}) cos(\phi_{lq}) + P_{lm_y} cos(\theta_{lq}) cos(\phi_{lq}) + P_{lm_z} sin(\phi_{lq}) \right)} \tag{B.3}$$

where the trigonometric expressions of the azimuth and elevation angles between the lth sensor array and the qth emitter can be written as

$$\sin\left(\theta_{l_q}\right) = \frac{\left(p_{q_x} - P_{lm_x}\right)}{\sqrt{\left(p_{q_x} - P_{lm_x}\right)^2 + \left(p_{q_y} - P_{lm_y}\right)^2}} \tag{B.4}$$

$$\cos\left(\theta_{l_q}\right) = \frac{\left(p_{q_y} - P_{lm_y}\right)}{\sqrt{\left(p_{q_x} - P_{lm_x}\right)^2 + \left(p_{q_y} - P_{lm_y}\right)^2}} \tag{B.5}$$

$$\sin\left(\phi_{l_q}\right) = \frac{\left(p_{q_z} - P_{lm_z}\right)}{\sqrt{\left(p_{q_x} - P_{lm_x}\right)^2 + \left(p_{q_y} - P_{lm_y}\right)^2 + \left(p_{q_z} - P_{lm_z}\right)^2}} \tag{B.6}$$

$$\cos\left(\phi_{l_q}\right) = \frac{\sqrt{\left(p_{q_x} - P_{lm_x}\right)^2 + \left(p_{q_y} - P_{lm_y}\right)^2}}{\sqrt{\left(p_{q_x} - P_{lm_x}\right)^2 + \left(p_{q_y} - P_{lm_y}\right)^2 + \left(p_{q_z} - P_{lm_z}\right)^2}} \tag{B.7}$$

The a_{lm} expression can be separated as

$$a_{q_{lm}} = b_{lq} \psi\, \gamma \tag{B.8}$$

where the expressions ψ and γ can be written as

$$\psi = e^{-j \cdot \frac{2\Pi\, w}{W\left(\frac{T}{K}\right)}\left(\tau_l(\boldsymbol{p_q})\right)} \tag{B.9}$$

$$\gamma = e^{-j\frac{2\Pi}{\lambda}\left(P_{lm_x}\sin\left(\theta_{l_q}\right)\cos\left(\phi_{l_q}\right) + P_{lm_y}\cos\left(\theta_{l_q}\right)\cos\left(\phi_{l_q}\right) + P_{lm_z}\sin\left(\phi_{l_q}\right)\right)} \tag{B.10}$$

The components of the $\boldsymbol{D_n}$ expression can be written for each emitter as

$$\boldsymbol{D_{q_n}} = \frac{\partial a_q}{\partial p_{q_n}} \tag{B.11}$$

where n is the index for the dimension vectors, i.e. x, y, z. The components of the $\frac{\partial a_q}{\partial p_{qn}}$ expression can be written for each dimension as

$$\frac{\partial a_{lm}}{\partial p_n} = b_{lq}\left(\frac{\partial \psi}{\partial p_n}\gamma + \frac{\partial \gamma}{\partial p_n}\psi\right) \tag{B.12}$$

And the components $\frac{\partial \psi}{\partial p_n}$ can be written as

$$\frac{\partial \psi}{\partial p_n} = -\psi j \frac{2\Pi w}{W\left(\frac{T}{K}\right)c} \frac{(P_n - P_{lm_n})}{\|\boldsymbol{P} - \boldsymbol{P}_l\|} \tag{B.13}$$
$$n = x, y, z$$

Also the components $\frac{\partial \gamma}{\partial p_n}$ can be written as

$$\frac{\partial \gamma}{\partial p_x} = -\gamma\, j \frac{2\Pi}{\lambda}\left(P_{lm_x}\left(\frac{\|\boldsymbol{P} - \boldsymbol{P}_l\|^2 - \left(P_x - P_{lm_x}\right)^2}{\|\boldsymbol{P} - \boldsymbol{P}_l\|^3}\right)\right.$$
$$- P_{lm_y}\left(\frac{(P_x - P_{lm_x})(P_y - P_{lm_y})}{\|\boldsymbol{P} - \boldsymbol{P}_l\|^3}\right) \tag{B.14}$$
$$\left.- P_{lz}\left(\frac{(P_x - P_{lm_x})(P_z - P_{lm_z})}{\|\boldsymbol{P} - \boldsymbol{P}_l\|^3}\right)\right)$$

$$\frac{\partial \gamma}{\partial p_y} = -\gamma\, j \frac{2\Pi}{\lambda}\left(P_{lm_x}\left(\frac{(P_x - P_{lm_x})(P_y - P_{lm_y})}{\|\boldsymbol{P} - \boldsymbol{P}_l\|^3}\right)\right.$$
$$- P_{lm_y}\left(\frac{\|\boldsymbol{P} - \boldsymbol{P}_l\|^2 - \left(P_y - P_{lm_y}\right)^2}{\|\boldsymbol{P} - \boldsymbol{P}_l\|^3}\right) \tag{B.15}$$
$$\left.- P_{lz}\left(\frac{(P_y - P_{lm_y})(P_z - P_{lm_z})}{\|\boldsymbol{P} - \boldsymbol{P}_l\|^3}\right)\right)$$

$$\frac{\partial \gamma}{\partial p_z} = -\gamma \, j \, \frac{2\Pi}{\lambda} \left(P_{lm_x} \left(\frac{(P_x - P_{lm_x})(P_z - P_{lm_z})}{\|\boldsymbol{P} - \boldsymbol{P_l}\|^3} \right) \right.$$

$$- P_{lm_y} \left(\frac{(P_y - P_{lm_y})(P_z - P_{lm_z})}{\|\boldsymbol{P} - \boldsymbol{P_l}\|^3} \right) \tag{B.16}$$

$$\left. - P_{lz} \left(\frac{\|\boldsymbol{P} - \boldsymbol{P_l}\|^2 - (P_z - P_{lm_z})^2}{\|\boldsymbol{P} - \boldsymbol{P_l}\|^3} \right) \right)$$

By obtaining each $\boldsymbol{D_n}$ expression, the FIM blocks, consequently the minimum achievable positioning error can be calculated.